GNSS Antenna Orientation Based on Modification of Received Signal Strengths

David Eugen Grimm

Zurich 2012

DISS. ETH N^O. 20806

GNSS ANTENNA ORIENTATION BASED ON MODIFICATION OF RECEIVED SIGNAL STRENGTHS

A dissertation submitted to

ETH ZURICH

for the degree of

Doctor of Sciences

presented by

DAVID EUGEN GRIMM

Dipl. Ing. ETH Zurich

born September 22, 1982

citizen of Embrach and Hinwil, ZH

accepted on the recommendation of

Prof. Dr. Hilmar Ingensand, examiner
Prof. Dr. Lambert Wanninger, co-examiner

2012

Abstract

This dissertation presents a concept to determine the orientation of a single GNSS antenna. When the orientation of the antenna is known, the presented approach can also be used for detection of multipath and reflected signals as well as spoofing signals.

The orientation of the antenna is calculated using the direction of arrival (DOA) of the satellites' signals. Because the DOAs of the satellites' signals are not detectable with a standard GNSS antenna, the directional antenna pattern of the antenna used is modified. The antenna pattern is modified by partially covering the antenna with a material that attenuates the signals in the band spectrum of GNSS. The attenuating material is rotated above the antenna, thereby influencing the received signal strength of the different satellites. The signal strength is indicated by the carrier-to-noise density C/N_0. Analysing the C/N_0 of different satellites allows determining the DOA of each satellite's signal in relation to the antenna. Knowing the satellites' positions from the broadcast ephemerides and the antenna position allows calculation of the antenna orientation as well as the theoretically expected DOAs. Based on the instant approach, the real DOA of each satellite's signal is determined. By comparing the expected DOAs with the real DOAs, multipath and reflected signals as well as spoofing signals are determinable. Excluding these signals from the position and orientation calculation can remove systematic biases and, therefore, improve the accuracy.

Knowledge of the orientation completes the positioning information and is necessary for navigation applications. For precise GNSS measurements, the orientation of the antenna must be known to implement correction models for the antenna phase centre offset (PCO) and phase centre variation (PCV).

Under optimal conditions, orientation information with an uncertainty of 5 degrees is achievable after a 2-minute measurement while an orientation with an uncertainty below 1 degree is achievable by measuring for several hours. Under poor conditions, an uncertainty of 5 degrees is achievable as well; however, because of systematic influences, the uncertainty will not improve significantly over a longer measuring time. A comparison of the obtained orientation value to a reference value verifies the correctness of the concept.

Abstract

Zusammenfassung

Die vorliegende Dissertation beschreibt einen Ansatz zur direkten Orientierungsbestimmung einer einzelnen GNSS-Antenne. Bei bekannter Orientierung der Antenne können Mehrwegsignale, reflektierte Signale oder Signale von Störsendern, welche von der Antenne empfangen werden, identifiziert werden.

Die Orientierung der Antenne wird aus der Eintreffrichtung der Satellitensignale berechnet. Um die Eintreffrichtungen der Signale mit einer handelsüblichen Antenne zu bestimmen, wird das Empfangsmuster der verwendeten Antenne (Antennen Pattern) modifiziert. Dies erfolgt durch partielle Abschattung der Antenne. Für die Abschattung wird ein Material verwendet, welches Signale im GNSS-Frequenzspektrum dämpft. Die partielle Abschattung wird so über der Antenne gedreht, dass die Signale der einzelnen Satelliten entsprechend ihrer Position (Azimut und Elevation) unterschiedlich abgeschwächt werden. Der Zusammenhang zwischen Signal-Rausch-Verhältnis (C/N_0) und der Position der Abschattung ermöglicht die Bestimmung der Eintreffrichtungen der Satellitensignale. Durch Kenntnis der Satellitenposition aus den Bahndaten und der Eintreffrichtung der Satellitensignale können sowohl die Orientierung der Antenne sowie auch die theoretisch erwarteten Eintreffrichtungen der Satellitensignale bestimmt werden. Ein Vergleich zwischen den erwarteten und den bestimmten Eintreffrichtungen ermöglicht die Identifikation von Signalen, welche die Antenne nicht aus der erwarteten Eintreffrichtung erreichen. Das Ausschliessen dieser Signale von der Orientierungs- und Positionsbestimmung, führt zu einer Reduktion systematischer Abweichungen und somit zu einer verbesserten Genauigkeit.

Kenntnis über die Orientierung der Antenne vervollständigt die Positionsinformation. Eine bekannte Orientierung erleichtert Anwendungen in der Navigation und ermöglicht das direkte Navigieren ohne Initialbewegung der Antenne. Weiter muss die Orientierung der Antenne für hochgenaue GNSS-Messungen bekannt sein, um Korrekturmodelle für Phasenzentrumsoffset und Phasenzentrumsvariation anbringen zu können.

Unter optimalen Bedingungen kann nach einer Messdauer von 2 Minuten die Orientierung mit einer Messunsicherheit von 5 Grad, und nach einer Messdauer von über 2 Stunden mit einer Messunsicherheit von unter einem Grad erreicht werden. Unter schlechten Bedingungen kann ebenfalls eine Messunsicherheit von 5 Grad erwartet werden, wobei sich diese, aufgrund von systematischen Einflüssen, mit einer längeren Messdauer nicht markant verbessert. Die Richtigkeit des Ansatzes wird durch einen Vergleich der erhaltenen Orientierung mit einem Referenzwert gezeigt.

Contents

1 Introduction

This thesis presents the implementation of a method for GNSS antenna orientation based on modification of received signal strengths. The presented approach requires only one standard geodetic GNSS antenna that need not be moved. The approach is meant to be applicable in situations in which traditional GNSS-based orientation fails and additional sensors would be required. To show functionality and test performance of the approach, the evaluation model *NORDIS* (NORth Direction Indication System) is designed. It will be introduced in Chapter 5.3.

The antenna orientation is realised by using the information of the satellite constellation, in which GPS and GLONASS satellites are used. By knowing the antenna's position and the satellites' positions, the satellites can be used as directional references. To use this information, the directions of arrival (DOAs) of the measured satellites' signals must be known with regard to the antenna. Because DOA is not a measurable quantity, the signal strengths of the different received satellites serve as a measurand.

Specifically, partial attenuation of the antenna can influence the measured signal strength from the received satellites depending on the satellites' locations. An attenuation shield rotated around the antenna causes partial electromagnetic-wave attenuation. Thus, a geometric relation can be effected between the received signal strength and the position of the attenuation shield. By analysing the signal strength in respect to the position of the rotating shield, the DOAs of the satellites' signals can be determined.

1.1 Global Navigation Satellite Systems (GNSS)

Global navigation satellite systems (GNSS) permit positioning a receiver anywhere in the world. The only conditions are having the ability to receive satellite signals and a sufficient satellite constellation. Depending on the equipment and methodology used, position uncertainty ranges from several metres to less than a centimetre. Whereas the constellation was once a significant limitation, today, the GNSS constellation is being constantly improved. The GNSS constellation has been expanded by completing the constellation of the Russian GLONASS system during the last years and is being expanded further by introducing such new systems as the European Galileo and the Chinese COMPASS.

Besides these global systems, regional networks are established to improve the GNSS accuracy locally. Such networks can use geostationary satellites (WAAS[1], EGNOS[2], GAGAN[3], etc.) or terrestrial transmitters (Swipos[4], Sapos[5], etc.) to send correction messages to receivers. Extra satellites, orbiting specific areas of the world (e.g. China's Beidou 1[6] and Japan's QZSS[7]), provide better satellite availability for locations in which the constellation of GPS only is insufficient (e.g. deep urban canyons).

As a result of the global availability and sufficient accuracy of many applications, GNSS has revolutionised determining a position. Thanks to ongoing improvements, GNSS still continues to grow in importance.

1.2   Why Orientation?

Orientation, used as a geometric term, is required for navigation. In contrast to static GNSS measurements, navigation entails more than knowing where something or someone is. It means showing how to get to a certain place, for which an indication of direction is needed.

Navigation and, hence, orientation is needed in many applications: guidance for construction- and farming machines; pedestrian navigation; and course indication for airplanes, ships, and cars, to name a few examples. In vehicle navigation, the moving direction (heading) is required to provide further route information. For construction machinery, guiding the orientation of the machine is needed for instance, to automatically control an excavator. For pedestrian navigation, providing orientation information is advantageous: knowing the viewing direction of a pedestrian enables a navigation device to give proper directions and help the user find a route or point of interest. Beside navigation, initial orientation is needed for surveying tasks. Furthermore, a pre-oriented sensor can be helpful to register point clouds from laser scanners and from photogrammetric images.

For a long time, orientation was derived from sighting of landmarks or from astronomical observations. The introduction of the magnetic compass and later the gyro compass simplified the orientation determination and made it weather independent. However, the azimuth determined by a magnetic compass is affected by magnetic influences of the surrounding field. Furthermore, the magnetic field has local declinations that must be considered to achieve accurate measurements. Gyro compasses are expensive and must be gimbal mounted. The shortcomings of these compass systems show a need for further improvement of orientation determination. GNSS simplified the determination of coordinates, so why should GNSS not simplify and improve orientation finding as well?

---

[1] Wide Area Augmentation System (US-System)
[2] European Geostationary Navigation Overlay Service (European System)
[3] GPS Aided Geo Augmented Navigation (Indian System)
[4] Swiss Positioning Service
[5] Satellite Positioning Service (German System)
[6] experimental regional navigation system, consisting of four satellites (China)
[7] Quasi-Zenith Satellite System, consisting of three satellites (Japan)

1.3 Determination of Orientation by GNSS

With conventional use of a GNSS antenna, the orientation of the antenna is not known, because the direction of arrival (DOA) of the received satellite signals cannot be measured. Such measurement was not intended and is not needed for position determination.

1.3.1 GNSS Antenna Orientation in General

Nonetheless, defining the orientation by GNSS has been an object of research since the early days of GNSS, and some solutions have been well established. State of the art technologies (presented in Chapter 2) can be categorised in two main groups: systems using two or more antennas and systems with only one antenna. Furthermore several systems use GNSS in combination with additional sensors. Multi-antenna systems determine orientation by using several antennas firmly mounted in one mobile unit. In moving-antenna systems, the orientation can be calculated through the bearing (see Section 1.4) using the trajectory of previous positions. If an antenna is not moving or the dynamic of the movement is too complex and if more than one antenna cannot be mounted, additional sensors are used to indicate orientation. Such can be magnetic compasses, inertial measurement units, or gyrocompass (see Sections 2.2.8. to 2.2.8.4).

1.3.2 GNSS Antenna Orientation with NORDIS

Research on GNSS Antenna Orientation started in our group in 2006 with the idea from Kahlmann and Ingensand to use modulation of signal strength for detecting the DOA of satellite signals. The measurement principle uses an attenuation shield as shown in Figure 1.1, which is the underlying idea of this thesis. The intention was to combine a 3D measurement camera or total station with an orientation-finding GNSS antenna, with the aim of georeferencing the measurements from the 3D camera as it was first presented in (Kahlmann et al., 2006). For modulation of the signal strength, three concepts have been presented, of which the first is implemented in NORDIS.

The first idea uses a rotating attenuation shield. The material used for the shield needs to have the properties to attenuate the GNSS signals. The second idea requires a cover for the antenna that comprises different shielded angular stripes. According to the stripes have to be placed in a radial way on the antenna at angles between 10 and 50 degrees with different signal reductions factors. The third idea is based on polarising effects that are different in one or more angular planes to allow for modulating the received satellite information in a different way, depending on the point of entry into the cover (Kahlmann and Ingensand, 2007).

All three ideas were submitted for patenting in 2007. However, the patent application was not accepted because of an already-existing patent presented by Wiklund (1992), which was found during the course of an international search. Wiklund's concept is also based on the idea of generating directional sensitivity of the antenna by introducing an attenuation shield he refers to as a *wing*. The wing is constructed as a signal attenuating device that is rotated around the edge of the antenna as shown in Figure 1.2. Either the wing itself is rotated, or the rod with the antenna and the wing are rotated together. However, beside Wiklund's patent specification, neither documentation which indicates an implementation of the idea nor further information regarding attenuating material or proposed hardware could be found.

1	measurement camera
4	satellite positioning system
5	shield
6	encoder
7	motor
8	protective cover
10	inclinometer, inertial navigation system/ inertial measurement unit
11	central axis
20	tripod
A	presented in the detailed view
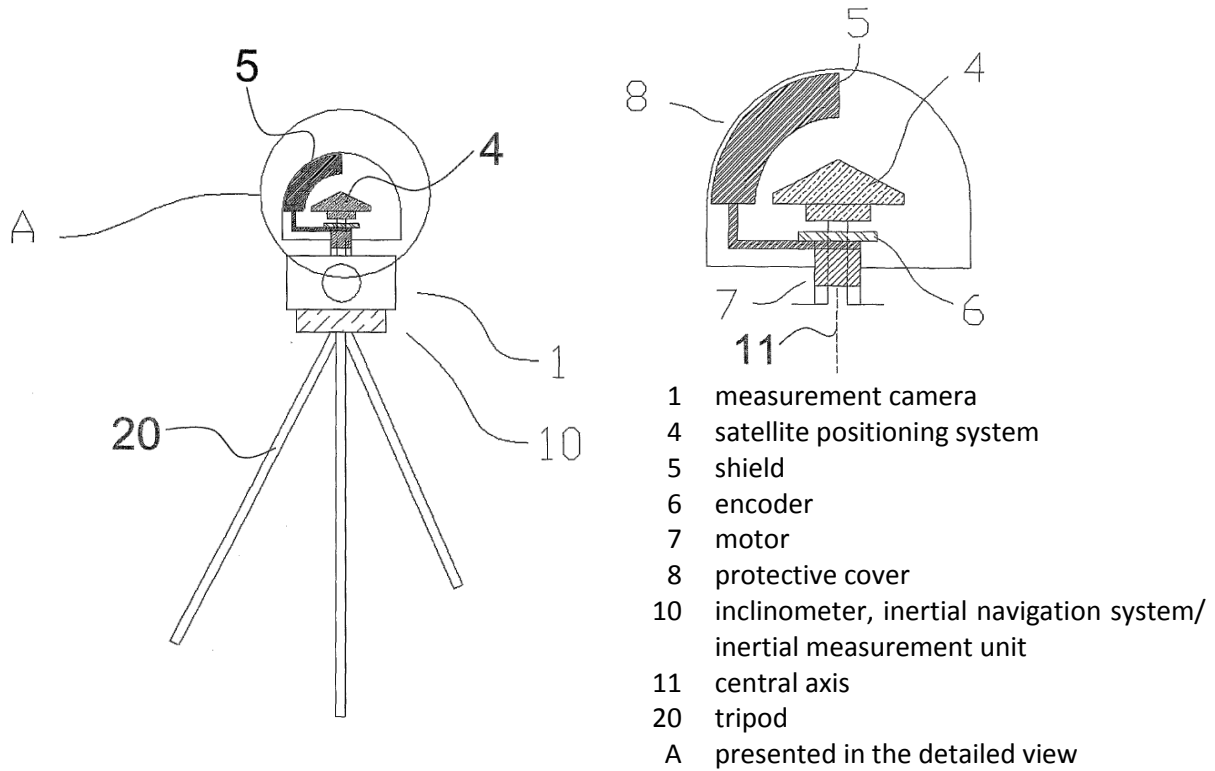
Figure 1.1 Measurement principle with a rotating attenuation shield (5) as it was presented in the patent application (Kahlmann and Ingensand, 2007).

1	GPS-antenna
2	Earth plane
3	central antenna element
4	rod
5	wing (attenuation)
6	motor + rotational angle sensor
7	stand (tripod)
8	sighting device
9	housing
10	horizontal angle indicator
11	computing unit
12	vertical angle indicator

Figure 1.2 Measurement principle with an attenuating wing as presented in .

Figure 1.3 Received signal strength as function of the angular rotation of the GPS-antenna (Wiklund, 1992).
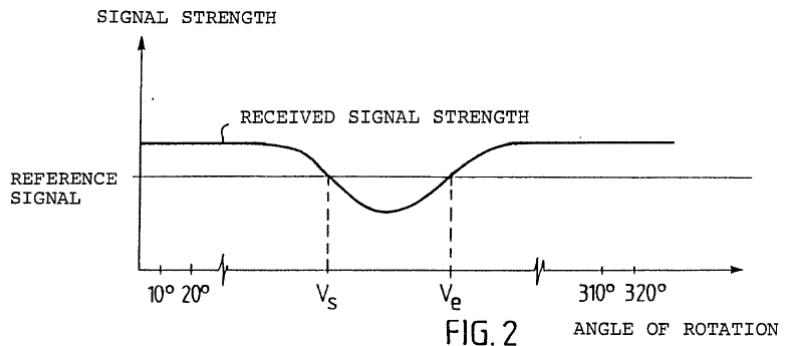
Figure 1.3 illustrates how the strength of an exemplary received satellite signal varies with the angle of rotation of the wing. According to the description, the wing can be constructed as a shield to attenuate the signals, as a reflector to amplify the signal, or as a combination of both. Theoretical considerations of how the different wing constructions influence the signal strength are shown in Figure 1.4.
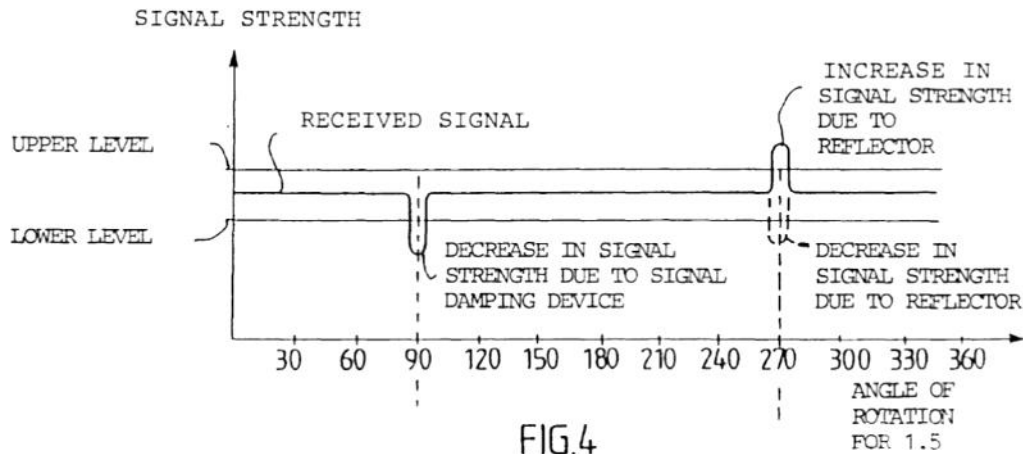
Figure 1.4 Influence of the wing as attenuator and as reflector (Wiklund, 1992).

1.3.3 Initial Implementations

The theoretical idea presented in Kahlmann and Ingensand (2007) was implemented in a first feasibility study in Grimm (2007a) and was further de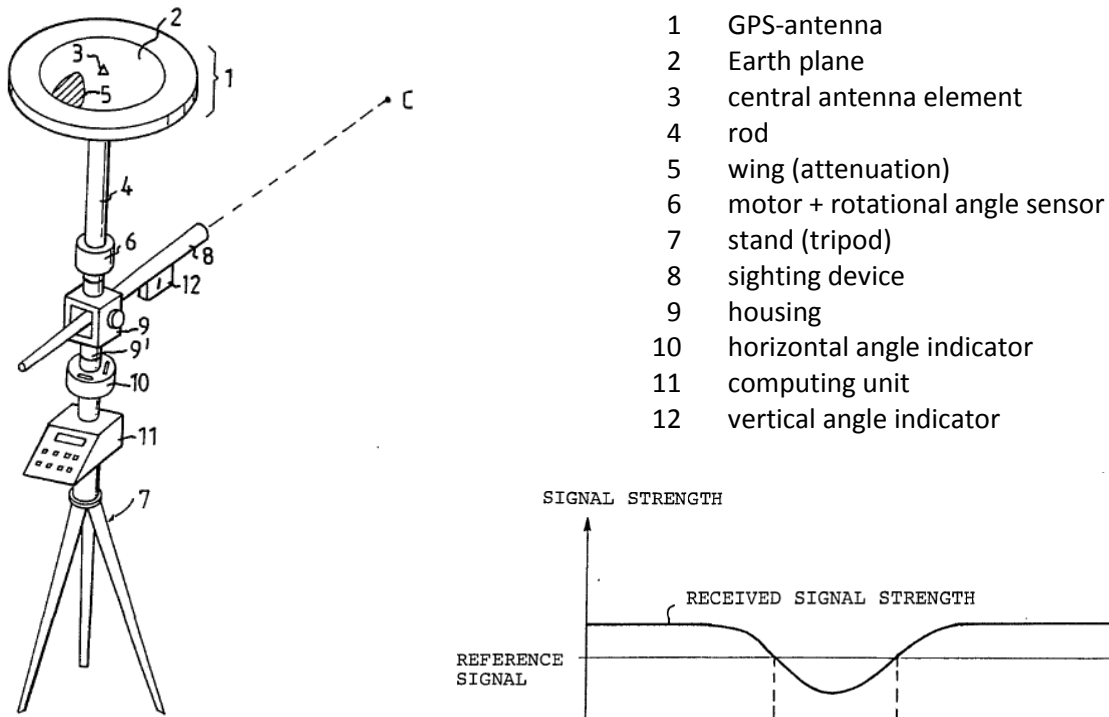veloped in Grimm (2007b). The first study was conducted to find suitable material and ideal shape for the attenuation shield. A motorised measurement setup using a u-blox L1 antenna (Figure 1.5) appears in Grimm (2007b). Results from measurements with this system are shown in Figure 1.6. The results are published in Grimm (2008a) and Grimm (2008b).
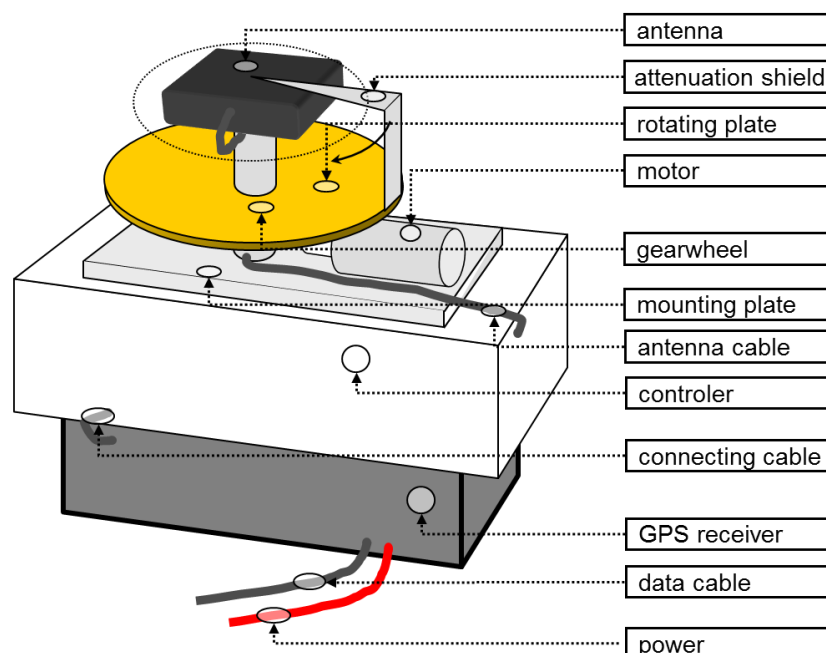
Figure 1.5 Measurement setup with L1 u-blox antenna and motorised attenuation shield (Grimm, 2007b).
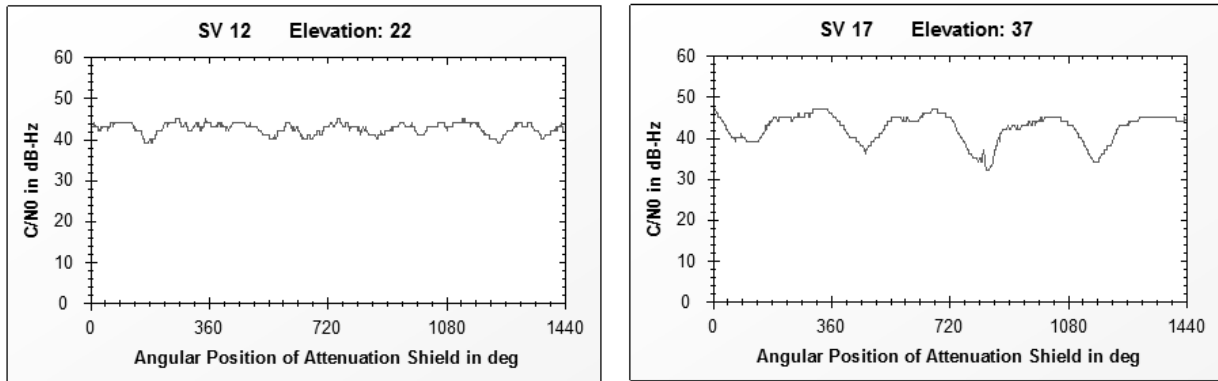
Figure 1.6 C/N$_0$ variation for 2 exemplary satellites during 4 revolutions of the attenuation shield.

The two graphs in Figure 1.6 show the C/N$_0$ during four revolutions of the attenuation shield shown in Figure 1.5. The graph on the left shows the C/N$_0$ of GPS satellite number 12 (SV12) and the graph on the right shows the C/N$_0$ of GPS satellite number 17 (SV17). Both satellites were observed at the same instant. It can be seen that the signal strength of SV 12 is not attenuated significantly while the signal strength of SV 17 shows the expected effect of the four revolutions of the attenuation shield. However, the attenuation effect on SV 17 varies across revolutions, and the shape of the graph is not identical for all revolutions. Accordingly, the measurement setup presented in Figure 1.5 shows that an attenuation shield could affect the C/N$_0$. Hence, the quality and repeatability of the measurements were not satisfactory. Therefore, the concept was modified to enable the use of a geodetic antenna, which has more stable antenna characteristics than the low-cost u-blox antenna has. For a first study, a motorised total station was used to rotate the geodetic antenna together with the attenuation shield as shown in Figure 1.7. The attenuation shield is fixed with an elastic band to the antenna.
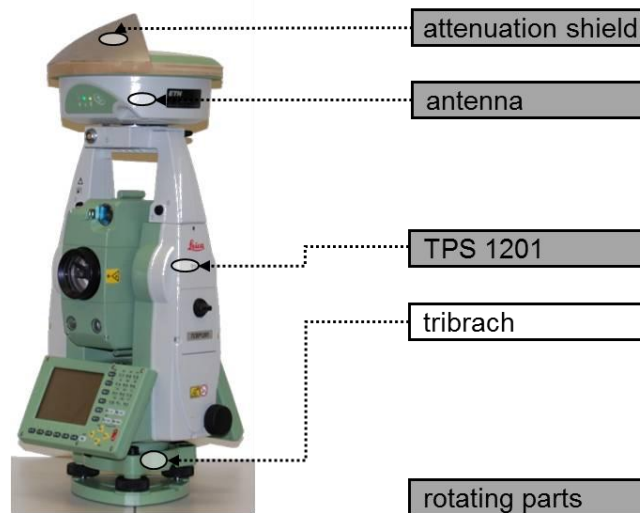
Figure 1.7 Geodetic antenna Leica ATX 1230 GG with attenuation shield on station Leica TPS 1201 (Smart Station). (Picture: D. Grimm)

Results from measurement with the ATX 1230 GG antenna and improved analysis concept are published in Grimm (2009). Figure 1.8 shows two graphs with the C/N$_0$ variation during 4 revolutions of the total station with the antenna on top. Compared with the measurements shown in Figure 1.6, the results from the geodetic antenna show a better repeatability of attenuation for each revolution.
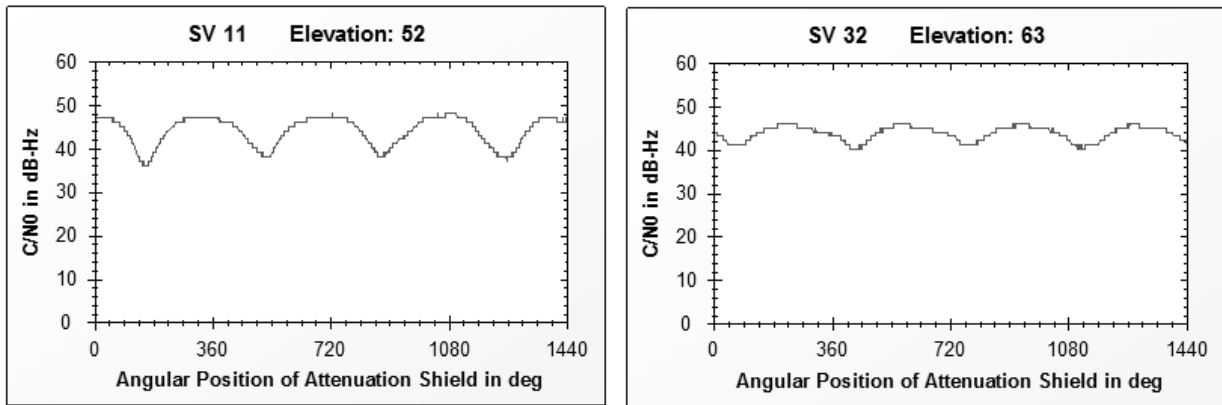
Figure 1.8 C/N$_0$ variation for 2 exemplary satellites during 4 revolutions of the total station with mounted antenna and attenuation shield.

The combination of a total station and the GNSS antenna would meet all requirements for testing the antenna orientation concept and can be useful in combination to determine the position and the initial orientation of the total station as it is presented in Section 8.2.1. Nevertheless there are several issues. First, it is not possible to rotate the attenuation separately; the antenna has to be turned as well. This approach would work for orientation determination, but the phase wind-up effect (see Section 2.2.3) affects the position accuracy. Furthermore, synchronising the measurement of the angular position with the GPS time when the total station is permanently in motion is problematic. Via the GeoCOM[8] interface, it is possible to control the motion of the total station with a desired velocity from a connected computer. In addition, it is possible to query the angular position. Because doing so must be done from an attached computer, the interface delay dilutes the accuracy of the angular position. However, these synchronising issues could be solved with full access to the on-board software of the total station and the GNSS receiver.

1.3.4 Implementation of NORDIS

The mentioned issues which had arisen during the pre-works led to the decision to develop the new measuring system NORDIS, which is described in Section 5.3.

1.4 Introducing the Term *Orientation*

In this thesis, the term *orientation* is used to describe the alignment of an object within a reference plane. The orientation is given at a certain position and points to a target point afield. Orientation indicates a reference direction, which in many cases is north (see Section 1.5). Different terms and definitions are commonly used to indicate direction information. Five terms significant to this thesis are the following:

- pointing direction (geodesy, geometry)
- azimuth (geodesy, astronomy)
- bearing/bearing angle (aviation, nautics, navigation, objects in motion)
- heading (aviation, nautics, navigation)
- attitude (aviation, astronautics)

In connection with a theodolite (Figure 1.9), the pointing direction indicates the direction of the line of sight from the theodolite (T) to the target point (P). The line of sight is realised through

---

[8] Interface for client applications for Leica instruments

the telescope. When the pointing direction refers to (true) north, the angle from north to the point is called the *azimuth*. In terms of flight dynamics, orientation is the yaw angle of the attitude, which corresponds to the heading (Figure 1.10).
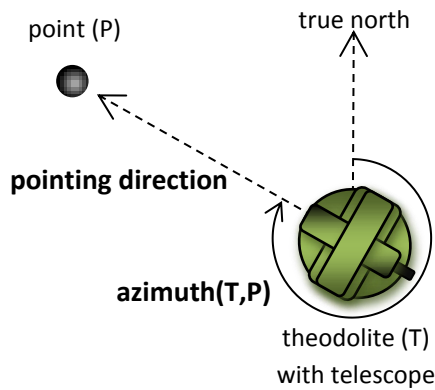
Figure 1.9 Pointing direction and azimuth in theodolite measurements.
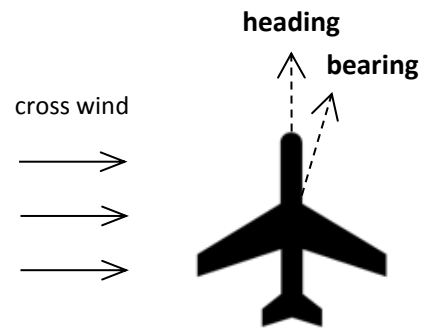
Figure 1.10 Heading and bearing of a flying airplane with cross wind.

1.4.1   Pointing Direction

The *pointing direction* indicates the direction a device (e.g., a telescope) is pointing to.

1.4.2   Azimuth

The *azimuth* describes the horizontal angle from (true) north to the line of sight between two points. This angle is measured clockwise from (true) north to the target point. Particularly in geodesy and astronomy, azimuth is a common term to indicate a direction.

1.4.3   Bearing/Bearing Angle

The term *bearing* is largely used for objects in motion (e.g., in nautics and aviation). In navigation, bearing is understood as a straight line from the object to the point the object is navigating toward. Beside this definition, the terms (often in combination with true-bearing, magnetic-bearing or compass-bearing) are used synonymous with the term azimuth. The orientation determined by GNSS from a trajectory indicates the bearing.

1.4.4   Heading

Heading is also frequently used in nautics or aviation. It describes the direction an object (e.g., an airplane or a ship) is pointing. In the case of a cross wind, the heading does not correspond to the bearing. A multi-antenna system on an airplane, for instance, indicates the heading (see Figure 1.10).

1.4.5   Attitude

The term *attitude* is different from the others, because it is three-dimensional information including the two-dimensional information of orientation. Attitude describes how a rigid body is placed in the space it is in. Attitude refers to the reference frame of the body (dotted line in Figure 1.11) and is indicated in relation to a defined coordinate system (solid line in Figure 1.11).
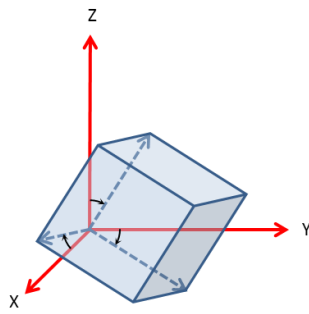
Figure 1.11 Attitude of a rigid body.
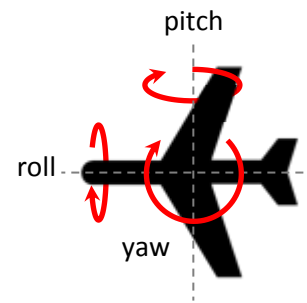
Figure 1.12 Attitude determination in flight dynamics.

In flight dynamics, the attitude of an airplane is indicated by three angles of rotation around the mass centre of the place: pitch, roll, and yaw (Figure 1.12). The yaw corresponds to the heading of the aircraft.

1.5   North Direction and Terrestrial Reference System

In many cases, the north direction serves as reference direction. However, the term *north* is ambiguous and must be specified. Astronomic north is defined with respect to the astronomic meridian, which varies under the influence of the local gravity. Grid north is defined with respect to the central meridian of a mapping projection. Magnetic north is the direction of the magnetic field of the earth, varying because of local anomalies. True north corresponds to geodetic north and is defined with respect to the ellipsoidal meridian. Geodetic north differs slightly (by a few arc seconds) from astronomic north because the local gravity at the pole does not correspond to the exact rotational axis of the Earth, resulting in a deflection of the vertical.

The ellipsoidal meridian is pointing along the Earth's surface toward the geographic North Pole. The geographic North Pole is defined by the Earth's rotation axis. Because the Earth rotation axis is subject to influences of nutation and wobbling, a conventional mean-rotation axis is introduced. The reference pole is defined within the Earth orientation parameters (EOP) provided by the International Earth Rotation Service (IERS). The IERS reference pole coincides with a standard measurement uncertainty of 0.1'', with the mean position of the rotation pole determined as Conventional International Origin (CIO) from 1900 to 1905 (Guinot, 2003).

GPS is embedded in WGS 84, a conventional terrestrial reference system (CTRS), where the rotation axis of the ellipsoid indicates north. WGS 84 is a right-handed, Earth-fixed orthogonal coordinate system, as shown in Figure 1.13.
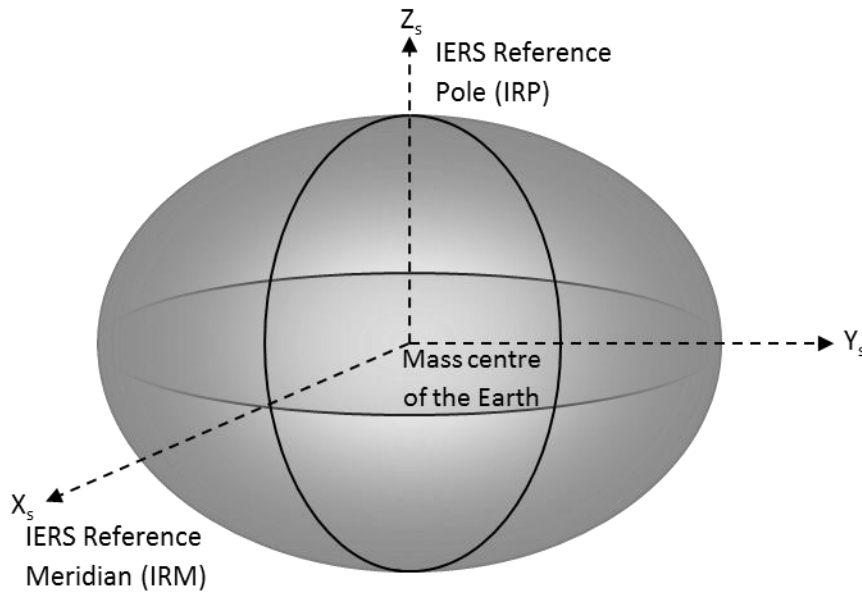
Figure 1.13 The WGS 84 coordinate system definition.

The origin of the ellipsoid is the idealised Earth mass centre. The orientation of the X-axis and the Z-axis was initially given in 1984 by the Bureau International de l'Heure (BIH), the predecessor of the IERS. The definition of the axis is defined by the National Imagery and Mapping Agency, U.S. Department of Defense (2000) as follows:

Z_s-Axis: The direction of the IERS Reference Pole (IRP). This direction corresponds to the direction of the BIH Conventional Terrestrial Pole (CTP) (epoch 1984.0) with a standard measurement uncertainty of 0.005''.

X_s-Axis: Intersection of the IERS Reference Meridian (IRM) and the plane passing through the origin and normal to the Z-axis. The IRM is coincident with the BIH Zero Meridian (epoch 1984.0) with a standard measurement uncertainty of 0.005''.

Y_s-Axis: Completes a right-handed, Earth-Centered Earth-Fixed (ECEF) orthogonal coordinate system.

To indicate coordinates determined by GNSS on the Earth's surface with an absolute sub-meter uncertainty, the coordinates must be brought into relation with the international terrestrial reference frame (ITRF) or a local terrestrial frame by using reference points. Coordinates given in the Swiss grid are referenced using the Swiss reference frame (CHTRF). Further information on the geodetic reference systems in connection with GNSS can be found in Leick (2003) in the first chapter.

1.6 Outline of this Thesis

The motivation for antenna orientation is given in this first chapter. In Chapter 2, state of the art methods and systems are discussed. Chapter 3 has an overview of antenna theory, including terminology, antenna types, and GNSS signals used in this work. Chapter 4 addresses the fundamentals for calculating the position of a satellite in a topocentric coordinate system, with the position being determined by azimuth and elevation values. Chapter 5 introduces the single GNSS antenna orientation approach NORDIS, the primary work of this thesis. In the first section of Chapter 5, performance requirements are listed, based on several applications found in literature. After an introduction of the developed measuring model, measuring principle, and preliminary hardware model, the data processing is presented in Chapter 6, with discussion of the results in Chapter 7. A summary and outlook are given in Chapter 8. Each chapter concludes with a short summary. The appendix contains further information on topics mentioned in the chapters and details of the software implementation.

2 State of the Art in GNSS Orientation Determination

Since early implementation of GPS, numerous approaches and systems for defining orientation by GNSS have been developed. Some systems are established and available on the market while others are still prototypes. Because the existing systems differ considerably in terms of functionality and performance, it is helpful to categorise them. The categorising property used in this thesis is the number of implemented antennas in a system. A distinction can be drawn between methods using only one antenna, called single-antenna systems, and methods using more than one antenna, called multi-antenna systems (Figure 2.1). The number of antennas is the driver for the measurement principle and influences the size and cost of a system.
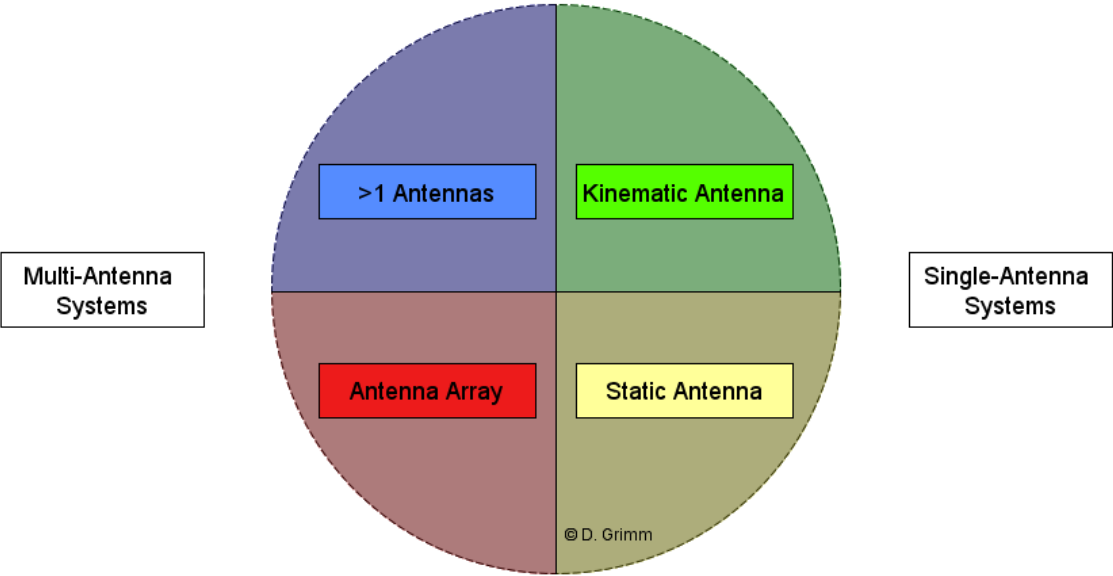
Figure 2.1 Categorisation of GNSS antenna orientation systems into four groups according to the number and use of implemented antennas.

To determine orientation, single-antenna systems can be used either in static applications or in kinematic applications, in which the antenna is placed on a moving platform (e.g., car, aircraft, ship, etc.). In multi-antenna systems, a distinction can be drawn between two or more-antenna systems and antenna arrays. Antenna arrays are normally manufactured in one piece and cannot be subdivided into single antennas. In contrast, multi-antenna systems are composed of several antennas that could possibly be removed and used independently. However, this distinction is a simplified proposition and is not always applicable. Dependent on the system type, different effects or concepts are used to determine the orientation. The orientation can be calculated using a single method or a combination of methods.

2.1 System Types

In Figure 2.2, the four system types are arranged in the inner circle, analogous to Figure 2.1. The effects or concepts used are arranged in the middle circle. Some effects can be used only in combination with specific system types while others can be used more freely. Typical combinations of effects/concepts and system types are drawn with solid lines; possible combinations that are not as common are drawn with dashed lines. The methods explain how the orientation is calculated and are arranged in the outer circle, connected with the corresponding effects/concepts by a dotted line. All system types and the corresponding effects/concepts and methods are explained in this chapter.
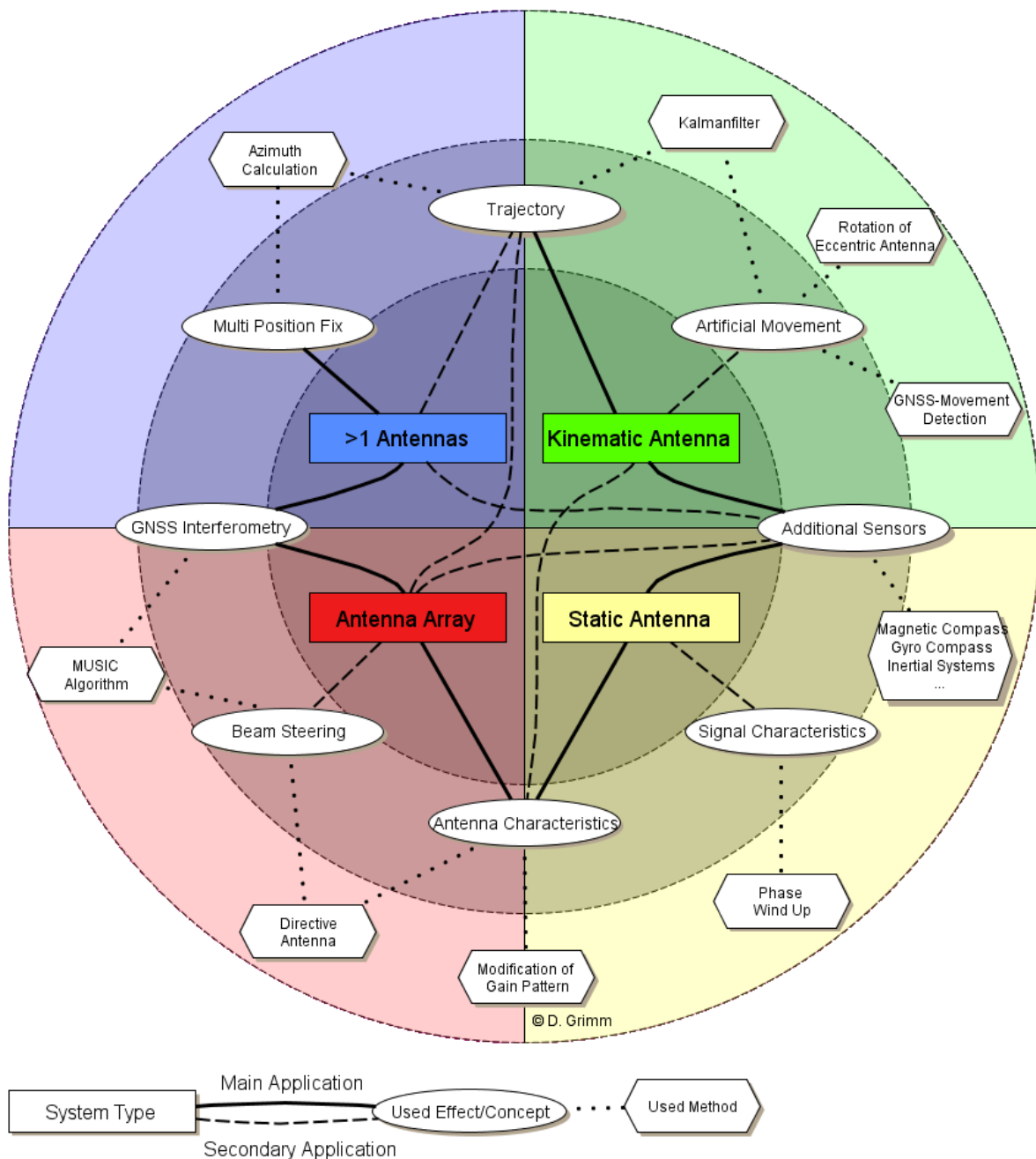
Figure 2.2 Graphical overview of the four GNSS antenna orientation systems (inner circle) with the underlying effects/concepts (middle circle) and correspondent methods (outer circle).

14

Single-antenna systems are often used when funds or available space is limited. Because most single-antenna systems use the trajectory for orientation determination, they work on moving objects only. Single-antenna systems are widely used in smart phones, with additional sensors providing coarse orientation information. Multi-antenna systems are typically used when more accurate results are required. Apart from different hardware components, there are two concepts concerning how the antennas are used. One concept uses the position solution of both antennas to calculate the azimuth of the baseline. The second concept uses the difference between the carrier phases of the two antennas, referred to as *GNSS interferometry*. Besides systems using several antennas in combination, antenna arrays have become common.

2.2 Description of the Effects and Concepts Used

The different system types use different effects or concepts for orientation determination. Depending on the requirements and possibilities of the system type, combinations of several effects of concepts can be used or implemented. Starting with the trajectory, the different effects and concepts are presented in this section, following Figure 2.2 clockwise. Because the use of additional sensors is not directly related to determining a GNSS-based orientation, such approaches are described at the end of Section 2.2.

2.2.1 Orientation from Trajectory (Kinematic)

An established method for navigation applications is calculating the orientation from the trajectories of previous positions. This method is frequently used for car navigation systems and is inexpensive because a single antenna is sufficient. The accuracy of both position and orientation can be improved by considering the constraints of vehicle dynamics. A prediction filter like Kalman[9]-filtering, which relies on previous positions, can lead to satisfying results when the dynamic of the movement is sufficiently predictable. The better the dynamic of the movement can be determined analytically, the better the orientation can be estimated. El-Mowafy and Mohamed (2005) showed that the use of an adaptive Kalman filter may improve the results. For vehicles moving along pre-determined routes, such as cars on streets, map-matching algorithms can also improve the solution.

This method works for moving objects only. When the object rotates around the antenna axis, the orientation is lost immediately. Consequently, this method works well for objects (e.g. vehicles) whose dynamics are subject to constrains.

2.2.2 Artificial Movement

For applications in which the antenna itself is not moving (e.g., antenna on laserscanner or tachymeter), a solution is to move the antenna artificially, thereby generating a trajectory of the GNSS positions. In connection with laserscanner or tachymeter, a GNSS antenna can be mounted eccentrically on top of the device. By rotating the device, a circular trajectory can be analysed as presented by Paffenholz et al. (2010).

A similar approach, using an arbitrary instead of a circular movement, is presented in Broumandan et al. (2007): "Instead of using multiple antennas with a multi-channel receiver, [. . .] an antenna array can be synthesised by moving a single antenna in an arbitrary direction" (p. 729). The antenna is mounted on a rotating arm to take spatial measurements. An inertial

---

[9] The explanation of the filter presented by Kálmán can be read in Kalman (1960).

measurement unit is used to estimate the trajectory of the moving antenna. Real antenna arrays collect data simultaneously; however, the synthetic antenna array takes time to move the antenna, possibly causing a problem for kinematic applications.

A method to detect small and rapid movements, G-MoDe©, is presented in Guillaume et al. (2012). The method can detect rapid movements above 5 mm horizontally and 10 mm in height significantly (95%) in real-time by using a single L1-GPS carrier phase receiver. This relative change of coordinates can be used to calculate the direction of the movement. Although not yet tested, this method could also be used to calculate the orientation of the antenna. To apply this calculation for static applications, small, highly frequent artificial movements of the antenna are necessary.

2.2.3   Signal Characteristics (Phase Wind-Up Effect)

Carrier phase wind-up is an effect that arises from relative rotation between a transmitting and receiving antenna using circular polarised electromagnetic waves (see Section 3.6.2). The rotation of one antenna by 360 deg changes the phase measurement by one wavelength. Because many satellites turn on their principal axis for stabilisation, phase wind-up has an effect on the signals sent or received by these satellites. The effects of satellite spin on ground-received signals have already been discussed in Bolljahn (1958) and Marini (1971). GNSS satellites do not spin; however, with GNSS, the effect occurs on the receiver side when the receiving antenna is turned on the boresight axis. According to Kim et al. (2006),

> the result is [. . .] a change in the measured phase. As one or both of the antennas rotate, the phase change accumulates and is referred to as *phase wind-up*. [. . .] In addition, the rotation of the receiving antenna causes an apparent change in the GPS carrier frequency. It is distinguished from the normal Doppler shift in that phase wind-up is carrier-frequency independent and does not affect ranging modulation group delay. (p. 58)

Because the phase wind-up effect is independent of the satellite elevation for pure rotation around the antenna boresight axis, it is usually absorbed by the clock estimation in navigation algorithms (García-Fernández et al., 2008). The effect can further be used to detect relative changes of the orientation of a GNSS antenna (Häberling and Geiger, 2010).

2.2.4   Antenna Characteristics

In literature several concepts for GNSS antenna orientation are referred to as *GNSS-attitude determination*. Most of these approaches are single-antenna systems that use antenna characteristics. However, many of them, for instance Axelrad and Behre (1999), do not determine the full three-dimensional attitude, but rather the direction of the antenna boresight axis (see Section 3.1.2), which is a combination of the roll and pitch angles as shown in Figure 1.12. An overview of GPS used for spacecraft attitude determination from 1992 until 1997 is given in Chu and Woerkom (1997).

2.2.4.1   Attitude Determination from Single-Antenna Carrier-Phase Measurements

A single-antenna method of partial attitude (orientation) determination is presented for the case of a simple dipole antenna in Krall and Bahder (2001) and for full attitude determination for an arbitrary antenna in Bahder (2002). The method is based on an electromagnetic behaviour regarding the satellite signal. According to Krall and Bahder, "The phase of the voltage $V(t)$ induced in a receiving antenna by the signal of a GPS satellite depends on the orientation of the

antenna with respect to the electric and magnetic field vectors **E** and **B** that describe the EM field" (p. 6513). To exploit the effect, the transmitting and receiving antennas should be fully characterised. Because the orientation of the receiving antenna is known only relative to the transmitting antenna, the attitude of the satellite antennas must be known. Therefore, the control segment of the system must monitor and control satellite attitude. Furthermore, this information must be made available in the navigation message. To determine all three angles of attitude, carrier-phase measurements to seven satellites must be taken. The presented approach looks very promising, but does not work until a future GNSS includes fully characterised antennas with parameters available along with satellite attitude information at the measuring time.

2.2.4.2   Approaches Using Signal Strength

In addition to code and phase measurements, GNSS receivers provide a value for the received signal strength, indicated as carrier-to-noise density C/N_0 (see Section 3.6.7) for each satellite in view. The main application for signal strengths is signal integrity checking and quality control. Satellites with low signal strength are typically not included in the processing. In addition, signal strengths are used for multipath estimation and could be used for orientation or attitude estimation.

The approach using signal strength for attitude determination is based on most GNSS antennas having the highest gain along the boresight vector (see Sections 3.3.2 and 3.6.5). The gain decreases with increasing zenith angle (θ) from the antenna boresight (see Section 3.1.2). Consequently, the C/N_0 for a particular satellite strongly depends on the angle between the antenna boresight vector and the line-of-sight vector from the antenna to the GNSS satellite. The off-boresight angle is calculated by comparing the actual observation with a predetermined calibration data set. An early description of this approach can be found in Hashida and Unwin (1993). Further variations of this approach are presented by Serrano et al. (1995), Duncan and Dunn (1998), and Axelrad and Behre (1999). The uncertainty for the roll and pitch angle is indicated in Axelrad and Behre as being 5 deg to 10 deg standard measurement uncertainty. However, the attitude uncertainty can be improved by modelling the GNSS transmission path as described in Wang et al. (2005).

For omnidirectional antennas, the azimuthal variations are small. Consequently, rotations around the antenna boresight axis are not observable at all or only poorly observable as long as the antenna has a homogeneous gain pattern in the azimuthal plane.

Nevertheless, Buist et al. (2000) present a possibility method to determine the yaw angle of the attitude of the same satellite (PoSAT-I) as described in Hashida and Unwin (1993):

> On PoSAT-I, the GPS antenna is placed on the same facet of the satellite as the gravity gradient boom [. . .]. The satellite is rotating round this boom axis (this is yaw rotation) and during every rotation the boom will block the antenna briefly, hence the yaw rotation may be determined from the frequent drop in the CNR. (p. 494; author's note: CNR corresponds in this case to C/N_0)

Accordingly, the antenna gain is disturbed by the boom, leading to larger azimuthal variations of the C/N_0, depending on the rotation angle of the boom. The NORDIS approach introduced in Chapter 5 is also based on signal-strength measurements. NORDIS uses a specific modification of the received signal strengths.

2.2.5 Beam Steering with Antenna Arrays

Antenna arrays include more than two antennas, normally manufactured in one piece. Depending on the placement of the antennas, different attitude angles can be determined. A linear placement of the antennas as shown in Figure 2.3 is used to determine the direction of arrival (DOA) within the plane, orthogonal to the antenna surface. A spatial distribution of the elements as shown in Figure 2.4 serves to determine all attitude angles.
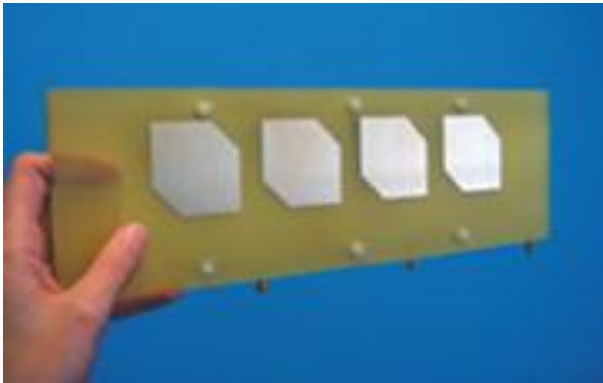
Figure 2.3 Array of four patch antennas (Fraunhofer Institut, 2011).

Figure 2.4 Sixteen element antenna array (Brown and Gerein, 2001).

In addition, antenna arrays can generate an adaptive antenna, which is able to steer the antenna gain pattern (see Section 3.3.2). By means of beam-forming (also referred to as *beam-steering*), the antenna array can focus in an arbitrary direction. The gain in this direction is higher while signals from other directions are nearly suppressed. Beam-forming is attained by reading out the different antenna elements with a specific delay. Figure 2.5 and Figure 2.6 show the gain patterns of an adaptive antenna for two different satellites. The positions of the satellites are indicated in Table 2.1.
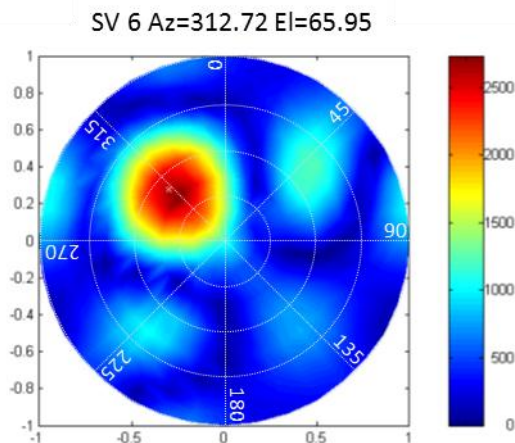
Figure 2.5 Gain pattern of a 16-element array adjusted for SV 6 (Brown et al., 2001). Coordinate grid added by the author.
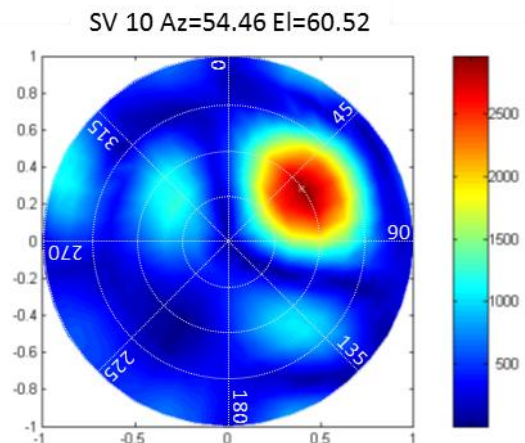
Figure 2.6 Gain pattern of a 16-element array adjusted for SV 10 (Brown et al., 2001). Coordinate grid added by the author.

Table 2.1 Satellite Positions at Measuring Time.

Satellite Identification	Azimuth in deg	Elevation in deg
SV 6	312.72	65.95
SV 10	54.46	60.52

Adaptive antennas are useful to suppress jammer and interference signals. Numerous papers regarding beam-forming with antenna arrays for multipath and jammer detection are published

on the NAVSYS[10] webpage. Direction of arrival calculation in connection with an antenna array is often performed using the MUSIC algorithm (see Section 2.2.6.1).

2.2.6 Carrier Phase Differences of Two or More Antennas (GNSS Interferometry)

The satellite carrier phase from a single satellite, measured by two or more antennas at the same instant, has a phase shift when the distances from the satellite to the antennas are not identical due to different positions of the antennas. This interferometer principle can be used to determine the orientation of the antennas in the case of two antennas and full attitude for at least three antennas. As a precondition, the antennas must be mounted on a common platform, and the integer cycle ambiguities must be solved in the data. This concept was presented by Spinney (1976) and later by Brown and Ward (1990). Because ambiguity resolving is not trivial, several proposals were made to handle this issue.

An approach that uses the change in phase measurements rather than phase measurements themselves is presented by Evans (1986). This approach works with one single, slowly moving antenna, removing the requirement that cycle ambiguities be solved. A similar possible solution for solving the ambiguities is moving the antennas around the common centre of rotation (TU et al., 1997). As soon as the ambiguities are resolved, rotating the antennas is no longer necessary.

For fast moving kinematic applications, such as attitude information for aircrafts, usually only measurements during the moving phase of the vehicle are available for ambiguity resolution. An investigation into ambiguity resolution on the fly is published in Cocard (1995). However, losing the ambiguity resolution in the air can cause difficulties. Therefore, Barrows et al. (1996) present a "more closely-spaced antenna configuration, to provide a more robust design for acceptable aircraft use" (p. 423). In this configuration, the distance between the antennas is smaller than the wavelength of the carrier, which is 0.19m for L1, with the result that there are no integer ambiguities. However, reducing the distance between the antennas decreases the orientation accuracy as well. A dependency between the orientation uncertainty and the length of the baseline is indicated in Schwieger and Hemmert (2008) for a 4-antenna system: The standard measurement uncertainty of the heading u_{A_h} is calculated in Equation (2.1), where d is the length of the baseline in m:

$$u_{A_h} = \frac{0.2\,\text{deg}}{d} \qquad (2.1)$$

Furthermore, a combination of a short- and long-baseline concept is presented in Eling et al. (2010). Three antennas are arranged in such a way that one short ($d < 19$ cm) and one long baseline are formed. The short baseline is used to compute an approximate solution, which should support resolution of the ambiguities for the second baseline. The longer baseline is used to deliver an accurate baseline-orientation. The uncertainty of orientation determined by the short baseline only is indicated with a standard measurement uncertainty of 0.8 deg by using the known baseline length as a constraint and with 0.95 deg for an unknown baseline length. The orientation uncertainty for the long baseline is indicated with a standard measurement uncertainty of about 0.1 deg without indicating the baseline length, however.

---

[10] **Nav**igation **Sys**tem Innovators

A different possibility is to enhance the ambiguity resolving procedure. Resolving the ambiguities traditionally requires searching all possible ambiguity combinations, leading to intense calculation effort and time consumption. However, optimised ambiguity resolution processes are presented in Brown (1992), Hill and Euler (1996), and Teunissen et al. (2011). Through introduction of boundary conditions like the known distances and angles between the antennas or the maximal slope of the baseline, the orientation of the antennas is not completely unknown. The effect of the optimised ambiguity resolution is described in Hill and Euler (1996): "In the example given, a total of 4913 potential candidates were reduced to just 66 candidates after applying the baseline distance and tilt restrictions" (p. 268). The authors applied for patent for this method in 2006 (Euler and Hill, 2006).

2.2.6.1 MUltiple SIgnal Classification (MUSIC) algorithm

The MUSIC algorithm evaluates measurements from multiple wave fronts arriving at the different elements of an antenna array. The signal and noise subspace eigenvectors are obtained from performing an eigenvalue-decomposition of a covariance matrix. For this purpose, the algorithm uses the orthogonal property of the noise subspace eigenvectors and the calculated signal vectors to provide asymptotically unbiased estimates of the following:

1. number of signals
2. directions of arrival (DOA)
3. strengths and cross-correlations among the directional waveforms
4. polarizations
5. strength of noise / interference

The algorithm was presented by Ralph O. Schmidt in 1979. The mathematical description of the algorithm is presented in Schmidt (1986). However, MUSIC needs "many array input data snapshots [. . .] to obtain a good performance [. . .] plus the incidence signals must be uncorrelated" (Kim et al., 2005, p. 1346). Consequently, a fast DOA estimation is presented in (Kim et al., 2005), one that can also estimate the incidence angle when the signals are correlated. An improved approach using the method of Kim et al. is presented in Wen et al. (2006).

2.2.7 Using the Position Fix of Two or More Antennas

The approach is based on the principle of measuring coordinates of two points and calculating the azimuth of the baseline. When the points are measured simultaneously, the relative coordinate uncertainty is relevant for the accuracy of the calculated azimuth. A simultaneous reading is needed when the antennas are mounted on a moving platform. In static cases, the two points can be measured one after another with the same antenna and receiver, in this case, the absolute coordinate uncertainty is relevant for the azimuth accuracy.

When the coordinates of point A (x_{tA}, x_{tB}) and point B (y_{tA}, y_{tB}) are given as local grid coordinates in a conformal coordinate projection, (e.g. Swissgrid), the azimuth of the baseline between the two antennas at station A and station B is calculated by using Equation (2.2), respecting the trigonometric quadrant rule[11].

$$Az(A, B) = \arctan \left[\frac{(y_{tB} - y_{tA})}{(x_{tB} - x_{tA})} \right]$$

(2.2)

---

[11] For $(x_{tB} - x_{tA}) < 0$, add 180 deg; for $(x_{tB} - x_{tA}) > 0$, add 360 deg if result <0.

$$d^2 = (y_{tB} - y_{tA})^2 + (x_{tB} - x_{tA})^2 \qquad (2.3)$$

In Equation (2.3) d is the distance between the two antennas. With ellipsoidal coordinates, the azimuth can be calculated by numerical integration of the differential equation of the geodetic line (shortest connection between two points on an ellipsoid's surface), as shown in Torge (2003).

The uncertainty of the calculated azimuth depends on the satellite geometry, performance of receiver, baseline configuration and attitude, and in particular, the distance d between the antennas. The influence of the position uncertainty and the baseline length is shown in Equation (2.4), according to Park et al. (1997).

$$u_{A_{Azi}} = \sqrt{\frac{2\left((\sigma_E \cos Azi_0) + (\sigma_N \sin Azi_0)\right)}{(d \cdot \cos Ele_0)}} \qquad (2.4)$$

$u_{A_{Azi}}$:   standard measurement uncertainty of the orientation

σ_E, σ_N: relative position accuracies in easting and northing.

Azi_0 and Ele_0:   azimuth and the elevation of the base line

d: length of the baseline

The equation is valid when both antennas receive signals from identical satellites and the influences of the ionosphere and troposphere on the received electromagnetic waves can be assumed as identical. According to Wanninger (2000), the influences of the ionosphere on single-phase measurements can be assumed as identical when the two antennas are placed within a few kilometres.

Using the distance as denominator in Equation (2.4) implies that the uncertainty of the orientation decreases with longer baseline. The terms σ_N and σ_E depend on the satellite constellation. Because of lack of satellites above the poles (caused by the orbit inclination of 55 deg towards the equator plane for GPS), σ_N is especially dependent on the latitude. Furthermore, an estimation of the azimuth (in the horizontal plane) is influenced by the cosine of the elevation of the baseline ($\cos Ele_0$). A calculation is no longer possible when the baseline is vertical because there is no horizontal component available ($\cos 90 = 0$). Consequently, orientation estimation with least variance can be obtained when the baseline is horizontal and aligned north-south (Park et al., 1997). The distance d can be used for quality check or as a constraint when previously known. Investigations relating to orientation determination using the position of two or more antennas can be found in Jablonski (1989), Flawn (1996), and Giorgi et al. (2011).

2.2.7.1 Two or More Antennas with Large Baseline

A large-scale version of a multiple-antenna system can be used for finding orientation in a geodetic network. Therefore, GNSS antennas are located at two or more stations of the network up to several kilometres apart. In contrast to shorter baselines (compare Section 2.2.7), the influences of the ionosphere and troposphere on the received electromagnetic must be considered. Experiences with GPS for network determination are presented in Frei et al. (1992) and Wiget and Schneider (1992). In comparison, a traditional geodetic approach for orientation of large networks uses astronomical azimuth measurements as described in Torge (2003). Saving time and being independent in terms of weather are reasons for replacing the traditional astronomical azimuth measurements by GNSS measurements. The azimuth obtained by GNSS

has been shown to be consistent with the astronomical azimuth with a standard measurement uncertainty of 1'' (Chang and Tsai, 2006), corresponding to 0.3 mgon.

2.2.8   Additional Sensors

Low-cost GNSS receivers are built in smart phones, laptops, and even digital cameras. In addition, the significance of location based services like location-dependent applications on mobile devices has increased rapidly. The combination of a mobile communication device and a positioning function in one device offers a wide range of opportunities in which orientation plays a major role. Because handheld devices should be as small as possible, it is not feasible to use more than one antenna. Embedding two antennas with a baseline of several decimetres or metres is even less feasible. Because pedestrians have very few constraints in their movement, orientation indication is not accurately possible by using the trajectory of the movement. Consequently, implementation of a prediction model is not practicable. In addition, pedestrians often stand still while using a GNSS handheld device or even turn around to find their point of interest. Due to the complexity of the situation, many GNSS navigation devices use additional sensors as support for the orientation determination by trajectory.

2.2.8.1   Magnetic Compass

Electronic compass sensors are integrated into many handheld devices (see Table 2.3). The uncertainty of the compass ranges from 2 deg up to 5 deg standard measurement uncertainty, depending on the device. However, a magnetic compass is subject to local deviations of the Earth's magnetic field and disturbances from magnetic or electromagnetic sources.

2.2.8.2   Gyroscope / Gyrocompass

A gyroscope is a fast-spinning disc that is gimbal-mounted on a platform. Because of the gimbal-mounting, external torque influencing the orientation of the disc is minimised. As a consequence, the orientation of the disc remains nearly stable. Hence, gyroscopes can be used to maintain an initial orientation independent of the movements of the platform. However, the orientation is valid only for a limited period of time because gyros are subject to drift. Gyrocompasses consist of a gyroscope with one degree of freedom fixed to the Earth-gravitational field. Therefore, the gyroscope is related to the rotation of the earth, which exerts a torque on the disc. Because of the principle of angular momentum, the rotation axis is forced to turn perpendicular to the torque. Consequently, the rotation axis of the disc is oriented along a line of longitude that indicates true north.

In aviation and nautical navigation, the size of the orientation system is less important than the reliability. Therefore, a gyrocompass offers a good option for obtaining accurate and reliable orientation information (Anschütz, 2012). A combination of a digital magnetic compass and a gyroscope is presented in Ladetto and Merminod (2002). Gyrocompasses are also available for geodetic application, largely in tunnelling and mining, in which GNSS-based orientation is not applicable. An introduction of geodetic compasses is given in Stier (1962) and in Halmos (1966). The uncertainty of a geodetic gyrocompass depends on the type and ranges from a standard measurement uncertainty of 1 mgon (DMT, 2012) to 6 mgon (GeoMessTechnik, 2012). However, the measurement uncertainty depends on the influence of the local vertical deflection and can drift with varying temperatures. Furthermore the measurement uncertainty increases with increasing latitude because the torque-induced precession D, which forces the gyroscope towards the direction of the Earth's rotation axis, is dependent on the centrifugal force of the Earth's angular momentum ω_E, as shown in Equation (2.5) (Zanini, 1992).

$$D = \omega_E \cdot R_G \cdot \cos\varphi \cdot \sin A_m \tag{2.5}$$

where R_G is the running axis of the gyroscope and A_m is the azimuth between the running axis and the local meridian. At latitudes greater than 70 deg, a gyrocompass is out of service.

A comparison in Beckmann et al. (1988 indicates that a successful combination of orientations from GPS azimuths with gyrocompass azimuths is possible, without reduction of accuracy.

2.2.8.3   Inertial Systems

An inertial system can be used to determine direction changes of a pedestrian who is turning but not moving forward. A description of inertial systems can be found in Mautz (2012):

> An INS is an electronic device that provides estimates of position, velocity and orientation from an IMU. The custom IMU consists of three orthogonally arranged accelerometers (motion sensors), three gyroscopes (angular rate sensors) and/or a magnetometer (3 perpendicular sensors for measuring the strength and/or direction of a magnetic field). If an initial position and orientation are known, subsequent positions, orientations and velocities (direction and speed of movement) of the moving platform are continuously updated via Dead Reckoning (DR) without the need for external reference positions. The main argument to use INS for pedestrian navigation arises from independent operability—at least temporarily—without external infrastructure, making navigation possible in environments, where the installation and maintenance of such infrastructure is not affordable. (p. 92)

The disadvantage of an inertial system in general is the low long-term stability. Inertial systems drift significantly within a short time (after a few minutes or even seconds) and need to be readjusted.

2.2.8.4   Dead Reckoning

Dead reckoning is a method used in navigation to bridge the positioning function during outages of the GNSS reception, mainly using input data from inertial systems. The calculated coordinates or the inertial system itself can be used to calculate the orientation. Investigations into combining GNSS and dead reckoning can be found in Kao (1991), Hayashi (1996), and Cannon et al. (2001). A summary description of dead reckoning is given in Mautz (2012):

> Dead reckoning is the process of estimating a position based upon previously determined positions and known or estimated speeds over the elapsed time. An inertial navigation system is the main type of sensor used. A disadvantage of dead reckoning is that the errors of the process are cumulative, so the error in the position fix grows with time. The reason is that new positions are calculated solely from previous positions. (p. 32)
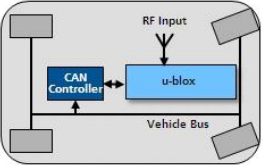
2.3   Overview of Existing Methods and Systems

The following tables give a summary of existing methods for GNSS-based direction finding. Some are only in the concept stage while others are already commercially available. The Tables show only an exemplary selection for the different methods.

Table 2.2 Exemplary Selection of Commercial Multi-Antenna Systems.

Figure (Image Source= Source)	Technology	Remarks	Update Rate	Baseline	Standard Measurement Uncertainty
	Azimuth calculation using differential position fix	Specially developed for alignment of mobile phone antennas	n/a	ca. 90 cm	0.4 deg
Source: (precise positioning management, 2012)					
	Two antenna element	Only L1 antennas	10 Hz	ca. 45 cm	0.5 deg
Source: (gpscompass, 2012)					
	Two antenna element	Only L1 antennas, dual antenna acquisition with a single cable	10 Hz	ca. 56 cm	0.5 deg
Source: (Thales Navigation, 2011)					
	Azimuth calculation using differential position fix	Optimised for machine control on excavators	10 Hz	5 m 10 m	0.08 deg 0.03 deg
Source: (Trimble, 2012)					
	Azimuth calculation using differential position fix	Low cos add-on antenna only for orientation determination	10 Hz	10 m	0.05 deg
Source: (Trimble, 2009)					
	GNSS interferometry between 4 antennas	3 cheap add-on antennas for attitude determination. The 4-antenna system and an IMU determine the inclination and adjust the calculated position accordingly.	20 Hz	0.5 m - 1 m	0.3 deg - 0.55 deg
Source: (Javad, 2011)					

24

Table 2.3 Exemplary Selections of Commercial Single Antenna Systems with Additional Sensors.

Figure (Image Source= Source)	Technology	Remarks	Update Rate	Standard Measurement Uncertainty
Source: (Garmin, 2011)	GNSS + electronic 3D-compass	3D compass is tilt-compensated; the device does not need to be level for compass measurement.	n/a	2 deg – 5 deg
Source: (xsens, 2012)	Sensor fusion: • accelerometer • magnetometers • thermometer • barometer • GNSS	Heading accuracy depends on sensor and scenario used	120 Hz	0.5 deg - 1 deg
Source: (Oxford Technical Solutions, 2012)	Combination of inertial navigations system (INS) and high quality GNSS receiver. Optional 1 or 2 antennas can be used.	Heading accuracy depends on model. The optional 2nd antenna improves heading accuracy.	100 Hz	0.1 deg – 0.2 deg
Source: (Leica, 2012)	Inertial measurement unit (IMU) GNSS receiver	High-end system developed for airborne applications	n/a	0.005 deg- 0.015 deg
Source: (u-blox, 2012)	Dead reckoning using information (e.g. odometer pulses, steering wheel ticks, etc.) from the vehicle data via CAN-bus	Dead reckoning bridges temporary limited gaps of GNSS reception.	n/a	n/a

Table 2.4 Example of Commercial Single Antenna Systems using Trajectory only.

Figure (Image Source= Source)	Technology	Remarks	Update Rate	Standard Measurement Uncertainty
Source: (AppStore, 2012)	Compass calculations based on consecutive GPS coordinate readings	Compass App for mobile devices with including GNSS receiver.	n/a	"not very accurate"
Source: (TomTom, 2012)	Compass calculations based on consecutive GPS coordinate readings	Orientation information included in the navigation software.	n/a	n/a

2.4 Chapter Conclusion

Orientation is highly important to various applications, particularly concerning navigation. GNSS systems offer a wide range of possibilities for providing orientation information. Some of the possibilities are already included in the everyday environment; for example, the GNSS car navigation system obtains the orientation information from the previous position fix. Multi-antenna systems are largely used in professional environments, whether for machine control and guidance, for alignment of mobile telephone broadcasting antennas, or for attitude determination on airplanes or ships. Since the beginning of GNSS much research was conducted to determine orientation or attitude by GNSS, an overview of the main approaches and commercially available systems was included in this chapter. In summary, solutions exist to address many requirements in whole or in part. However, no satisfactory solution includes only a single, non-moving antenna without using auxiliary sensors.

3 GNSS Antennas and Signals

This chapter covers the basics of antenna terminology, antenna parameters, and signals used in this thesis. Most information in this chapter is applicable to antennas in general, although the chapter focuses on GNSS antennas.

3.1 Antennas

An emitting antenna receives power from a cable connection and radiates the power into free space. The electromagnetic energy escapes from the antenna and, unless reflected or scattered, does not return (McLean et al., 2002a). Because electromagnetic waves propagate along electrical wires and in free space, an antenna can be seen as the link between the wire and the free space. According to the reciprocity theorem, the same antenna could be used as an emitting or a receiving antenna. Consequently, the architecture/design is, in principle, the same for both types of antennas. However, this conclusion is not applicable for active antennas because of the integrated amplifier. Antennas for GNSS measurements are active antennas and, thus, used for receiving signals only. A standardisation of antenna terminology was published in 1983 under the title "IEEE Standard Definitions of Terms for Antennas" (Institute of Electrical and Electronics Engineers [IEEE], 1983). Several of the following explanations are based on this standard.

3.1.1 *Antenna* as Term

In literature, the term *antenna* is used ambiguously. Generally speaking, the term *antenna* is used in the sense of a complete system including electronic parts, connectors and enclosure. However, it is also used to describe only the core part of such a complete system. According to the IEEE (1983), an antenna is "that part of a transmitting or receiving system which is designed to radiate or to receive electromagnetic waves". In this thesis, *antenna* is used according to this definition.

3.1.2 Antenna Coordinate System

The most commonly used coordinate system for describing an antenna and the associated electromagnetic fields is the spherical coordinate system. In the context of antennas, the zenith angle is usually denoted with θ while the azimuth is denoted with φ. To distinguish from geodetic coordinates, the subscript A (for Antenna) is henceforth added. A zenith angle of $\theta_A = 0$ corresponds to the antenna boresight vector. On the other hand, $\varphi_A = 0$ corresponds to zero degrees longitude, defining the orientation of the coordinate system (McLean et al., 2002b). The longitude φ_A increases counter clockwise, toward the antenna boresight vector. Thus, the coordinate system is right-handed. Figure 3.2 shows the antenna coordinate system.
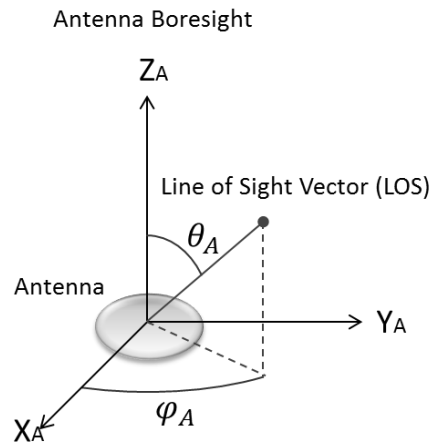
Figure 3.1 Definition of the antenna coordinate system.

3.1.3 The Size of Antennas

An antenna has a physical size L and an electrical size L/λ_w, where λ_w is the wavelength of the electromagnetic wave. The subscript w is used again to distinguish from geodetic coordinates. The physical size determines the design size of the antenna while the electrical size determines the characteristics of the antenna. The electrical size of an antenna is important to the directivity of an antenna (see Section 3.3.3).

Antennas with an electrical size below a certain level are referred to as *electrically small* antennas. The first definition dates back to Wheeler (1947), who defined an antenna as electrically small when the maximal dimension L of the antenna is smaller than the *radian length l*. The definition of radian length is given in Equations (3.1) and (3.2).

$$L < l \tag{3.1}$$

$$l < \frac{\lambda_w}{2\pi} \tag{3.2}$$

Wheeler's definition does not take into account other influence factors but can be used as an approximation for many applications. Bevelacqua (2011) describes an antenna as electrically small if the total size L is smaller than $0.25 - 0.5\ \lambda$.

3.1.4 Bandwidth of an Antenna

The bandwidth of an antenna refers to the range of frequencies an antenna can receive. The optimal efficiency can be achieved by designing an antenna particularly for a specific frequency. The dimensions of the antenna element should fit the corresponding wavelength. However, the ability to receive more than one frequency with the same antenna is often desired, for instance, to receive GPS L1 and L2 simultaneously or to listen to different FM radio stations without using several antennas.

For this reason, most antennas are designed for a certain bandwidth. The bandwidth of an antenna describes "the range of frequencies within which the performance of the antenna, with respect to some characteristic, conforms to a specified standard" (Institute of Electrical and Electronics Engineers [IEEE], 1983). Antennas allowing reception of several frequencies are called *multi-band antennas*. However, multi-band antennas are compromised by the trade-off between bandwidth and design for a specific frequency, resulting in different electrical phase centres for each band and different behaviours with multipath effects.

3.1.5 Phase Centre Offset and Variation

The electrical phase centre does not necessarily correspond to the mechanical antenna reference point. According to Geiger (1988), a constant phase centre offset and a phase centre variable term can be determined for each antenna. The phase centre offset is dependent on the antenna type and frequency and is defined in terms of easting and northing coordinates in the antenna plane, and the height offset is given. The constant offset is overlaid by the smaller term of the phase centre variation, influenced by the direction of arrival of the signals. Normally, the values for easting and northing are within 1 cm to 3 cm. The value for the height can be up to 15 cm or more. The phase centre variation behaves as a function of the satellite's position, with the range of variation normally below 1 cm. Antennas of the same model have largely identical antenna phase centre offsets (Wanninger, 2000).

3.1.6 Aperture Blockage

The IEEE definition describes *aperture blockage* as "a condition resulting from objects lying in the path of rays arriving at or departing from the aperture of an antenna" (Institute of Electrical and Electronics Engineers [IEEE], 1983). In this sense, the attenuation shield used in NORDIS (see Chapter 5.3.3) can be seen as an aperture blockage. However, the attenuation shield covers only part of the antenna and does not totally block all parts of it.

3.2 Antenna Fields

The surrounding area of an antenna is divided into two primary regions:

- Far-field region
- Near-field region

Dependent on the electrical size of the antenna, the near field region can be subdivided into:

- Reactive near-field region
- Radiating near-field (Fresnel) region (not applicable to electrical small antennas)

The regions are defined depending on the distance to the antenna as shown in Figure 3.2. The regions for electrical small antennas with a missing radiating near field are shown in Figure 3.3. The symbol in the centre stands for an antenna element with dimension L.

The Radius R_1 for the near field is

$$R_1 = 0.62 \sqrt{\frac{L^3}{\lambda_w}} \tag{3.3}$$

and for the far field

$$R_2 > \frac{2L^2}{\lambda_w} \tag{3.4}$$

where $R_2 \gg L$ and $R_2 \gg \lambda_w$, L is the largest dimension of the antenna, and λ_w is the wavelength.

For the GPS L1 signal (see Chapter 3.6) and an antenna of the size of $L = 9.525 \, cm$ the values are for $R_1 = 4.18 \, cm$ and $R_2 = 9.52 \, cm$.
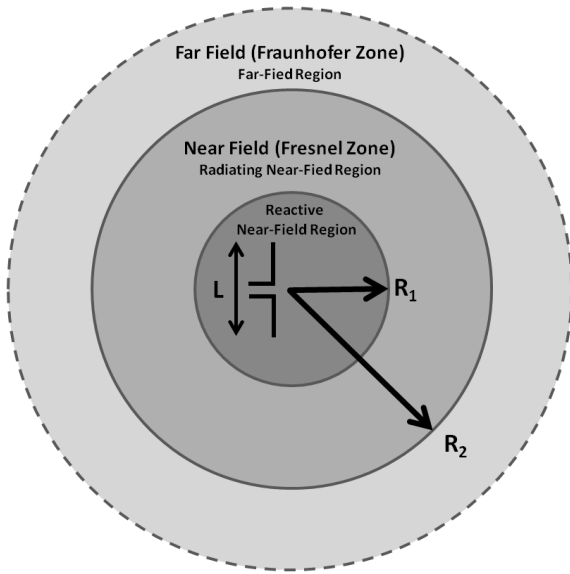
Figure 3.2 Antenna near- and far-field according to (Menge, 2003).
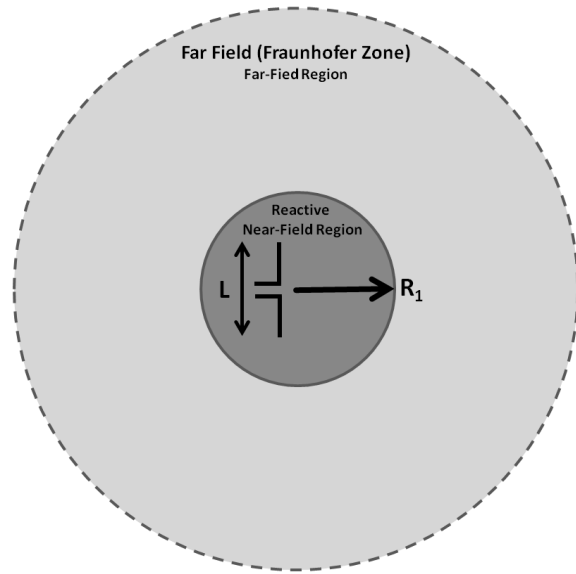
Figure 3.3 Antenna near- and far-field for electrical-small antennas (missing radiating near-field region) adapted from (Menge, 2003).

3.2.1   Far-Field (Fraunhofer) Region

When the range between the emitting and receiving antennas is larger then R_2, as shown in Equation (3.4), the oncoming wave front at the receiving antenna can be assumed to be planar and the rays to be approximately parallel. As shown in Figure 3.4, in the far field the spherical surface of uniform power density appears flat to a receiving antenna because the receiving antenna is very small compared to the surface of the sphere. In the far-field region, the characteristic of the wave is independent from the distance. The far field is the most important region for many applications because antennas are usually used to communicate over a distance that is larger than the near-field region.

The far field is also called the *Fraunhofer Zone* because of the Fraunhofer diffraction that describes the diffraction when planar waves are passing through a small aperture in blocking material. This effect occurs for electromagnetic waves as it occurs for acoustic waves or waves in fluids as long as they are parallel, a condition only true in the far field.
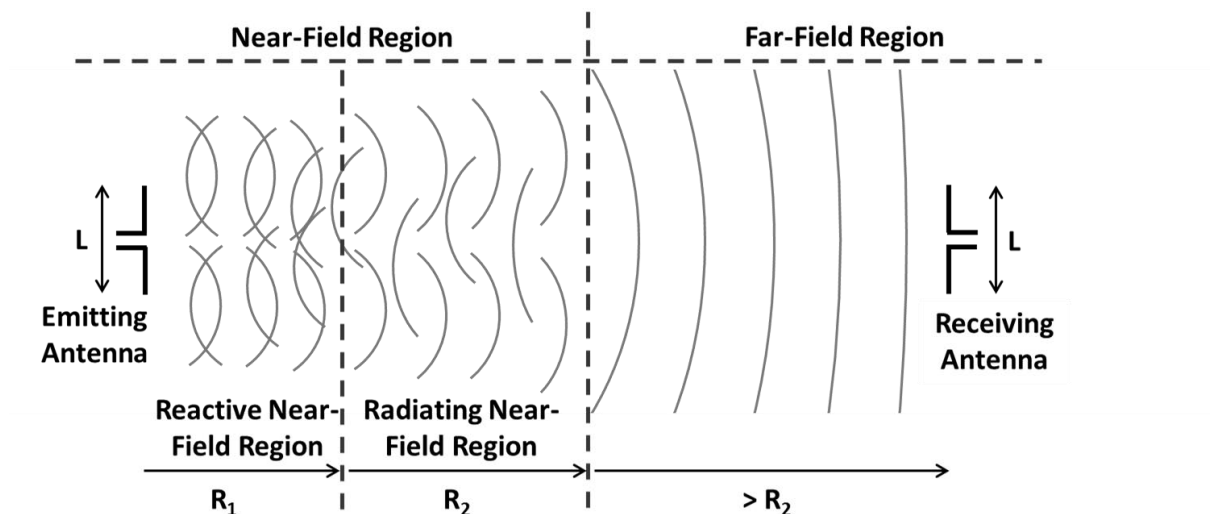
Figure 3.4 Transition from the near-field region to planar waves in the far-field region according to (Djuknic, 2003).

3.2.2 Near-Field Region

The region limited by the radius smaller than R_2 is called the *near-field region*. In contrast to the far-field region, the relation between E and H field is very complex in the near-field region:

> In the near-field region the radiation pattern is dependent on the distance from the antenna as well as the observation angle. This is because the distance from different parts of the antenna to the observation point varies considerably and consequently the phase and amplitude of field contributions from the different parts changes proportionally. (Rudge, 1982)

3.2.3 Reactive Near-Field Region

The nearest region of the antenna is called the *reactive near field*. This field is dominated by non-radiating field components. "In this region, the fields are predominately reactive fields, which means that the E- and H- fields are out of phase by 90 degrees to each other" As Rudge (1982) noted, "The reactive field arise from the electromagnetic charges on the structure, they do not radiate but form an essential part of the radiating mechanism". The limitation of this region is given by Equation (3.4).

3.2.4 Radiating Near-Field (Fresnel) Region

According to Bevelacqua (2011), "The radiating near field or Fresnel region is the region between the near and far fields. In this region, the reactive fields are not dominating; the radiating fields begin to emerge". The waves are clearly not planar and have phase shifts. With increasing distance from the antenna, the E and H fields begin gradually to be in phase, a prerequisite for radiation. The radiating near field does not exist for electrical small antennas.

3.3 Antenna Characteristics

Based on the antenna fields, antenna characteristics such as gain, antenna pattern, directivity, polarisation and radiated power can be derived.

3.3.1 Antenna Gain

The antenna gain is a performance indication combining the antenna's directivity and electrical efficiency. The gain of an antenna is a relative factor in terms of a reference antenna. As a theoretical reference, an isotropic antenna is often used.

An *isotropic antenna* is a hypothetical antenna with equal radiation intensity in all directions. One can imagine an isotropic antenna as a light bulb that illuminates the whole surrounding (Figure 3.6) and, in contrast, a directive antenna as a spotlight, illuminating only a certain area (Figure 3.5). Assuming both shine with the same energy, the light intensity in the spot area will be higher. Antennas with exact isotropic radiation patterns do not exist in practice but are used as theoretical references for comparison with real antennas.

Figure 3.5 Directive antenna.
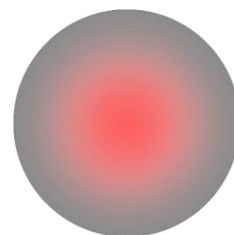
Figure 3.6 Isotropic antenna.

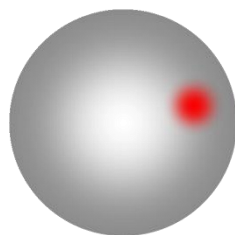The absolute gain is the ratio of the radiation intensity in a given direction to the radiation intensity that would be obtained if the power accepted by the antenna were radiated isotropically (Institute of Electrical and Electronics Engineers [IEEE], 1983).

> A gain of 3 dB means that the power received far from the antenna will be 3 dB (twice as much) higher than what would be received from a lossless isotropic antenna with the same input power. Gain is sometimes discussed as a function of angle, but when a single number is quoted the gain is the "peak gain" over all directions. (Bevelacqua, 2011)

For passive antennas, the directivity increases the gain as opposed to the isotropic antenna. Furthermore, an active antenna has an amplifier to increase the power gain.

3.3.2 Antenna Pattern

The antenna pattern describes the electromagnetic field generated by an antenna. In spherical coordinates, it is the distribution of a quantity describing the electromagnetic field over θ and φ for the fixed radial distance R (McLean et al., 2002b). An antenna pattern can be created for several quantities. According to McLean et al. (2002b), the following quantities are generally of interest:

- Power flux density
- Radiation intensity
- Directivity
- Gain
- Phase
- Polarisation
- Field strength (electric or magnetic)

As McLean et al. (2002b) noted, "In particular, the radiation pattern is a representation of the angular distribution of radiated power density in the far field. [...] In the far field, the power flux density and the radiation intensity are identical. [...] Thus, the radiation pattern can be simply taken as representation of the tendency of an antenna to radiate electromagnetic energy as a function of direction in the far field region." Usually, the radiation pattern is drawn using two-dimensional cuts as shown in Figure 3.7 and Figure 3.8. At this point, it is important to note that the angle at which the cuts are taken is important. To completely describe the radiation characteristics of an antenna, a three-dimensional model must be used.

The radiation pattern of an antenna is indicated by the parameter directivity. The normalised directivity D_A is calculated in Equation (3.5), where $F(\theta_A, \varphi_A)$ is the radiation pattern, written as a function in spherical coordinates.

$$D_A = \frac{1}{\frac{1}{4\pi} \int_0^{2\pi} \int_0^{\pi} [F(\theta_A, \varphi_A)]^2 \sin \theta_A \, d\theta_A \, d\varphi_A} \tag{3.5}$$

As noted by Bevelacqua (2011), "A normalised radiation pattern is the same as a radiation pattern, just scaled in magnitude such that the peak (maximum value) of the magnitude of the radiation pattern [F in Equation (3.5)] is equal to 1". The numerator indicates the maximum value of F, and the denominator represents the "mean power radiated over all directions" (Bevelacqua, 2011).

Figure 3.7 shows the vertical radiation pattern of a simulated right-handed circular polarised (see Section 3.6.2) patch antenna for zenith angles φ_A = 0 deg (magenta), 45 deg (blue), and 90 deg (brown). Figure 3.8 shows the corresponding horizontal radiation pattern of the same antenna for horizontal angle θ_A = 0 deg (magenta), 45 deg (blue), and 90 deg (brown). The behaviour of the antenna is perfectly omnidirectional for satellites located in the zenith of the antenna (θ_A= 0 deg), but the omnidirectionality worsens with increasing zenith angle. The simulated antenna has characteristic directivity at a zenith angle of 70 deg.
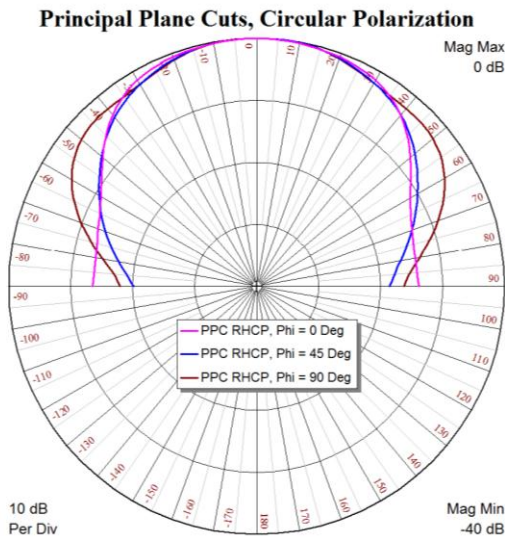
Figure 3.7 Radiation pattern, side view of the antenna. The radial scale shows the C/N$_0$, and the circular scale shows the parameter θ_A. (Simulation created in AWR Microwave Office, 2009).
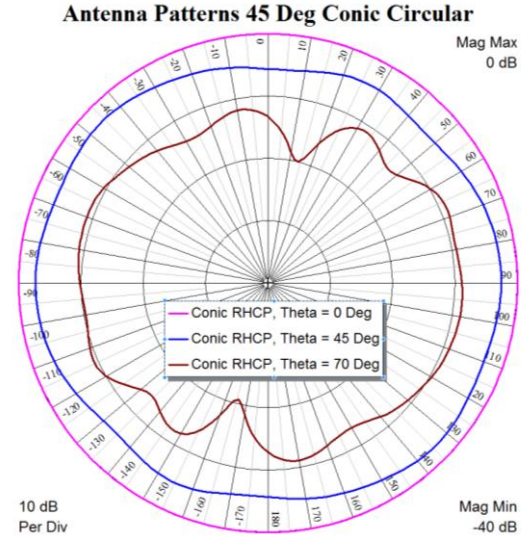
Figure 3.8 Radiation pattern, plan view of the antenna. The radial scale shows the C/N$_0$, and the circular scale shows the parameter φ_A. (Simulation created in AWR Microwave Office, 2009).

3.3.3 Influence of the Satellite's Elevation on Received Signal Power

A typical radiation pattern for the Pinwheel™ antenna (see Section 3.5.1) is shown in Figure 3.9, where "the amplitude rolloff from antenna boresight to horizon is about 15 dB" (Kunysz, 2000). The calculated radiation pattern is confirmed by the measurements in Figure 3.10. "The graphs show data collected over a 24-hour period for all satellites tracked in that period. [...] The variations of C/N$_0$ (see Section 3.6.7) for a given elevation angle (specifically below 30 deg of elevation angle) is mainly due to multipath" (Kunysz, 2000).
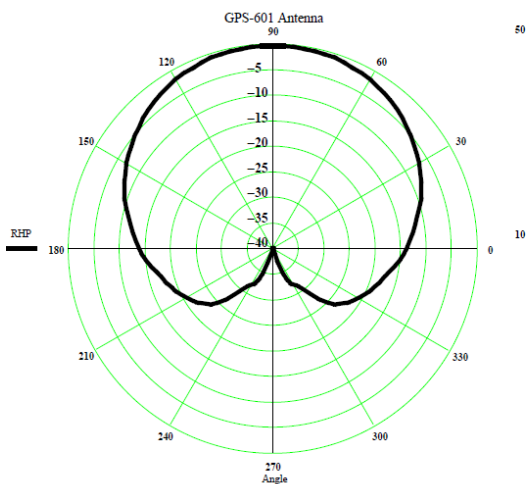
Figure 3.9 L1 Channel amplitude radiation pattern for Pinwheel™ antenna (GPS-601) (Kunysz, 2000).
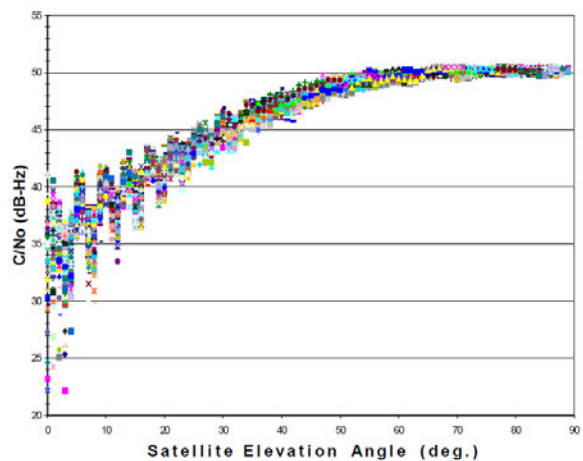
Figure 3.10 L1 C/N$_0$ for Pinwheel™ antenna (Kunysz, 2000).

Because NORDIS is based on measuring the received signal power, the dependency between received signal power and satellite elevation have to be considered (see Section 6.2).

3.3.4 Omnidirectional Antenna

An omnidirectional antenna is an antenna with an essentially non-directional pattern in a given plane of the antenna and a directional pattern in any orthogonal plane (Institute of Electrical and Electronics Engineers [IEEE], 1983). That is, the pattern is nearly isotropic for a single plane. Usual GNSS antennas are built as omnidirectional antennas in the horizontal plane because the satellites are received from all over the sky above the antenna. To build an antenna with low directivity, the antenna has to be electrically small (see Section 3.1.3).

Figure 3.11 shows the omnidirectional gain pattern of the Leica AT504GG antenna, measured in the antenna measuring chamber at University of Bonn. The maximal gain in the zenith is set to 0 dB. The gain decreases by 15.8 dB to the horizon (Zeimetz, 2010).
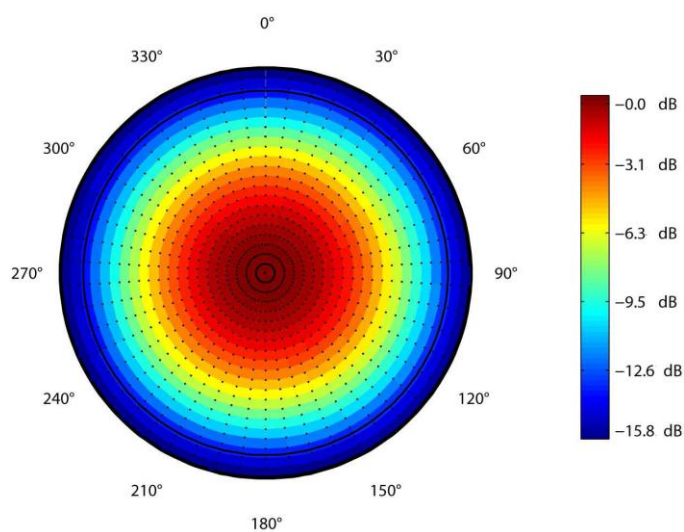
Figure 3.11 Directivity of Leica AT504GG antenna plotted for L1 (Zeimetz, 2010).

To proof the directivity independently from the measurements performed in the antenna measuring chamber, a measurement of real satellites data was performed at ETH. For this purpose the antenna was rotated around the boresight vector while measuring the C/N_0 density. Figure 3.12 shows the C/N_0 densities of all satellites in view (GPS and GLONASS), measured with the Leica smart antenna ATX1230 GG. For the measurement, the antenna was turned four times around its boresight axis. All measured C/N_0 densities have no significant variation during the revolutions, although the received satellites have different elevations. Consequently, the antenna has a non-directional pattern in the horizontal plane even for different elevations and is, therefore, omnidirectional.
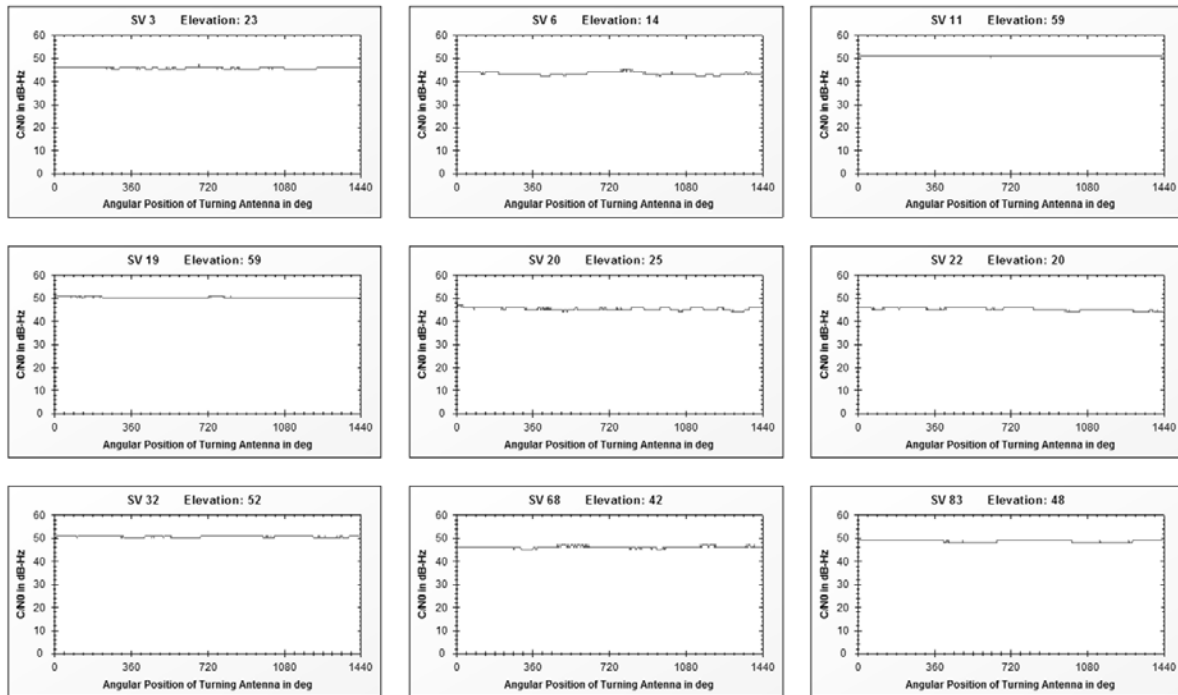
Figure 3.12 C/N$_0$ density for 9 satellites during four revolutions of the Leica antenna ATX1230 GG. The constant curves prove the omnidirectionality of the used antenna.

3.4 GNSS Antenna Types

In connection with GNSS measurements, three antenna types are quite common.

- Patch antenna
- Helix antenna
- Spiral antenna

However, beside these three types, other antenna types exist.

3.4.1 Patch Antenna

The patch antenna is a very common antenna type. Its small size, weight and low cost make this antenna type widely applicable. Hence, for most applications, low-cost GNSS patch antennas are used. Nonetheless, patch antennas are also built into geodetic receivers, where the patch is often mounted on a metallic disk as ground plane, allowing for increasing the gain and decreasing the back lobe. Patch antennas appear as a conductive microstrip, which works as an electrical transmission line. The microstrip is separated from a ground plane by a dielectric layer (substrate).
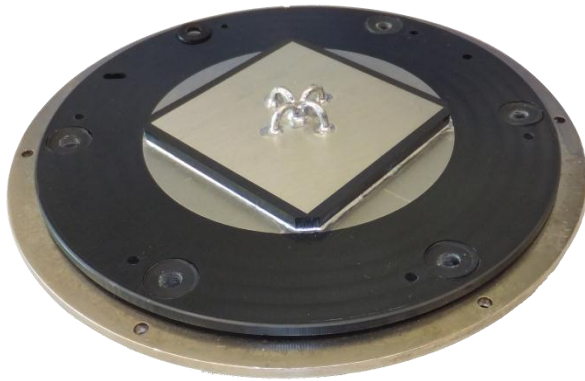
Figure 3.13 Geodetic patch antenna used in Trimble antennas. (Picture: D. Grimm)
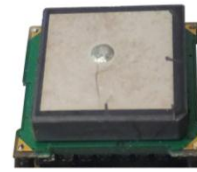
Figure 3.14 u-blox patch antenna. (Picture: D. Grimm)

The edge length of a patch antenna is dependent on the wavelength λ_w and the dielectric constant ε_r of the substrate and is calculated according to Equation (3.6).

$$L = \frac{\lambda_w}{2 \cdot \sqrt{\varepsilon_r}}$$

(3.6)

For GPS L1 with a wavelength of $\lambda_w = 19.05 \; cm$ and a ceramic substrate with a dielectric constant of $\varepsilon_r = 20$, an edge length of 2.1 cm results.

3.4.2 Helix Antenna

Helix antennas have a 3-dimensional structure with a helical shape. The winding of the helix corresponds to the circular polarisation and the wavelength. The antennas on the Block II GPS (Figure 3.15) satellites, for instance, are the helix type. Some GNSS receivers also use helix antennas (Figure 3.16).

Figure 3.15 Helix antennas mounted on a GPS-Block-2 satellite (Lockheed Martin, 2005).

Figure 3.16 u-blox receiver with helix antenna. (Picture: M. Kunz)

3.4.3 Spiral Antenna

The spiral type antenna consists of one or more conducting wires or tapes arranged as a spiral (Institute of Electrical and Electronics Engineers [IEEE], 1983). Such antennas are usually classified according to the shape of the surface. For example, they can be conical or planar

spirals or, according to mathematical form, equiangular or Archimedean. An example of a spiral antenna is the Pinwheel™ Antenna discussed in Section 3.5.1.

3.4.4 Wire and Slot Antennas

Both helix and spiral antennas can be formed as wire or slot antennas. For wire antennas, the antenna elements consist of one or more conducting wires. In the case of a spiral antenna, the conducting wires are formed in the shape of a spiral. The length of the spiral arms is chosen to correspond with the wavelength or an integer part of the wavelength (half or quarter wavelength). As shown in (Booker, 1946), Babinet's principle of complementary screens, which was applied to optics, is applicable in reference to antennas. That is, a slot in a conducting sheet has the same effect as a conducting wire of the same shape. However, "voltage must be developed *along* wires but *across* slots" (Booker, 1946). Therefore, the slot antenna is rotated 90 deg against the wire antenna to receive the same signals.
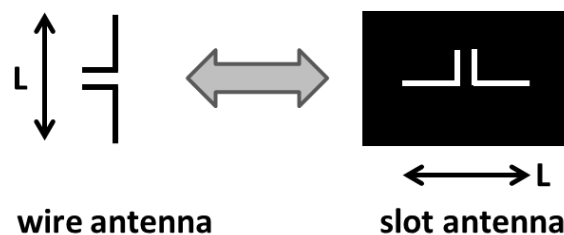
Figure 3.17 Babinet's principle applied to antennas.

Slot antennas are popular because they can be cut out in the desired shape from a conducting planar surface. The helix antennas shown in Figure 3.15 and Figure 3.16 are wire antennas while the spiral antennas shown in Figure 3.19 and Figure 3.20 are slot antennas.

3.5 Geodetic GNSS Antennas

Typical requirements for precise surveying applications are described in (Kunysz, 2000) as followed:

> For precise surveying applications, ideally the antenna should receive only signals above the horizon and reject all signals below the horizon plane of the antenna, have a known and stable phase centre that is co-located with the geometrical centre of the antenna, and have perfect circular polarisation characteristics to maximize the reception of the incoming right-hand polarized (RHP) signal. (p. 2506)

Further, a contemporary antenna should be able to receive signals from all GNSS providers. A wide bandwidth is needed to do so. However, it is difficult to construct an antenna with an identical phase centre for different wavelengths.

An often-used method to suppress the signals from the rear side of the antenna is to mount the antenna on a choke ring ground plane.

3.5.1 Pinwheel™ Antenna

The Leica AX1202 GG (Leica 1200) and the Leica ATX1230 GG (smart antenna) antennas are planar spiral antennas. The antenna type was developed and produced by NovAtel and named *Pinwheel™*, according to its appearance. The type was developed to improve the former antenna used in the Leica system 500. The spiral antenna consists of a conducting plane with slotted openings arranged in a spiral form on the upper side of a PCB print (see Figure 3.18 and Figure

3.19). The openings (81, 83, 85 and 87 in Figure 3.18) receive the signals and guide them to a microstrip spiral on the back side (61 in Figure 3.18), where the signals are transmitted via coax cable to the preamplifier.

3.5.2 Characteristics of the Pinwheel™ Antenna

The first Pinwheel™ antenna was designed for GPS-signals L1 and L2. The antenna has 6 slotted openings with a corresponding length to the L1 signal and 6 slotted openings corresponding to the length of the L2 signal. As shown in Figure 3.19, the slots for L1 and for L2 are arranged alternately in a spiral pattern, which is designed for right-hand polarised signals. The antenna has omnidirectional gain characteristics due to its symmetry.
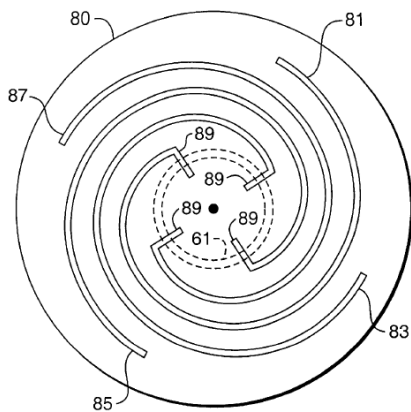
Figure 3.18 Concept of aperture coupled slot array antenna (Kunysz, 2002).

Figure 3.19 Pinwheel™ antenna for L1 and L2 modified picture from (NovAtel, 2006).

In a further development, the pinwheel antenna was modified to enable a wider bandwidth. This was necessary to receive more frequencies, for instance, the signals from GLONASS and Galileo satellites. According to NovAtel (2006),

> the modifications include interconnected slots shaped to begin as spiral slots that flare at the end into fractal loop configurations. These loops are coupled to another loop in an adjacent slot. The radiating structure of interconnected apertures creates many RF paths that open the bandwidth. They also provide a common phase centre for the new frequencies. (p. 2)

This antenna design is used in the Leica Smart Pole antenna (Figure 3.20 left).

Figure 3.20 Pinwheel™ antenna Leica ATX1230 GG (left) and patch antenna Leica 500 (right). (Photos: D. Grimm)

The antenna on the right is a patch antenna (shown in the same scale). The microstrip patch is placed on the substrate (white). Behind the rectangular substrate, the metallic ground disc can be seen.

3.5.3   Advantages of the Pinwheel Antennas in Comparison to Patch Antennas

The spiral form of the slotted openings realises an almost-constant and well-defined electrical phase centre. For precise geodetic measurements, these qualities are a fundamental prerequisite. Furthermore, the phase centre is the same for all enabled frequencies. An advantage is the light weight, made possible because the metallic ground disc is not required.

3.6   GNSS Signals

In this thesis, GPS and GLONASS signals are used, so they are the only signals discussed. However, the use of Galileo, COMPASS or other GNSS systems would be possible, but their use has not been tested.

3.6.1   Frequencies of GPS and GLONASS Signals

Satellite transmission frequencies are assigned and regulated by the World Radio Conference (WRC) of the International Telecommunication Union (ITU). Table 3.1 shows the band classification of typical microwave electromagnetic transmission frequencies used by satellite communication and navigation as specified in ITU-R V.431-7.

Table 3.1 Satellite Communication and Navigation Frequencies

Band	Frequency
L-Band	1.0 GHz to 2.0 GHz
S-Band	2.0 GHz to 4.0 GHz
C-Band	4.0 GHz to 8.0 GHz
X-Band	8.0 GHz to 12.0 GHz
Ku-Band	12.0 GHz to 18.0 GHz
K-Band	18.0 GHz to 27.0 GHz
Ka-Band	27.0 GHz to 40.0 GHz

Source: International Telecommunication Union (2000).

All GPS satellites transmit the civilian C/A code and the military P(Y) code on the same L1-frequency and a second military P(Y) code on the same L2-frequency. The different satellites are distinguished by their pseudorandom noise code number (PRN).

$$L1 = 1575.42 \text{ MHz} \quad \lambda_w 1 = 19.05 \text{ cm}$$

$$L2 = 1227.60 \text{ MHz} \quad \lambda_w 2 = 24.45 \text{ cm}$$

$$L5 = 1176.45 \text{ MHz} \quad \lambda_w 5 = 25.48 \text{ cm}$$

where λ_w is the wavelength.

GLONASS satellites transmit two codes (C/A and P Code). In contrast to GPS, each satellite broadcasts the same code but at a different frequency to distinguish the satellites.

$$L1 = 1602 \text{ MHz} + (n \cdot 0.5625 \text{ MHz})$$

$$L2 = 1246 \text{ MHz} + (n \cdot 0.4375 \text{ MHz})$$

$$L3 = 1202.025 \text{ MHz (latest GLONASS-K1 satellites)}$$

$$L3 = 1207.14 \text{ MHz (GLONASS-K2 satellites)}$$

where n is the identification number for each satellite ($n = 0, 1, 2, \dots$).

According to Table 3.1, GPS and GLONASS satellites broadcast within the L-Band. Hence, the GPS frequencies are called L1 and L2. Satellites of type GPS IIF (Block 2, Follow-On) and of type GPS III broadcast on the additional frequency L5. In this work, only L1 and L2 are used.

The relation between wavelength λ_w and frequency f is given in Equation (3.7).

$$c = \frac{\lambda_w}{T} = \lambda_w \cdot f \tag{3.7}$$

The propagation velocity c of waves is dependent on the medium the wave has to pass through and on the wave type (electromagnetic, acoustic, light). The value for electromagnetic waves in air is $c = 2.9979 \cdot 10^8$ m/s.

3.6.2 Polarisation

Simple antennas like dipole antennas emit an electromagnetic wave as a sinusoidal oscillation in a plane defining the electrical field **E**. It is perpendicular to the magnetic field. Usually, the **E**-field is in a horizontal or vertical plane, depending on the mounting of the emitting antenna. A corresponding receiving antenna has to be mounted in the same plane to be able to detect the electromagnetic wave (reciprocity theorem).

In contrast to the mentioned linear polarisation, an antenna can have a circular polarisation. In this case, the electromagnetic wave propagation describes a helix with the electrical field vector.

Depending on the direction of rotation of the helix, seen from the direction of the wave propagation, the circular polarisation is considered to be right handed or left handed. The GPS signal has a right-hand circular polarisation (RHCP).
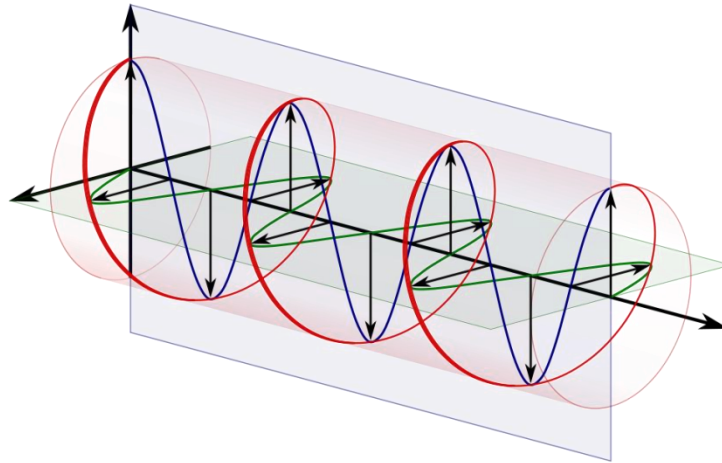
Figure 3.21 Right-hand polarised wave. Horizontal components in green and vertical components in blue (Right Handed Circular Polarization, 2011).

While antennas for linear polarisation must be aligned in the plane of the wave, antennas designed for circular polarisation are omnidirectional (see 3.3.2). That is, the antenna has a wider opening angle from which signals can be received. Consequently, antennas with circular polarisation are convenient for moving devices, for instance, for cellular phones or GNSS, for which constantly realigning the antenna is not convenient. The direction of the polarisation of the antenna must correspond to the wave polarisation direction. Thus, a RHCP-antenna does not receive LHCP-signals. The type of polarisation is crucial to the antenna type and shape.

3.6.3   Signal Refraction

Electromagnetic waves, propagating from the satellites to a receiving antenna on the Earth's surface, have to pass through the exosphere, the ionosphere (upper part of the atmosphere), the mesosphere, the stratosphere, and finally the troposphere (Dodel and Häupler, 2004). The ionosphere delays the propagation velocity while the troposphere attenuates the signal. These effects have a direct impact on the GNSS measurements, resulting in limiting position accuracy. Therefore, propagation models like that presented in Scappuzzo (2009 for different media are required to improve the results. Early approaches concerning atmospheric effects on geodetic space measurements are collected in Bauersima et al (1988.

3.6.4   Signal Diffraction

When an electrometric ray encounters an obstacle, edge diffraction can occur. For diffraction to occur, the obstacle needs a sharp edge (knife-edge). The obstacle works like a wide screen through which no energy can pass (Figure 3.22). Consequently, the line of sight from the transmitter S to the receiver E is masked by the screen. Although there is no direct view, the receiver still receives energy because of the diffraction. Signal diffraction in association with GNSS measurements can lead to decreased position accuracy because the determined range is not the shortest line to the satellite. A numeric approach for diffraction modelling is presented in Brunner et al. (1999).

However, Fresnel (1816) discovered that diffraction over an absorbing plane can be explained by Huygen's principle, stating that every point of a wave-front may be considered as a source of secondary spherical wavelets.
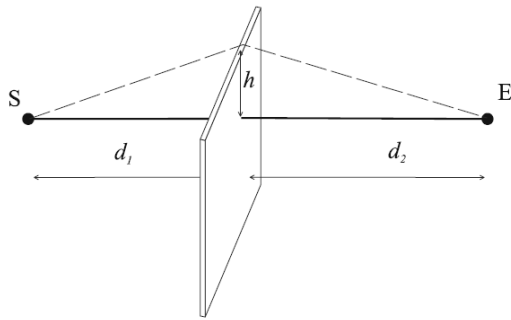
Figure 3.22 Edge diffraction through an absorbing screen (Benkner, 2007).
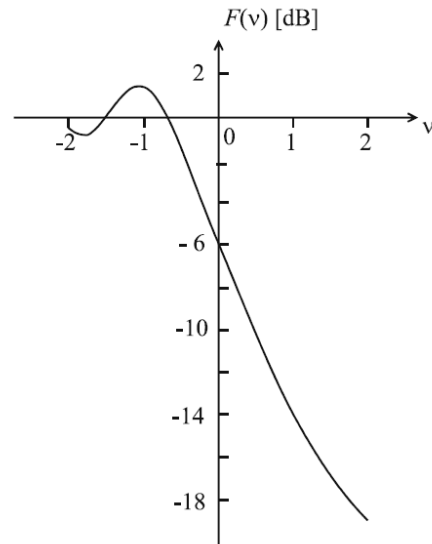
Figure 3.23 Edge diffraction attenuation in function of the Fresnel diffraction parameter v (Benkner, 2007).

The energy behind the screen can be expressed as *propagation loss F(v)*, which indicates the quotient between the diffracted field E and the incident field E_0. This quotient is calculated with the complex Fresnel integral (3.8).

$$F(v) = \frac{E}{E_0} = \frac{1+j}{2} \int\limits_{v}^{\infty} \exp\left(-\frac{j\pi t^2}{2}\right) dt \tag{3.8}$$

The Fresnel diffraction parameter v depends on the distance to the screen d_1, d_2 and the height of the screen h (see Figure 3.22).

$$v = h \cdot \sqrt{\frac{2(d_1 + d_2)}{\lambda d_1 d_2}} \tag{3.9}$$

As shown in Figure 3.23, the energy behind the screen can be even higher than it is without the screen. Accordingly, the attenuation implemented in NORDIS (see Section 5.3.3) does not hold back all the energy. Because of the diffraction, the antenna still receives the satellite signal, although the line of sight is screened by the attenuation.

3.6.5 Signal Power

The signal power of a GNSS satellite is commonly expressed in decibels (dB) on a logarithmic scale, indicating the ratio of the power to a reference power level. The reference power level value is in the same units as the power. Typical reference levels are one watt or one milliwatt. A power in decibel-milliwatts (dBm) can be computed from a power expressed in milliwatts according to (Northwood Labs, 2003) as

$$P_{P/mW} = 10 \cdot \log \frac{P_{mW}}{1\text{mW}} \text{ dBm}$$

where P_{mW} is the power in mW.

Power in decibel-watts (dBW) is expressed according to (Northwood Labs, 2003) as

$$P_{P/W} = 10 \cdot \log \frac{P_W}{1\text{W}} \, \text{dBW} = 10 \cdot \log \left(\frac{1}{1000} + \frac{P_{mW}}{1\text{mW}} \right) \text{dBW} = -30 + 10 \cdot \log \frac{P_{mW}}{1\text{mW}} \, \text{dBW}$$

where P_W is the power in W and P_{mW} is the power in mW.

The formula for conversion of power in decibel-milliwatts to power in decibel-watts is

$$P_{P/W} = P_{P/mW} - 30$$

"A power level of 100mW can therefore be expressed as a power of 20 dBm or -10 dBW" (Northwood Labs, 2003).

The signal power depends on the emitted power of the satellites. Relevant for the user is the amount of signal power available at the receiver. This amount is indicated in literature as having a value of at least -160dBW for the C/A Code on L1. A precise value is noted in U.S. Coast Guard Navigation Center (2008): "This signal is transmitted with enough power to ensure the minimum signal power levels of -158.5 dBW for L1 C/A-code under the conditions defined in IS-GPS-200." Table 3.2 shows the link budget analysis between satellite and receiver.

Table 3.2 Carrier Link Budget Analysis for L1 Modulated with the C/A code

Influencing Factors	Gain +/Loss -	Absolute Value
Power at the satellite transmitter		13.4 dBW (43.4 dBm=21.9 W)
Satellite antenna gain (due to concentration of the signal at 14.3 deg)	+13.4 dB	
Radiate power EIRP (Effective Integrated Radiate Power)		26.8 dBW (56.8 dBm)
Loss due to polarization mismatch	-3.4 dB	
Signal attenuation in space	-184.4 dB	
Signal attenuation in the atmosphere	-2.0 dB	
Gain from the reception antenna	+3.0 dB	
Power at receiver input		-160 dBW (-130 dBm)

Source: Zogg (2009).

3.6.6 Amount of power at the receiver (GPS)

The common power values for GPS L1, L2 and L5 are:

$$L1 \; C/A \; CODE: \; -160 \; \text{dBW} \; (10^{-16} \, \text{W})$$

$$L1 \; P \; CODE: \quad -163 \; \text{dBW} \; (5 \cdot 10^{-17} \, \text{W})$$

$$L2 \; P \; CODE: \quad -166 \; \text{dBW} \; (2.5 \cdot 10^{-17} \, \text{W})$$

$$L5: \qquad\qquad -157.9 \; \text{dBW} \; (1.6 \cdot 10^{-16} \, \text{W})$$

The GLONASS signals have similar signal power (Langley, 2011).

To assess the amount of power, the power at the receiver must be compared to the power of the noise. Noise sources generate power in proportion to the bandwidth of the affected system (GPS or GLONASS). Hence, the power level has to be described in relation to a bandwidth unit

according to the power spectral density. According to Northwood Labs (2003), "The power spectral density for noise is"

$$N = k \cdot T_a \tag{3.10}$$

where $k = 1.38 \cdot 10^{-23} \, J/K$ is the Boltzmann constant and T_a is the absolute temperature.

Important for GNSS receivers is the power of the thermal background noise in the ambient noise of the receiver. This ambient thermal noise N_T is typically calculated at 290 K (16.85 C). 290 K is a reference generally taken as the effective noise temperature of the Earth ()(Northwood Labs, 2003, Northwood Labs, 2003):

$$N_T = kT = 1.38 \cdot 10^{-23} \frac{J}{K} \cdot 290 \text{ K} = 4.00 \cdot 10^{-21} J \tag{3.11}$$

Because 1 J corresponds to 1 Ws, Equation (3.11) can be expressed in watts per Hertz (Northwood Labs, 2003):

$$N_T = 4.00 \cdot 10^{-21} \frac{W}{Hz} = -204 \frac{dBW}{Hz} = -174 \frac{dBm}{Hz} \tag{3.12}$$

With a spectral power density of the thermal background noise of about –174 dBm/Hz (at a temperature of 290 K), the maximum received signal power is approximately 14 dB below the thermal background noise level.

3.6.7   Carrier-to-Noise Density (C/N$_0$)

The relation of the carrier power to the noise power spectral density is defined as carrier-to-noise density C/N$_0$. The carrier-to-noise density is standardised at the thermal noise floor $N_0 = N_T$.

Using the value for the carrier power for L1 from Table 3.2 and the thermal noise floor from Equation (3.12), the carrier-to-noise density for L1 is as follow:

$$\frac{C}{N_0} = \frac{-160 \text{ dBW}}{-204 \text{ dBW/Hz}} = 44 \text{ dB Hz.} \tag{3.13}$$

3.6.8   Carrier-to-Noise Density (C/N$_0$) and Signal-to-Noise Ratio (SNR)

As to Badke (2009) indicated,

> Note that C/N$_0$ is not the same as SNR (signal-to-noise ratio), although the terms are sometimes used interchangeably. Effectively, C/N$_0$ assumes that the noise has infinite bandwidth (and thus power) and therefore characterizes it using a density, that is, as the amount of noise power per unit of bandwidth (i.e., watts/Hz).
>
> Conversely, SNR considers the total noise power in a certain bandwidth (i.e., watts). C/N$_0$ can be derived from SNR if the noise bandwidth of the SNR measurement is known. For example, one manufacturer's GPS receiver displays SNR as a figure of merit for a GNSS signal. However, in this receiver, C/N$_0$ is typically 30 decibels higher than the displayed SNR.
>
> C/N$_0$ provides a metric that is more useful for comparing one GNSS receiver to another than SNR because the bandwidth of the receivers is eliminated in the comparison. (p. 20)

Therefore, the following is independent of the receiver's characteristics.

$$\frac{C}{N_0} dBHz = SNR[dB] + 10 \cdot \log_{10}\left(\frac{2 \cdot NBW}{f_S \cdot \tau}\right) \qquad (3.14)$$

NBW :   noise bandwidth
f_S A/D :   sampling frequency
τ :   accumulation period

As seen in Equation (3.14), the SNR value is heavily dependent on the chosen NBW. Because this value is set by the receiver manufacturer, SNR values for receivers from different companies are not evidently comparable. Thus, the C/N_0 density is commonly used. Table 3.3 gives an overview of often-used quantities for corresponding units.

Table 3.3 Quantities describing signal strength.

Quantity	Unit	Name
C/N_0	dB Hz	carrier-to-noise density
C	W	carrier power
N_0	W/Hz	noise power
SNR	dB	signal-to-noise ratio

3.6.9 Receiving the Signal

To be received, the very low power of the signal must be despreaded. As Zogg (2009) indicated,

> The demodulation and despreading of the received GPS signal causes a system gain G_G of:

$$G_G = \frac{Modulation\ rate\ of\ C/A - Code}{Data\ rate\ of\ information\ signal} = \frac{1023\ bps}{50\ bps} = 20.500 = 43\ dB \qquad (3.15)$$

> After despreading, the power density of the usable signal is greater than that of the thermal or background signal noise.

Subsequently, the analogue signal must be filtered, amplified, and down converted. After these steps are completed, a typical value for L1 C/A code, as indicated in Joseph (2010), is

$$C/N_0: {\sim}37\ to\ 45\ dBHz$$

3.6.10 Satellite Separation

Because all satellites broadcast on the same frequency, the signals from the different satellites cannot be distinguished in an analogous way. Hence, the code and Doppler effects are exploited in a first step to distinguish the satellites. In a second step, the signal strength is calculated.

The concept in this section is adapted from Sayre (2003, p. 18-26, Ward et al. (2006, p. 155-156 and Hofmann-Wellenhof et al. (1997, p 83) and is illustrated in Figure 3.24.

After the signal from the antenna is amplified with a low noise preamplifier, the GNSS receiver must process the incoming GNSS signal and ambient noise. Therefore, the signal and the noise are downconverted to an analogue intermediate frequency IF, which is achieved by mixing the signal with frequencies from local oscillators (LOs). The LOs are synthesised frequencies deriving from the reference oscillator. Because only the lower frequency band of the in-phase plus noise component is desired, low pass filters eliminate the upper band. "The signal Dopplers

and the PRN codes are preserved after the mixing process" (Ward et al., 2006). The analogue IF signals are then sampled and quantised by the analogue-to-digital converter (A/D converter), using an automatic gain control (AGC) function. At this point, the digitised IF signals enter multiple receiver channels, in which the same signal processing is performed on different satellites in parallel. Hence, the signal from a specific satellite must be identified. To separate the different signals, a reference C/A code in the receiver is used to identify the different PRN codes by code correlation techniques. Detailed information on separating the satellite signals is given in Braasch and Van Dierendonck (1999).
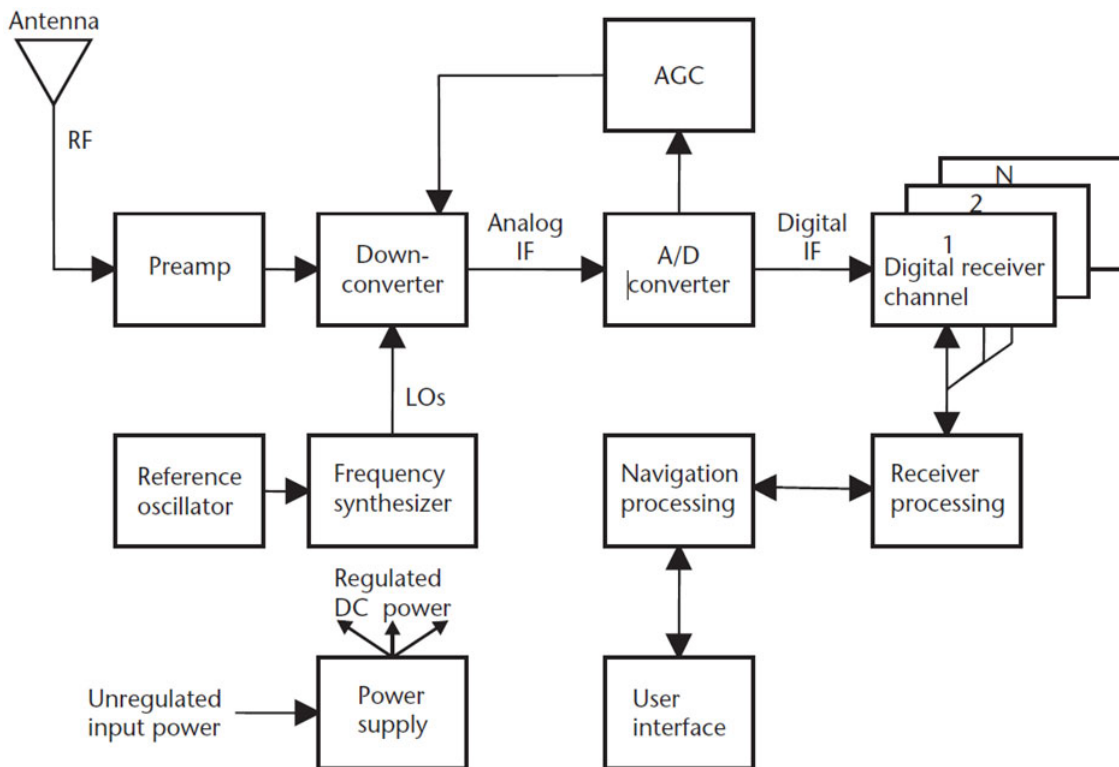
Figure 3.24 Generic digital GPS receiver block diagram (Ward et al., 2006).

The pseudorange measurements are then performed in tracking loop circuits within the different receiver channels. "The code ranges are determined in the delay lock loop (DLL) by using code correlation techniques" (Hofmann-Wellenhof et al., 1997). For the code correlation, a local replica of the PRN code must be available on the receiver. The reference signal is correlated with the received satellite signal. Then, the signals are shifted with respect to time so that they optimally match. Because of the motion of the satellites, the frequencies of the received signals are Doppler shifted. For this reason, the tracking loops must be tuneable; that is, the local code is adapted to the Doppler shift of the received signal. "After removing the PRN code from the incoming signal, the unmodulated (Doppler shifted) carrier wave is obtained. This carrier wave is then passed to the phase lock loop (PLL) where the signal is compared with a carrier replica (generated in the receiver) to give the (fractional) phase offset between the two signals" (Hofmann-Wellenhof et al., 1997).

A common method to estimate C/N_0 for each satellite is to compare the signal plus noise power over two different bandwidths. First, the signal-to-noise ratio SNR is calculated for two different bandwidths and then the C/N_0 is provided through the *Narrowband-Wideband power ratio* (NWPR) method, which is explained in (Van Dierendonck, 1996). In a last step, navigation processing is performed using the pseudoranges from the different channels.

3.7   Chapter Conclusion

In this thesis, signal strength is an important observable because it is used to determine the direction of arrival of the entering satellite signals. Therefore, basic understanding of GNSS antennas and signal propagation is important. Accordingly, this chapter introduced relevant antenna terminology and the antenna coordinate system. After discussion of the antenna gain pattern and antenna types theoretically, the antenna gain pattern of the Leica antenna ATX1230 GG was tested. It could be seen that the antenna gain is perfectly omnidirectional in the case of an undisturbed antenna. In the GNSS signal section, the carrier link budget for GPS L1 was analysed and discussed. The nominal C/N_0 density that a typical geodetic antenna receives without attenuation, ranges from 37 to 45 dBHz. However, the value depends strongly on the elevation of the satellite. Both the omnidirectional characteristic of the Leica antenna ATX1230 GG and the nominal value for received signal power are important in the development of NORDIS.

4 Mathematical Models for Satellite Orbits

To calculate the antenna's orientation, the satellites' positions are used as reference. For this purpose, the satellites' positions must be known in respect to the antenna. Therefore, a topocentric horizontal coordinate system is chosen, one in which the origin of the coordinate system is based on the position of the receiving antenna. Thus, the positions of the satellites are indicated by azimuth and elevation angle as shown in Figure 4.1. Because the GNSS satellites are not stationary, a sufficient update rate for the satellite's positions is necessary to ensure optimal accuracy. In this chapter, the calculations of the satellite's positions and velocities are shown starting from the Keplerian elements. The calculations are shown for GPS; however, they also apply to GLONASS with the necessary modifications.
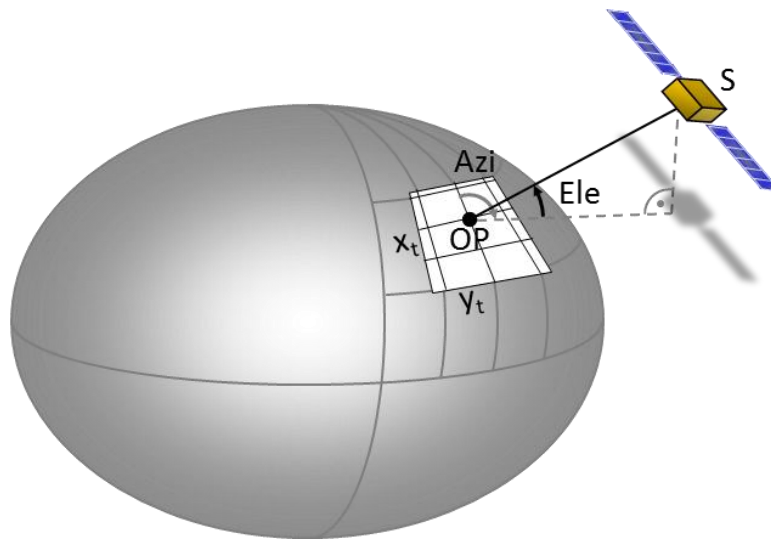
Figure 4.1 Observation vector from observation point OP at Earth's surface to satellite S.

4.1 Broadcast Ephemerides, Almanac, and GPS Time

GPS satellites circle the Earth on different orbits. The mathematical description of each orbit is specified in ephemerides, which are defined by Kepler elements (see Section 4.1.1). Each satellite broadcasts its own ephemeris to the receiver, allowing reconstruction of the orbit in meter-level uncertainty in real-time (Petovello and Driver, 2008). The data are called *broadcast ephemerides*. In addition, each satellite broadcasts orbital information for every other GPS satellite in the so-called *almanac*. According to Petovello and Driver, "The almanac was developed as a coarse equivalent to the precise ephemeris, reducing the number of bits required to transmit the necessary data at the cost of reduced accuracy of orbital propagation. The

propagated orbits are, however, still accurate enough for the intended purpose of determining which satellites are above the horizon" (p. 14). The almanac enhances the process of identification of other GPS satellites, thereby speeding up position fix at a GPS receiver.

4.1.1 Ephemerides

Table 4.1 shows the definition of the orbital parameters. Besides the six Keplerian elements, the reference time and perturbation parameters are given. The use of the perturbation parameters is explained in Section 4.2.3.

Table 4.1 Ephemeris Data Definitions

Time Parameters	
t_{0e}	Reference Time Ephemeris
Keplerian Parameters	
$\sqrt{A}$	Square root of the semi-major axis
e	First numerical eccentricity
i_0	Inclination angle at reference time
Ω_0	Longitude of ascending node of orbit plane at weekly epoch
ω	Argument of perigee
M_0	Mean anomaly at reference time
IODE	Issue of data ephemeris[12]
Perturbation Parameters	
Δn	Mean motion difference from computed value
$\dot{\Omega}$	Rate of right ascension
IDOT	Rate of inclination angle [13]
C_{us}	Amplitude of the sine harmonic correction term to the argument of latitude
C_{uc}	Amplitude of the cosine harmonic correction term to the argument of latitude
C_{is}	Amplitude of the sine harmonic correction term to the angle of inclination
C_{ic}	Amplitude of the cosine harmonic correction term to the angle of inclination
C_{rs}	Amplitude of the sine harmonic correction term to the orbit radius
C_{rc}	Amplitude of the cosine harmonic correction term to the orbit radius

4.1.2 Almanac

GPS receivers process the broadcasted almanac. However, the almanac is not only broadcasted via satellite but is also available for download. "The 2nd Space Operations Squadron[14] makes the almanacs available via their web site in the SEM and YUMA formats" (Petovello and Driver, 2008, p. 14). Both SEM and YUMA almanacs contain orbital elements. The two almanacs differ in some points. The YUMA format is easier to read for humans while the SEM almanac contains more information and the orbit elements are more precise. As an example, the almanac for two satellites in the YUMA format is shown in Table 4.2. The GPS almanacs and constellation status for GPS and GLONASS can be downloaded from the Celestrak website[15], which obtains the data from the 2nd Space Operations Squadron and from the U.S. Coast Guard Navigation Centre.

---

[12] IODE: Ephemeris Issue of Data, unique identifier for the current set of navigation data.

[13] IDOT stands for a small letter *i* with a dot representing the first derivative. It is written out because the dot cannot be distinct from the normal dot of the letter *i.*

[14] The 2nd Space Operations Squadron is a component of the 50th Operations Group, 50th Space Wing, Schriever Air Force Base, Colorado Springs. The squadron performs the command and control mission for the GPS satellite constellation.

[15] http://celestrak.com/GPS/

Table 4.2 Example of almanac data for two satellites.

```
******** Week 568 almanac for PRN-02 ********
ID:                     02
Health:                 000
Eccentricity:           0.9606838226E-002
Time of Applicability(s): 319488.0000
Orbital Inclination(rad):  0.9393024445
Rate of Right Ascen(r/s): -0.8225470083E-008
SQRT(A)  (m 1/2):         5153.543945
Right Ascen at Week(rad): -0.1525243163E+001
Argument of Perigee(rad):  3.105541110
Mean Anom(rad):          -0.1649649858E+001
Af0(s):                  0.2727508545E-003
Af1(s/s):                0.3637978807E-011
week:                    568

******** Week 568 almanac for PRN-03 ********
ID:                     03
Health:                 000
Eccentricity:           0.1333570480E-001
Time of Applicability(s): 319488.0000
Orbital Inclination(rad):  0.9277019501
Rate of Right Ascen(r/s): -0.8029019227E-008
SQRT(A)  (m 1/2):         5153.668457
Right Ascen at Week(rad): -0.2678444624E+001
Argument of Perigee(rad):  1.008704305
Mean Anom(rad):          -0.1742982268E+001
Af0(s):                  0.5817413330E-003
Af1(s/s):                0.3637978807E-011
week:                    568
```

4.1.3   GPS Time

GPS time is counted in GPS weeks (time of week) and GPS seconds beginning with 6 January 1980 at 00:00:00h. Because the week indication in the navigation message is transmitted as a 10-Bit message, the range is limited from 0 to 1023. Hence, the week number restarts at 0 every 1024 weeks. This renumbering occurred for the first time on 22 August 1999.

To determine the observation date, 1024 must be added to the week in the example in Table 4.2.

$$568 + 1024 = 1592 \tag{4.1}$$

Thus, the almanac shown in Table 4.2 is from July 2010.

4.2   Orbit Calculation

Both almanac and ephemerides contain the six Keplerian elements:

1. Semi Major Axis a
2. First numerical eccentricity e
3. Longitude of Ascending Node Ω

4. Inclination i
5. Argument of Perigee ω
6. Mean anomaly at epoch M_0

The three laws Kepler presented in *Astronomia Nova* (Kepler, 1937) and in *Harmonice Mundi* (Kepler, 1940) are a description of the motion of a first body in an orbit around a second body under ideal circumstances. This is a special case of the *two-body problem*. Thus, a description in Keplerian elements is only valuable assuming an undisturbed orbit without other elements

beyond the two objects. The respective masses must be considered to be point masses or homogeneous bodies with spherical mass distribution. In the case of a satellite, its own mass can be negligible in comparison to the mass of the Earth. The inhomogeneous Earth body, however, causes undeniable perturbation of the satellite's orbit.

To take into account orbital perturbations, GPS ephemerides contain correction terms next to the Keplerian elements. The correction values are given as harmonic coefficients for modelling time independent sine and cosine oscillations. The correction terms are valid for a short arc of the orbit, from 2 hours before to 2 hours after the time of calculation. Every 60 minutes, new data are available. Consequently, GPS orbits are composed of multiple 60-minute length arc sections, leading to small leaps between the curve-fit intervals that can be smoothed by interpolation methods.

The derivation in Section 4.2 closely follows the derivation provided by (Seeber, 2003). However, it differs from Seeber (2003) in that the transformation from the geocentric Cartesian coordinates (X_s, Y_s, Z_s) into the topocentric horizontal system (x_t, y_t, z_t) and the calculation of azimuth and elevation are additionally provided. More detailed information regarding GPS satellite orbits, including calculation of the mean orbit elements, and a discussion of numerical integration methods can be read in Beutler (1996).

4.2.1 Orbit Geometry and Undisturbed Orbital Motion

First, the orbits are calculated as undisturbed orbits. Although orbital perturbations are discussed in Section 4.2.3, the secular drift Δn, which is included in the correction terms (see Table 4.3), is used in this section.
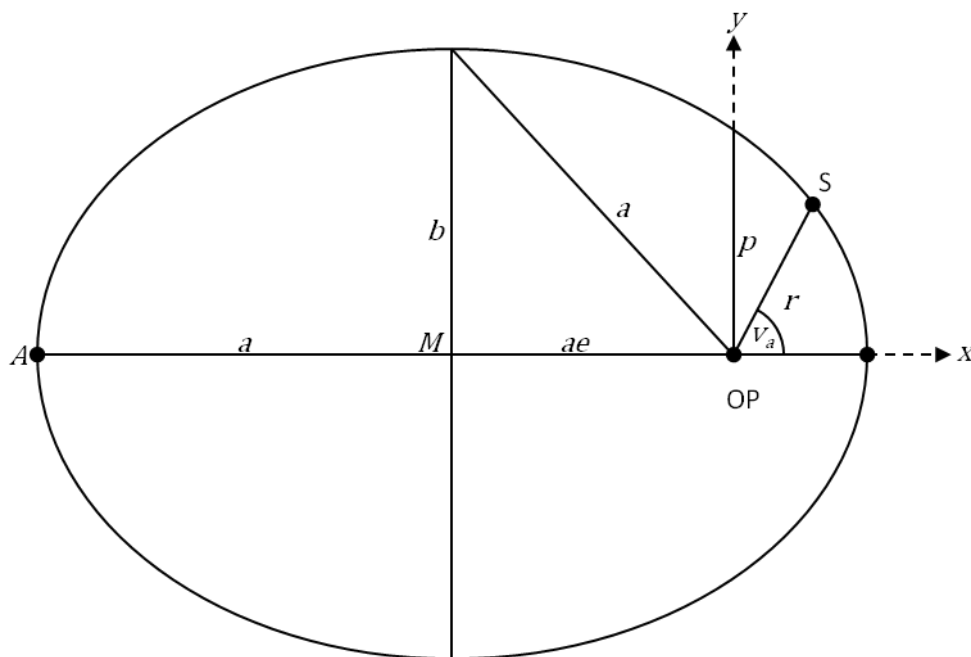
Figure 4.2 Geometry of the orbital ellipse according to Seeber (2003), with the satellite's position S.

The geometric locus of the satellite S is described by the ellipse shown in Figure 4.2. The ellipse is coplanar with the orbital plane. One focal point of the ellipse, OP is defined by the Earth.

The distance of the position vector $r(v_a)$ of a satellite S in the orbital plane is given by

$$r(v_a) = \frac{P}{1 + e \cdot \cos v_a} \tag{4.2}$$

where the symbol P represents the ellipse parameters (sometimes also referred to as *semi-latus rectum*):

$$P = a(1 - e^2). \tag{4.3}$$

Equation (4.3) uses the semi major axis a and the first numerical eccentricity e.

$$r(v_a) = \frac{a(1 - e^2)}{1 + e \cdot \cos v_a} \tag{4.4}$$

Equation (4.4) is written in polar coordinates and represents a conic section. The function $r(v_a)$ of the true anomaly v_a describes the perigee passage. The value v_a depends on the elapsed time t_C since the reference epoch t_{0e} given in the ephemerides. The prerequisites for the calculation of v_a are shown in Equations (4.5) to (4.10) while the calculation of v_a is shown in Equation (4.11).

$$t_C = t - t_{0e} \tag{4.5}$$

In Equation (4.5), t is the time of observation. The term M_C in Equation (4.6) is the corrected mean anomaly:

$$M_C = M_0 + n \cdot t_C \tag{4.6}$$

where n is the corrected mean motion and M_0 is the mean anomaly at reference time.

$$n = n_0 + \Delta n \tag{4.7}$$

The term Δn is the difference between the mean motion and the computed mean motion n_0. The term Δn is given in the ephemeris.

$$n_0 = \sqrt{\frac{GM}{a^3}} \tag{4.8}$$

The mean motion n_0 is computed using the semi major axis a and the WGS 84 constant for geocentric gravity GM.

$$GM = 3.986005 \cdot 10^{14} \ [\text{m}^3/\text{s}^2] \tag{4.9}$$

The Keplerian equation for the eccentric anomaly must be solved by iteration, using $E_0 = M_C$ as a starting value.

$$E_C = M_C + e \sin E_C \tag{4.10}$$

Finally, the true anomaly v_a can be calculated:

$$v_a = 2 \cdot \arctan\left(\sqrt{\frac{(1 + e)}{1 - e}} \cdot \tan\frac{E_C}{2}\right) \tag{4.11}$$

For further calculations, it is helpful to write the Cartesian coordinates x_s and y_s of the satellite in the orbital system (Figure 4.2) as follows. Because the satellite is within the orbital plane, z_s is zero.

$$x_s = r(v_a) \cdot \cos v_a$$
$$y_s = r(v_a) \cdot \sin v_a$$

(4.12)

The position vector in the orbital system $\vec{r}_o$ is

$$\vec{r}_o = \begin{pmatrix} r(v_a) \cdot \cos v_a \\ r(v_a) \cdot \sin v_a \\ 0 \end{pmatrix}.$$

(4.13)

4.2.2 Transformation into Equatorial System

So far, the position of the satellite is known within its orbit. To bring the position into context with all satellites and the Earth system, the coordinates must be transformed from the orbital plane to the equatorial system. The transformation is realised by using the rotation matrix $\mathbf{R}$:

$$\mathbf{R} = \mathbf{R}_3(-\Omega)\mathbf{R}_1(-i)\mathbf{R}_3(-\omega)$$

(4.14)

$$\mathbf{R} = \begin{pmatrix} \cos \Omega_0 & -\sin \Omega_0 & 0 \\ \sin \Omega_0 & \cos \Omega_0 & 0 \\ 0 & 0 & 1 \end{pmatrix} \begin{pmatrix} 1 & 0 & 0 \\ 0 & \cos i & -\sin i \\ 0 & \sin i & \cos i \end{pmatrix} \begin{pmatrix} \cos \omega & -\sin \omega & 0 \\ \sin \omega & \cos \omega & 0 \\ 0 & 0 & 1 \end{pmatrix}$$

(4.15)

In matrix notation

$$\vec{r}_e = \mathbf{R}\,\vec{r}_o$$

(4.16)

where $\vec{r}_e$ is the position vector in the equatorial system, subscript "e" refers to the equatorial system and subscript "o" to the orbital coordinate system. In Equations (4.14) and (4.15), i represents the orbital inclination and ω the argument of perigee. In general astronomy, Ω represents the right ascension angle, measured from the vernal equinox. In the GPS message, Ω_0 is measured from the Greenwich meridian.

$$\vec{r}_e = \begin{pmatrix} X_S \\ Y_S \\ Z_S \end{pmatrix}$$

(4.17)

According to the addition theorem for trigonometrically functions, Equation (4.16) can be rewritten to

$$\begin{pmatrix} X_S \\ Y_S \\ Z_S \end{pmatrix} = r(v_a) \begin{pmatrix} \cos(v_a + \omega) \cos \Omega_0 - \sin(v_a + \omega) \sin \Omega_0 \cos i \\ \cos(v_a + \omega) \sin \Omega_0 + \sin(v_a + \omega) \cos \Omega_0 \cos i \\ \sin(v_a + \omega) \sin i \end{pmatrix}.$$

(4.18)

To simplify, $r(v_a)$ is factored out in Equation (4.18).

Finally, the coordinates of the satellite are given in a geocentric elliptic, Cartesian coordinate system, in which the origin is the Earth's centre of mass (see Figure 1.13).

4.2.3 Consideration of Orbital Perturbations

This section describes the calculation of the final coordinates of the satellite's position, taking the perturbation factors into account. In the following, variables with subscript C represent the corrected value. The correction terms used are presented in Table 4.3.

Table 4.3 Description of Correction Terms

Symbol	Description
C_{us}, C_{uc}, C_{is}, C_{ic}, C_{rs}, C_{rc}	Short periodic effects of the second zonal harmonic, higher order effects and short periodic effects of lunar gravitation at the moment of shortest distance between space vehicle and the moon, and further small-term perturbations.
IDOT	Rate of change of inclination.
Δn	Secular drift in $d\omega/dt$ due to the second zonal harmonic. Also absorbs effects of sun and moon gravity and solar radiation pressure over the interval of fit.
$\dot{\Omega}$	Secular drift in right ascension of the node due to the second zonal harmonic. (Includes effects of polar motion)

Source: Seeber (2003)

In the following, the equations for the corrected values are explained. First, the final formula is shown, followed by the equations for all used parameters. The formulas are from Seeber (2003).

4.2.4 Corrected Values for Earth Fixed Coordinates

$$X_C = X'_C \cos \Omega_C - Y'_C \sin \Omega_C \cos i_C \qquad (4.19)$$

$$Y_C = X'_C \sin \Omega_C + Y'_C \cos \Omega_C \cos i_C \qquad (4.20)$$

$$Z_C = X'_C \sin i_C \qquad (4.21)$$

The corrected value of longitude of ascending node Ω_C is used.

$$\Omega_C = \Omega_0 + (\dot{\Omega} - \varpi_e)t_C - \varpi_e t_{0e} \qquad (4.22)$$

Ω_0 is the longitude of the ascending node of the orbital plane at the weekly epoch, and $\dot{\Omega}$ is the correction rate of the right ascension value. Both values are given in the ephemerides. ϖ_e is the WGS 84 value of the Earth rotation rate, whose value is

$$\varpi_e = 7.292115 \cdot 10^{-5} \frac{rad}{s} . \qquad (4.23)$$

Next, the approximation values for X'_C and Y'_C must be calculated:

$$X'_C = r_C \cos u_C \qquad (4.24)$$

$$Y'_C = r_C \sin u_C \qquad (4.25)$$

The approximation values are calculated using a corrected radius r_C and a corrected argument for latitude u_C and radius correction factor δr_C. (The correction factors are introduced below.)

$$r_C = a(1 - e \cos E_C) + \delta r_C \qquad (4.26)$$

where E_C is the eccentric anomaly as shown in Equation (4.10).

The corrected latitude argument used in Equations (4.24) and (4.25) is calculated by using the latitude correction factor δu_C.

$$u_C = \Phi_C + \delta u_C \tag{4.27}$$

The corrected inclination used in Equations (4.19) to (4.21) is calculated by using the inclination correction factor δi_C.

$$i_C = i_0 + IDOT\, t_C + \delta i_C \tag{4.28}$$

where IDOT is the rate of inclination angle given in the ephemeris.

4.2.5 Correction Factors

Radius correction factor:

$$\delta r_C = C_{rc} \cos 2\Phi_C + C_{rc} \sin 2\Phi_C \tag{4.29}$$

Latitude correction factor:

$$\delta u_C = C_{uc} \cos 2\Phi_C + C_{uc} \sin 2\Phi_C \tag{4.30}$$

Inclination correction factor:

$$\delta i_C = C_{ic} \cos 2\Phi_C + C_{ic} \sin 2\Phi_C \tag{4.31}$$

Using the argument of latitude,

$$\Phi_C = v_C - \varpi \tag{4.32}$$

The corrected true anomaly, finally, is calculated by the cosine

$$\cos v_C = \frac{\cos E_C - e}{1 - e\,\cos E_C} \tag{4.33}$$

4.2.6 Satellite Position in Topocentric Horizontal System

To calculate the observation equation at observation point OP, the geocentric Cartesian coordinates (X_s, Y_s, Z_s) need to be transformed into the topocentric horizontal system (x_t, y_t, z_t). Therefore, the coordinates of the observation point OP must be known.
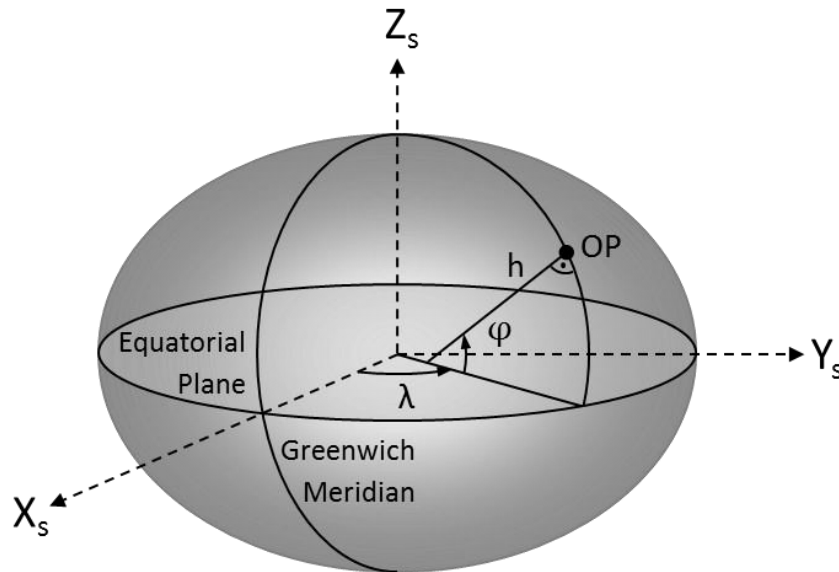
Figure 4.3 Schematic Earth with ellipsoidal coordinate system (WGS 84 ellipsoid).

The transformation according to Kahle (2004) is

$$\begin{pmatrix} x_t \\ y_t \\ z_t \end{pmatrix} = \begin{pmatrix} -\sin\varphi\cos\lambda & -\sin\varphi\sin\lambda & \cos\varphi \\ -\sin\lambda & \cos\lambda & 0 \\ \cos\varphi\cos\lambda & \cos\varphi\sin\lambda & \sin\varphi \end{pmatrix} \begin{pmatrix} X_s \\ Y_s \\ Z_s \end{pmatrix} \tag{4.34}$$

where φ is the geodetic latitude and λ the geodetic longitude of point OP.

Assuming the antenna at the origin of the coordinate system $(x_t, y_t, z_t = 0)$, azimuth and elevation values of the satellites can directly be calculated using the Equations (4.35) and (4.36), respecting the trigonometric quadrant rule[16].

$$azimuth = \arctan\left(\frac{y_t}{x_t}\right) \tag{4.35}$$

$$elevation = \arctan\left(\frac{z_t}{\sqrt{x_t^2 + y_t^2}}\right) \tag{4.36}$$

4.3 Satellite Motion

In addition to the position of the satellite, knowing how fast the satellites are moving is important. In this section, first, an exemplary satellite ground track is shown, followed by an estimation of the apparent motion of the satellites. The calculations apply the formulas introduced in Section 4.2 and are computed for GPS satellites.

4.3.1 Satellite Ground Track
The height of GPS satellites is about 20200 km above the Earth's surface. Thus, the orbits are considered to be medium Earth orbits (MEO). The orbital period for GPS satellites is half of an astronomic day (11 hours and 58 minutes). An exemplary GPS orbit is shown in Figure 4.4. Because of the Earth's rotation, the same satellite appears at the same position over the Earth

---

[16] For $x < 0$, add 180 deg; for $x > 0$, add 360 deg if result <0.

after every astronomic day (23 hours and 56 minutes). The arrows indicate the Earth's rotation and the bearing of the satellite.
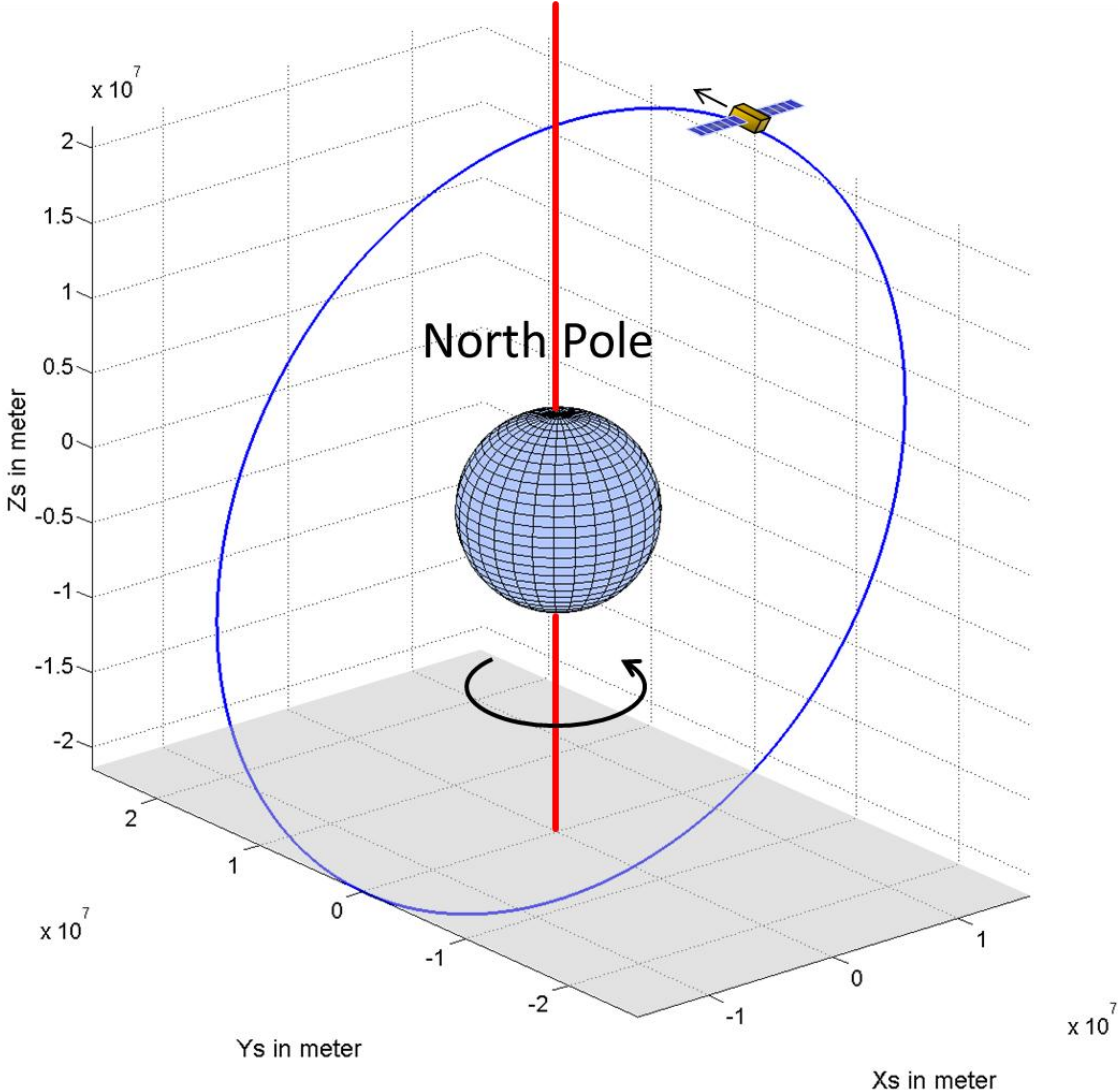
Figure 4.4 GPS satellite orbiting schematic Earth.

The ground track of a GPS satellite is shown in Figure 4.5.
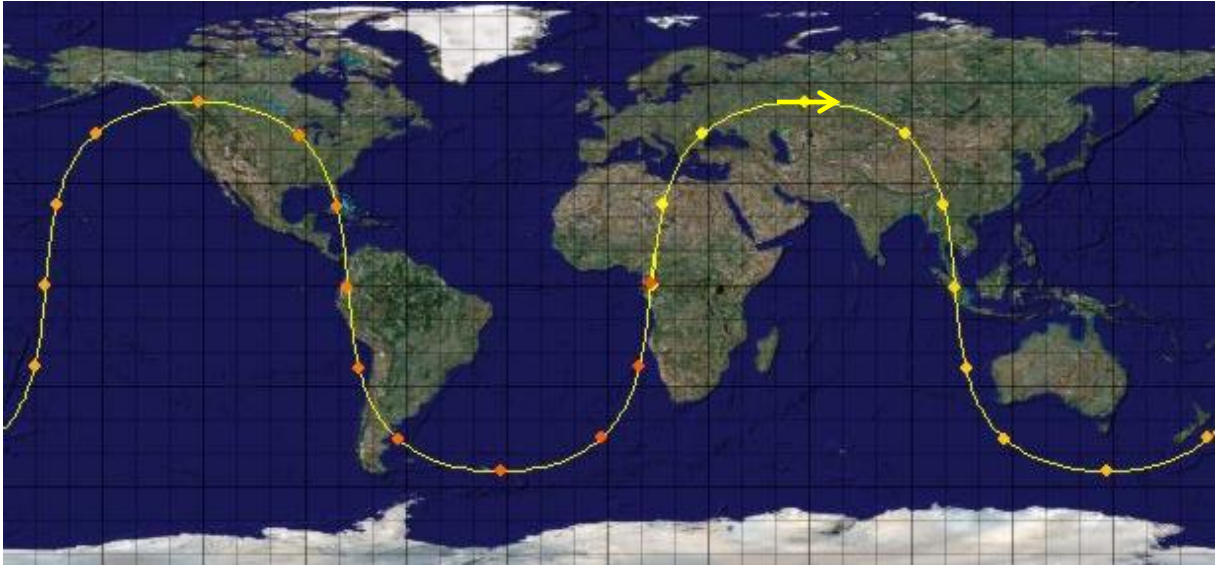
Figure 4.5 GPS ground-track (GPS Groundtrack, 2012).

Figure 4.6 and Figure 4.7 show the projection of the GPS ground track on a sphere from two different viewing angles.
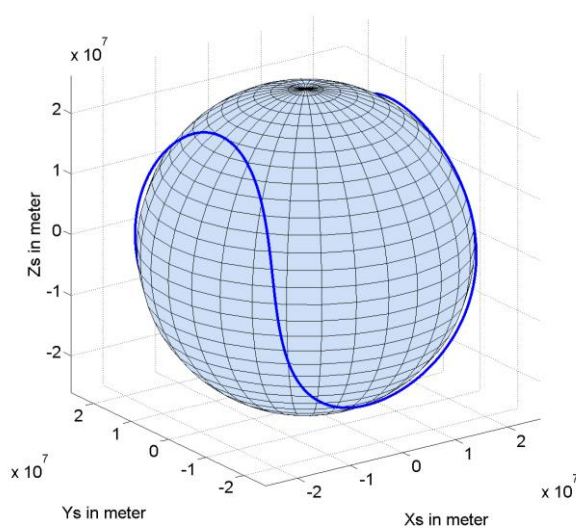
Figure 4.6 GPS ground track (viewing angle 1).
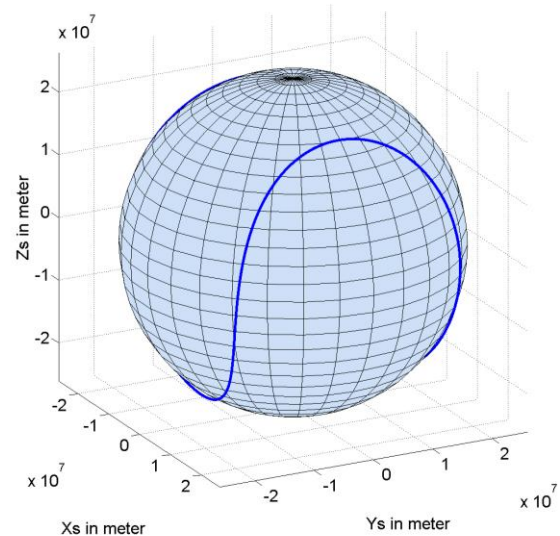
Figure 4.7 GPS ground track (viewing angle 2).

4.3.2 Apparent Motion of GPS Satellites

The apparent motion of a satellite describes the satellite's movement, seen from a specific observation point. The observation point is situated on the Earth's surface and is defined by its coordinates and height. Of specific interest for NORDIS is the change in azimuth and elevation during the period of observation.

The apparent motion of a satellite depends on the following factors:

- satellite orbit parameters (six Keplerian elements, see Section 4.2)
- Earth parameters (rotation, constant for geocentric gravity)
- position of the observer (longitude, latitude, and height)
- actual position of the satellite relative to the observer (time of observation)

The following simplified assumptions are made to estimate the influence of the motion:

- Earth is spherical, with a central symmetric gravity field
- orbital elements of the satellites do not change during one orbit
- further influences (nutation, precession, etc.) are ignored

Figure 4.8 shows the velocity of a GPS satellite in the spatially fixed system (dotted line) and the velocity in the Earth-fixed system (solid line) over one astronomic day. In the spatially fixed system, the velocity oscillates around 3.8 km/s because of the orbit eccentricity (Kepler's 2nd law). In the Earth-fixed system, the effect is superimposed with the Earth's rotation. The satellite's velocity over ground varies between 2.7 km/s and 3.2 km/s. In the Earth-fixed system, the relative velocity is smaller because the movement of the satellites is in the same direction as the Earth's rotation.
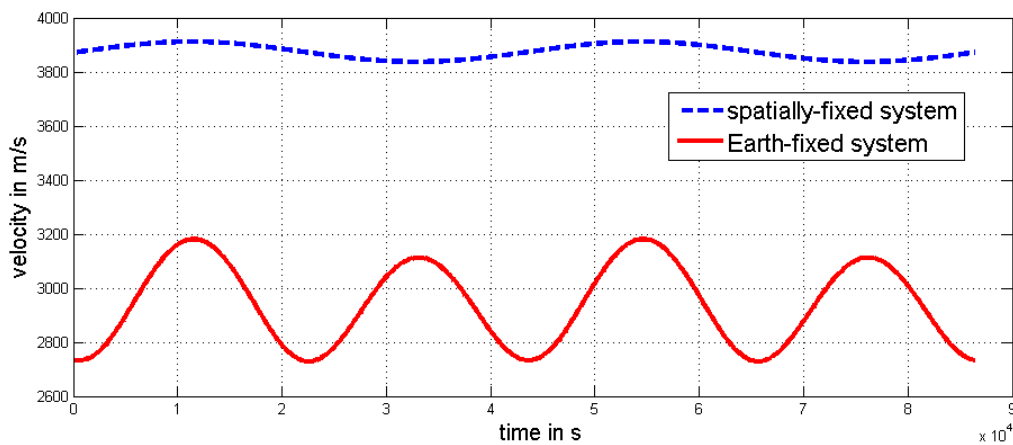
Figure 4.8 Velocity of a GPS satellite, comparing the spatial reference frame and the Earth frame.

Figure 4.9 shows the change of azimuth and elevation over one astronomic day for one satellite. The curves are calculated for an observation point in Zurich ($\varphi = 47°, \ \lambda = 8°, h = 590$ m). The satellite is visible only when the elevation is above zero.
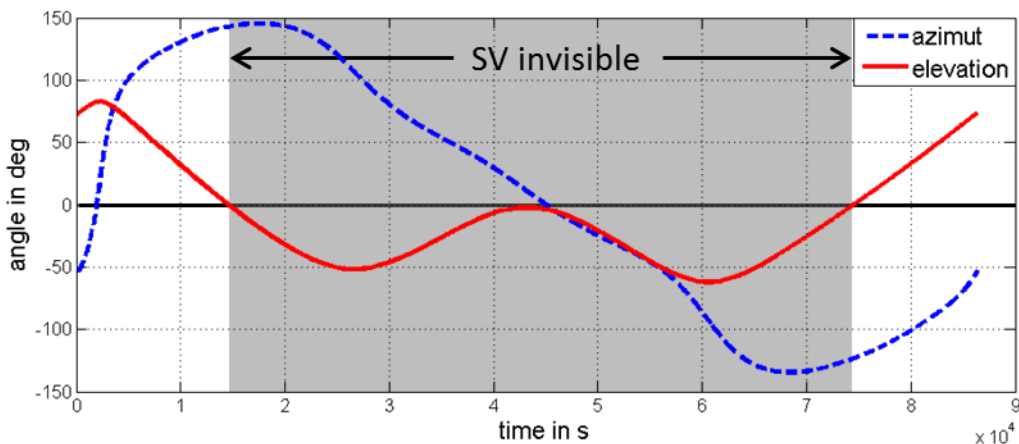
Figure 4.9 Elevation and azimuthal change over 1 astronomic day for 1 specific SV, observed at $\varphi = 47°, \lambda = 8°, h = 590$ m.

In dependence of the latitude and the longitude of the receiver and the satellite orbit, satellites can be visible once (Figure 4.9), twice (Figure 4.10) or even three times per astronomic day.
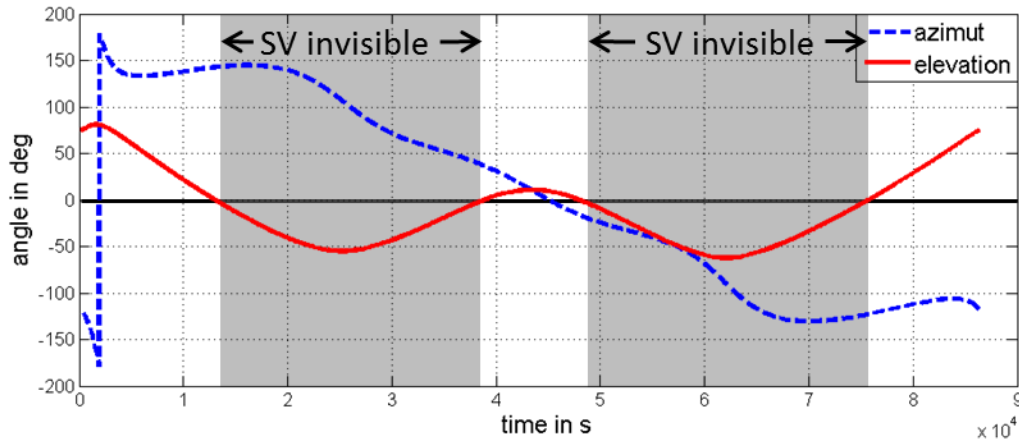
Figure 4.10 Elevation and azimuthal change over 1 astronomic day for 1 specific SV, observed at
$\varphi = 60°, \lambda = 8°, h = 590$ **m.**

Figure 4.11 shows the gradient of the change of azimuth and elevation for the data in Figure 4.9. The maximal gradient for azimuthal change is 0.062 deg/s, and the maximal gradient for elevation change is 0.0075 deg/s.
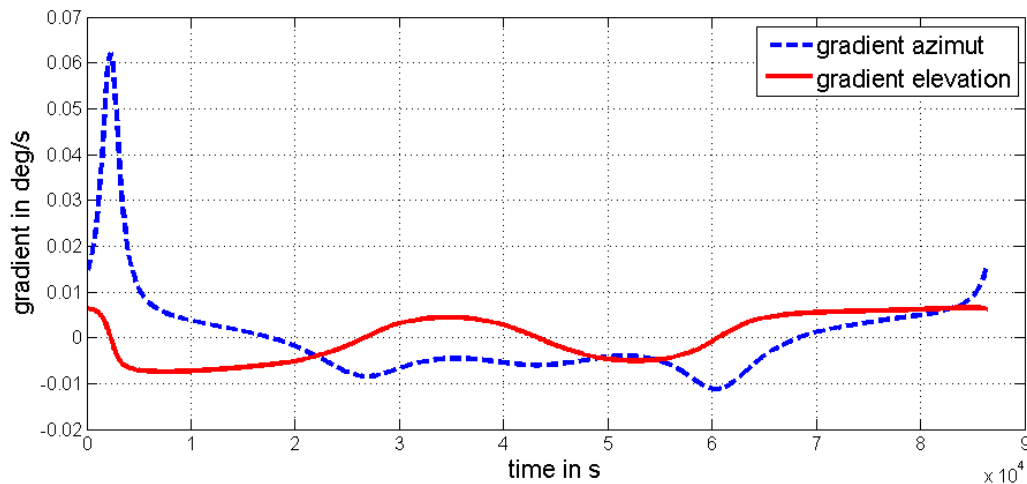
Figure 4.11 Gradient of the change of elevation and azimuth over 1 astronomic day.

4.4 Chapter Conclusion

For a detailed understanding of the coordinate systems used for the GNSS antenna orientation, the mathematic transformations between different systems were shown. The orbit calculation is discussed because, in NORDIS, the satellites' azimuth and elevation are required. The description of the orbit is based on Kepler's law. However, Kepler's law applies only under ideal circumstances. Because GNSS is under the physical influences of the Earth and other factors, several correction terms must be used to improve the quality of the orbit estimation. The apparent motion of a GNSS satellite is dependent on the orbit parameters, the coordinates of the observation place, and the Earth's rotation. It could be shown that a GPS satellite shows a maximal azimuthal change of 0.062 deg/s for an observation place in Zurich, corresponding to a maximal change of 2.28 deg per revolution of the attenuation shield. Consequently, the azimuth of the satellites cannot be assumed constant during one revolution and is, thus, corrected for each of the 720 measurements per round, as shown in Equation (6.9).

5 Orientation Finding with NORDIS

Orientation finding refers to determination of the orientation of a GNSS antenna. The orientation of the antenna is indicated as an azimuth within a specified plane of a coordinate system. This plane is either a tangent plane on the surface of the ellipsoidal coordinate system WGS 84 or the plane of a topocentric horizontal projection system. The orientation of an antenna is towards geodetic north (see Section 1.5). When using local grid coordinates, the meridian convergence must be corrected.

In the present work, three preconditions must be met:

- GNSS signal reception is possible
- the antenna is not moving during the measurement
- the antenna is levelled[17]

5.1 Required Accuracy

The projected goal for the accuracy of the antenna orientation with NORDIS is defined by the requirements of three exemplary-use cases. To comply with most of the requirements listed, accuracies for absolute orientation of the antenna with a standard measurement uncertainty of 1 deg are the goal. To achieve this threshold of 1 deg, the measurement uncertainty of all used system components for the inner and outer orientation must match this level of accuracy.

5.1.1 Initial Orientation for Total Station (Tachymeter)

The initial orientation of a total station derived from NORDIS can serve as a rough orientation. The rough orientation should be accurate enough that the total station can use *Automatic target recognition* (ATR) on a reference prism for precise orientation determination. The ATR field of view of a Leica TPS 1200 is 1.5 deg (Leica, 2007b). Accordingly, the standard measurement uncertainty of the rough orientation has to be below 1.5 deg. However, ATR can also find a prism outside the ATR field. Therefore, an ATR searching window can be defined. Generally, 5 deg is a reasonable range for the ATR searching window.

5.1.2 Orientation for Laserscanner

For georeferencing objects measured by a laserscanner, points of the object must be known by coordinates. To enable coordinate calculation beyond the scanner coordinates, one possibility is

---

[17] By means of inclination sensors, tilt of the antenna can be measured and compensated for; however, these sensors are not implemented in NORDIS.

to determine the scanner position and measuring direction. The required standard measurement uncertainty of the orientation for such application is indicated in Hesse (2007) at $u_{A_{Azi}} = 0.1$ deg.

5.1.3 Machine Control and Guidance

Besides indicating the position of a construction machine, orientation is needed for many machine control tasks, as already mentioned in Section 1.2. In Stempfhuber (2007), a standard measurement uncertainty below 1 deg is determined to be a general requirement for machine orientation. However, the required accuracy varies by machine. A standard measurement uncertainty below 1 deg is required for paving and milling machines. Earth-moving machines, such as graders (Figure 5.1), dozers (Figure 5.2), or excavators, require an orientation standard measurement uncertainty ranging from 2 deg to 20 deg.

Figure 5.1 Grader with two GNNS antennas to control the blade. Picture (L. Steiner)

Figure 5.2 Dozer with prism for height control with tachymeter. Picture (D. Grimm)

5.2 Measurement Concept of NORDIS

The measurement principle of orientation determination with NORDIS is based on signal-strength measurements. The measurand used is the C/N_0 density (see Section 3.6.7) of each satellite, which is an output from the receiver (see Section3.6.10).

5.2.1 Measurement Method

The measured C/N_0 densities are modified by a material that partially attenuates the antenna (see Figure 5.6). An attenuation shield that can be rotated around the antenna is designed (see Section 5.3). The attenuation shield is the size of a quarter of the antenna. Attenuation of the received energy is dependent on the azimuth and elevation of the satellite and the angular position of the attenuation shield. When the azimuth and elevation of the satellite and the angular position of the attenuation shield are known, the DOA of the satellites' signals can be calculated.

5.2.2 Measurement Model

The measurement model of NORDIS can be described by the following measurement function:

$$\bar{O} = f(Azi_{SV_t}, \alpha_t, \tau, C/N_{0_t}, Ref_{Ele_\alpha}) \tag{5.1}$$

where the output quantity $\bar{O}$ is the averaged orientation of the antenna [see Equation (5.4)] and the input quantities are:

Azi_{SV_t}:   azimuth of satellite SV at time t

α_t: angular position of the attenuation shield at time t

τ: transformation of the antenna orientation into the superior coordinate system

$C/N_{0_{SV_t}}$:   carrier-to-noise density of satellite at time t

Ref_{Ele_α}:   value of the reference curve for the corresponding elevation at angular position α (see Section 6.2)

Because the used quantities (bold face in Table 5.1) are derived quantities, their uncertainties depend on the uncertainties of their base quantities as shown in Table 5.1.

Table 5.1 Base and Derived Quantities Used in the Measuring Model

No.	Base Quantity		Derived Quantity	Standard Measurement Uncertainty	Specification	Type
1.1	solution of GNSS receiver	⇨	position of the antenna	2 m	navigation solution	A
1.2	ephemerides	⇨	position of the satellites	3 m	broadcast ephemerides	A
⇩	⇩		⇩	⇩	⇩	⇩
1	ephemerides and antenna position	⇨	azimuth of the satellite Azi_{SV_t}	**0.0002 deg**	calculated from 1.1 and 1.2 with a distance between antenna and satellite of 20200 km	A
2	event timestamp and revolution speed	⇨	angular position of the attenuation shield α_t	**0.03 deg**	uncertainty of the inner orientation (see Section 7.2.3)	B
3.1	uncertainty of theodolite measurement	⇨	autocollimation	0.0003 deg	value from literature (Ingensand, 2004)	B
3.2	uncertainty of pillar coordinates = 3 mm	⇨	uncertainty of reference azimuth	0.007 deg	calculated for 2 pillars with 34 m distance	A
3.3	uncertainty of the gear transmission	⇨	uncertainty of offset between collimation mirror and pulse encoder	0.03 deg	measured with a second autocollimation mirror (see Section 5.3.8)	A
⇩	⇩		⇩	⇩	⇩	⇩
3	autocollimation and uncertainty of reference azimuth	⇨	outer orientation (NORDIS- body) τ	**0.03 deg**	combined from 3.1, 3.2, and 3.3	C
4	output from GNSS receiver	⇨	C/N$_0$ (carrier-to-noise density) $C/N_{0_{SV_t}}$	0.5 dBHz ⇩ **?? deg** ⇩ **0.75 deg**	value from literature (National Instruments, 2010) assumption	B
5	averaged reference measurements	⇨	reference value for cross-correlation Ref_{Ele_α}	**0.1 deg**	comparison of two independent data sets (see Section 7.1)	A

The measurement uncertainty of the satellites' azimuth (No. 1 in Table 5.1) depends on the positions of the satellites and the antenna. From the two position uncertainties, one angular uncertainty can be derived. The measurement uncertainty of C/N_0 (No. 4 in Table 5.1) cannot be converted geometrically into an angular value. Therefore, the measurement uncertainty is determined empirically using multiple measurements. In addition, this value depends on the number of satellites used and the total number of measurements. An analysis of this influence is described in Chapter 7. For the estimation of the combined standard measurement uncertainty of NORDIS, an a priori value of 0.75 deg is assumed. The values for the degrees of all uncertainties of the input quantities are summarised in Table 5.2.

Table 5.2 Numerical Values of the Uncertainties of the Input Quantities

Input Quantity	Uncertainty of Input Quantity	Value in deg	Type	No.
Azi_{SV_t}	$u_{A_{Azi}}$	0.0002	A	1
α_t	u_{A_α}	0.03	B	2
τ	u_{A_τ}	0.03	C	3
$C/N_{0\,SV_t}$	$u_{B_{C/N_0}}$	0.75	B	4
Ref_{Ele_α}	$u_{C_{Ref}}$	0.01	A	5

Finally, the combined standard measurement uncertainty $u_{c_{\bar{O}}}$ of the output quantity $\bar{O}$ can be calculated using Equation (5.2), whereby the uncertainty of the carrier-to-noise density $u_{B_{C/N_0}}$ is the limiting factor for $u_{c_{\bar{O}}}$.

$$u_{c_{\bar{O}}} = \sqrt{0.0002^2 + 0.03^2 + 0.03^2 + 0.75^2 + 0.1^2} = 0.77\ deg. \tag{5.2}$$

Figure 5.3 illustrates the measurement model.
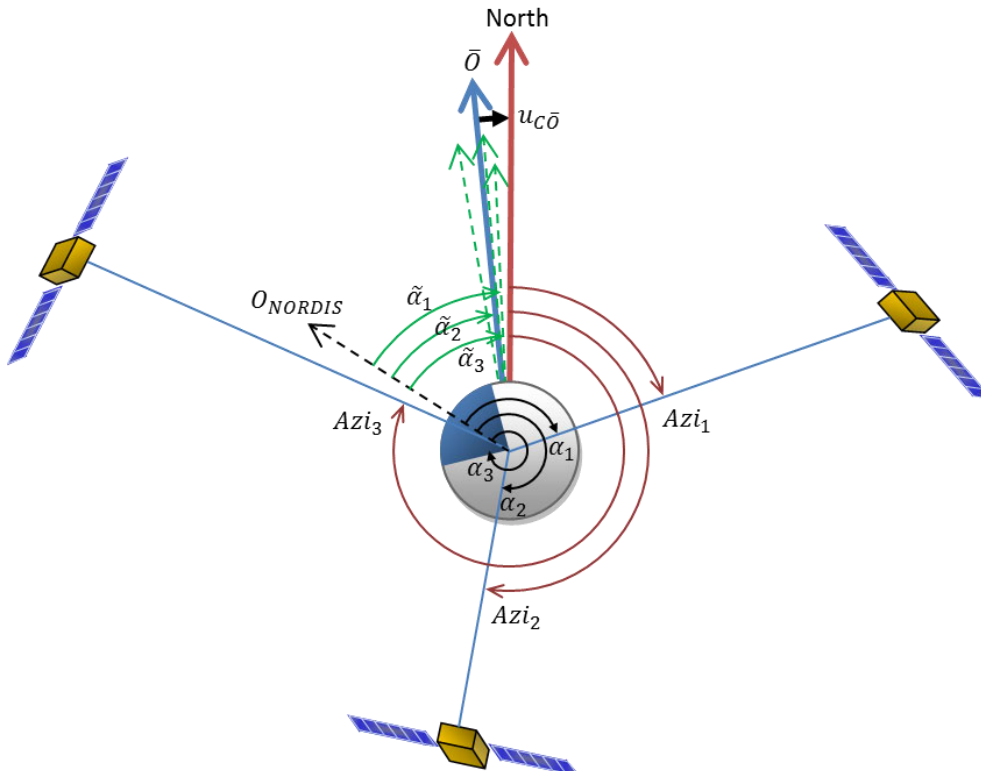
Figure 5.3 Illustration of the measurement model.

The values α_j (drawn in black) indicate the angle of entrance of the satellites' signals, calculated from the C/N$_0$ densities of the different satellites. These angles are indicated in regard to the zero direction of the inner orientation O_{NORDIS}, which is thus unknown. The values Azi_j (drawn in red) are the satellites' azimuth values, calculated from the antenna position and the satellites' positions given in the ephemerides. The values $\tilde{\alpha}_j$ (drawn in green) indicate an approximation of the north direction for each satellite, calculated by subtracting the satellites' azimuth from the observed angle of entrance of the satellites' signals [see Equation (5.3)].

$$\tilde{\alpha}_j = \alpha_j - \mathrm{Azi}_j \tag{5.3}$$

The values $\tilde{\alpha}_j$ vary because of the measurement uncertainty of the input quantities used (see Table 5.1). The resulting orientation $\bar{O}$ is calculated by

$$\bar{O} = \frac{\sum \tilde{\alpha}_j}{n} \tag{5.4}$$

and has a combined measurement uncertainty of $u_{C_{\bar{O}}}$, as indicated by Equation (5.2).

5.2.3 Measurement Procedure

To perform the measurement, NORDIS is mounted on a geodetic pillar or tripod. The measuring system has to be levelled, and direct reception of GNSS signals must be possible. The GNSS measurements (including C/N$_0$ density and GPS timestamp) are recorded on the GNSS receiver at a rate of 20 Hz. The attenuation shield is rotating continuously with a revolution period as close to 36 s as possible to ensure a resolution of one C/N$_0$ density value per 0.5 deg. The rotation speed of the attenuation shield is kept constant by the motor controller. After each complete revolution, the encoder triggers a pulse that is time tagged with GPS time by the GNSS receiver and recorded in a text file. Once the measurement has been taken, the GNSS C/N$_0$ data and the recording of the timestamps are combined, to time reference the C/N$_0$ measurements and the angular position of the attenuation shield. The procedure for combining the data and timestamps and the data analysis are described in Appendix 9.9.

5.3 Measuring System

To test the concept and take test measurements, preliminary hardware was designed (see Figure 5.4). The NORDIS hardware includes a geodetic GNSS receiver and can be operated with different types of antennas. For georeferencing of the measurements, NORDIS can be mounted on a tripod or on a geodetic pillar. The attenuation shield must be able to turn above the antenna for a period of time ranging from several minutes to 24 hours and must not impede the cable connection between the antenna and the receiver. The position of the attenuation must be known with respect to the body of the hardware and with respect to the superior coordinate system. The orientation between attenuation and the hardware body is the *inner orientation*, realised by an encoder. Correspondingly, the connection between the hardware body and the superior coordinate system is the *outer orientation*, realised by autocollimation (see Section 5.3.7).

The functional model of NORDIS consists of the following components:

- GNSS antenna
- GNSS receiver
- attenuation shield (see Figure 5.5 and Figure 5.6)
- turntable for attenuation
- encoder for inner orientation
- autocollimation mirror for outer orientation
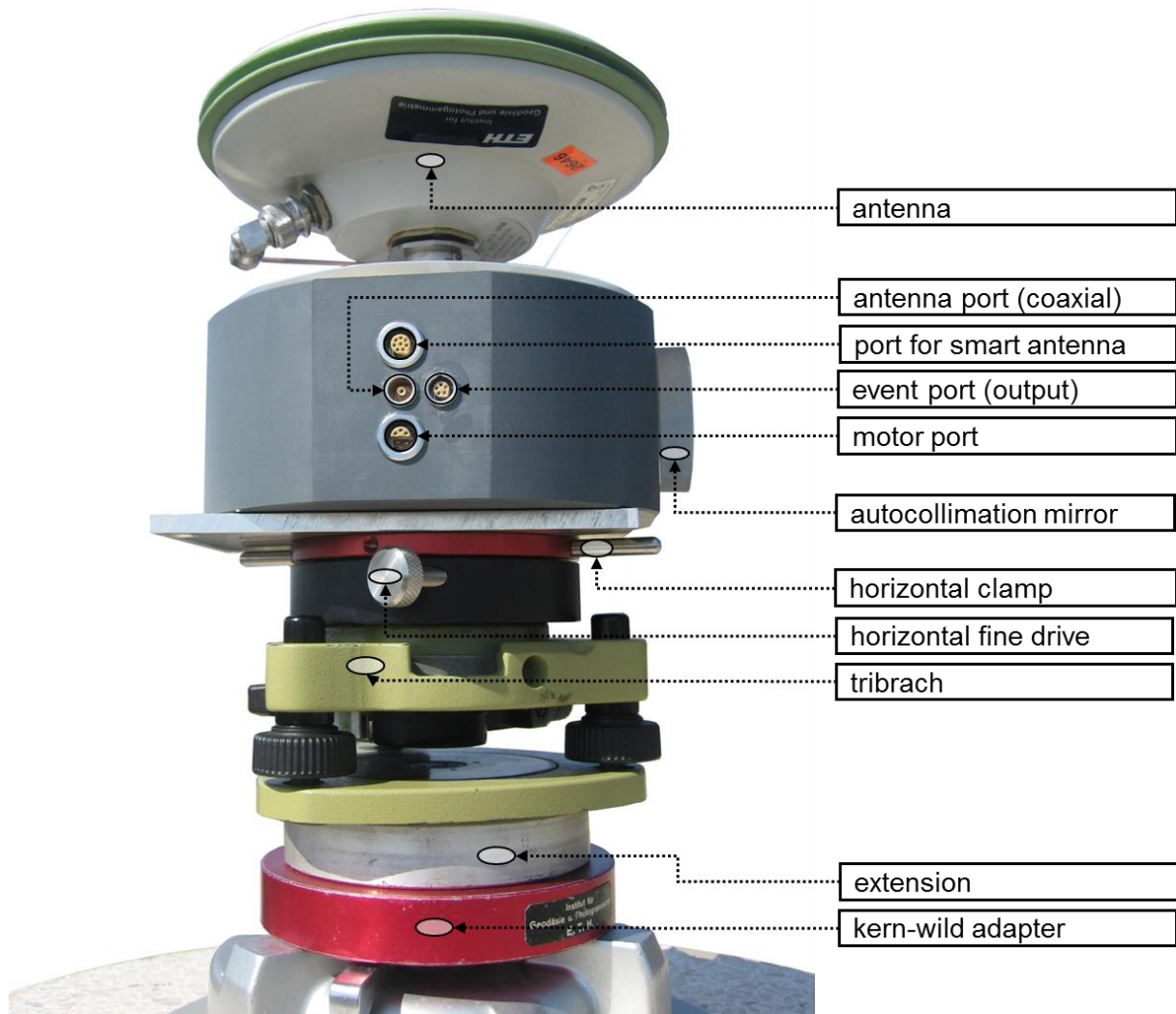
Figure 5.4 Front view of NORDIS with labelled components. (Picture: D. Grimm)

Figure 5.4 shows the measuring system NORDIS mounted on a geodetic pillar. Because the pillar has a Kern locking device, an adapter is used. An extension brings the autocollimation mirror to the same height as the telescope of the theodolite (see Section 5.3.7). The tribrach serves to level the measuring system while the horizontal fine drive is used to align NORDIS towards the autocollimation theodolite. The motor port serves as the power supply (12 V) and regulates the motor. The coaxial antenna port is used to connect an analogue (e.g. Leica ATX 1202 GG[18]) antenna with the receiver by a coaxial cable connection. For antennas with inbuilt receiver (e.g. Leica ATX1230 GG "smart antenna"), a digital port is added.

---

[18] *GG* stands for GPS and GLONASS.
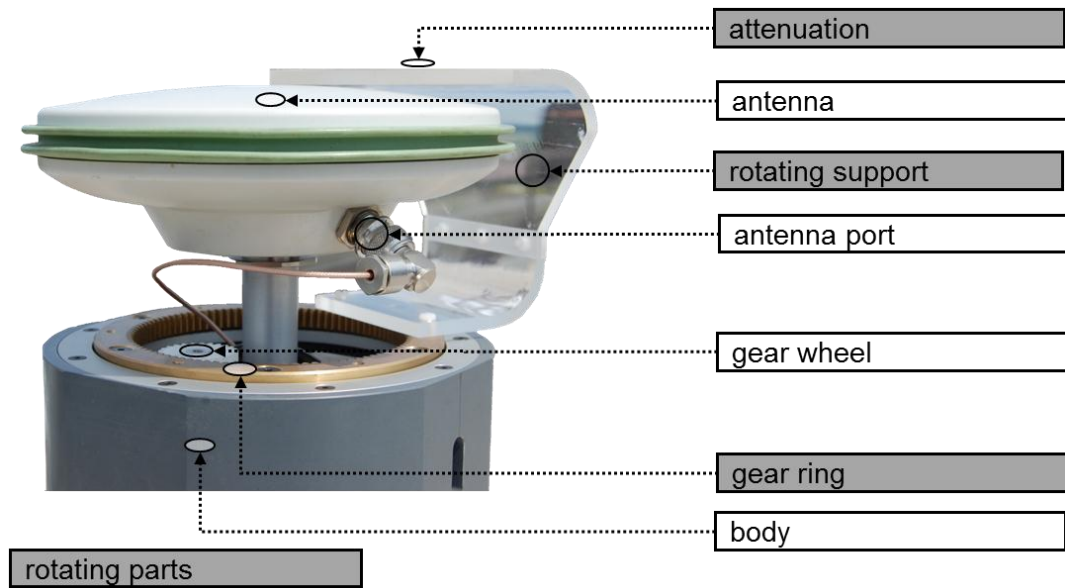
Figure 5.5 Detailed view of the rotating parts (grey in the legend) of NORDIS. (Picture: D. Grimm)
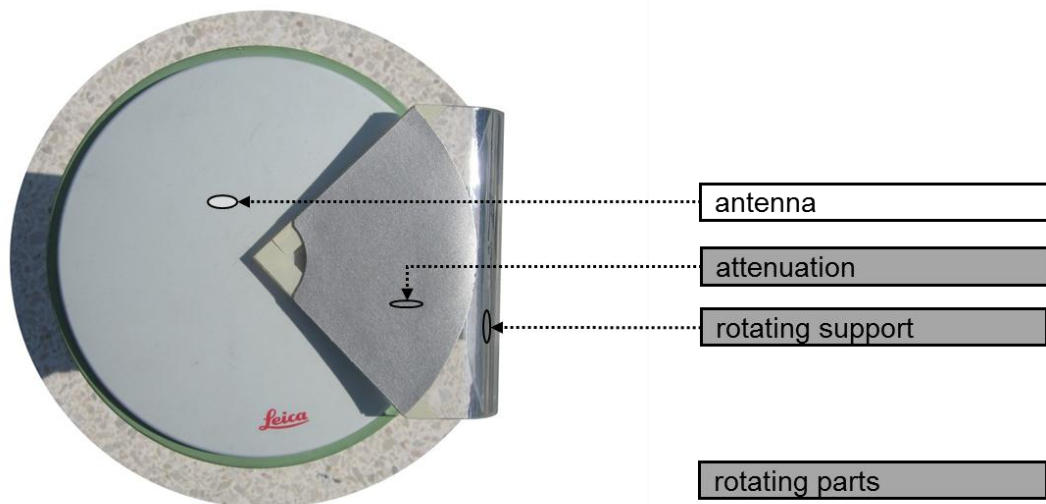
Figure 5.6 Top view of NORDIS with antenna and attenuation. (Picture: D. Grimm)

5.3.1 GNSS Antennas

The following antennas have been used for test measurements:

- Leica AX1202 GG (Leica 1200)
- Leica ATX1230 GG (smart antenna)

The Leica 1200 was connected with the receiver via coaxial cable. The Leica smart antenna and was connected via the digital port or Bluetooth® link. For description of the antennas, see Section 3.4.

5.3.2 GNSS Receiver

The receiver must match the antenna type used. In addition, the receiver must have an event input interface (see Appendix 9.5) to receive the pulses from the encoder of the inner orientation. The received pulses are tagged with GPS time and sent via COM port to the computer, where the timestamp is logged.

5.3.3   Attenuation

The signal propagation can be influenced by introducing a particular material to serve as attenuation between the antenna and the transmitter. The material must have specific characteristics to attenuate the intensity of an electromagnetic wave in the 1.5 GHz L-band. It should not absorb the signal completely. The signal has to be constantly detectable to maintain the normal positioning functionality. The influence the attenuation shield has on the position solution is discussed in Section 7.2.1. In Grimm (2008a), the specifications for the material were defined as follows.

When electromagnetic waves hit any material, one of the following physical effects occurs:

- Transparency: The material reflects the energy. Reflection occurs when the material consists of a highly conductive surface, such as metal.
- Penetration: The energy is transmitted through the material. Transmission occurs when the material has non-conductive characteristics.
- Absorption: The energy is absorbed. In this case, the material is able to absorb the wave completely or partially. In the absorption process, the energy is converted into heat.

Figure 5.7 and Figure 5.8 show test measurements performed with different materials. To evaluate the attenuation factor ε of the materials, the antenna was covered sequentially by different absorbing materials. The thin curve shows the C/N_0 during the test. In the time between the samples, the antenna was completely uncovered and the signal intensity increases to the regular value of about 47 dB.
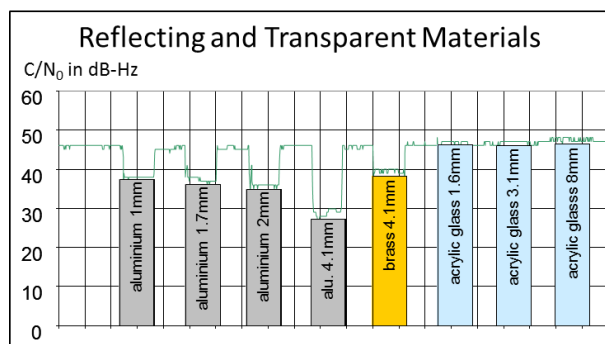
Figure 5.7 C/N_0 for different reflecting and transparent materials (Grimm, 2008a).
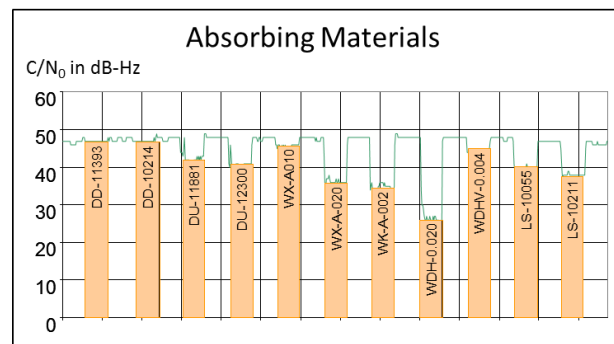
Figure 5.8 C/N_0 for different absorbing materials (Grimm, 2008a).

Figure 5.7 shows five samples of reflecting and three samples of transparent materials. Aluminium and brass attenuate the signal power dependent on its thickness while acrylic glass does not influence the signal at all. Figure 5.8 shows 11 samples of absorbing materials. The material designations are written on the bars. Specifications for the different materials can be found in Appendix 9.6. Beside the material, the absorption rate depends on the signal wavelength. According to the specifications, the materials in Figure 5.8 have been specially designed and developed for electromagnetic influence suppression and absorption. Nevertheless, the materials are also reflective. For that reason, whether the attenuation effects shown in Figure 5.8 derive from the absorption or from the reflection of the energy cannot be determined.

5.3.4   Turntable for Attenuation Shield

The turntable consists of a bracket, the rotating support used to hold the absorbing material. The rotating support is made of acrylic glass, which does not affect the incoming signals, as shown in Figure 5.7. The rotating support is mounted on a gear ring, which is driven by a gear

wheel on top of the motor. Figure 5.9 shows the C/N_0 density measured with a Leica antenna ATX1230 GG during four revolutions of the rotating support without absorbing material. As can be seen by the constant values in Figure 5.9, the acrylic bracket does not influence the C/N_0 density of the measured satellites. The C/N_0 densities for the nine satellites differ because of the different elevations (see Section 3.3.3).
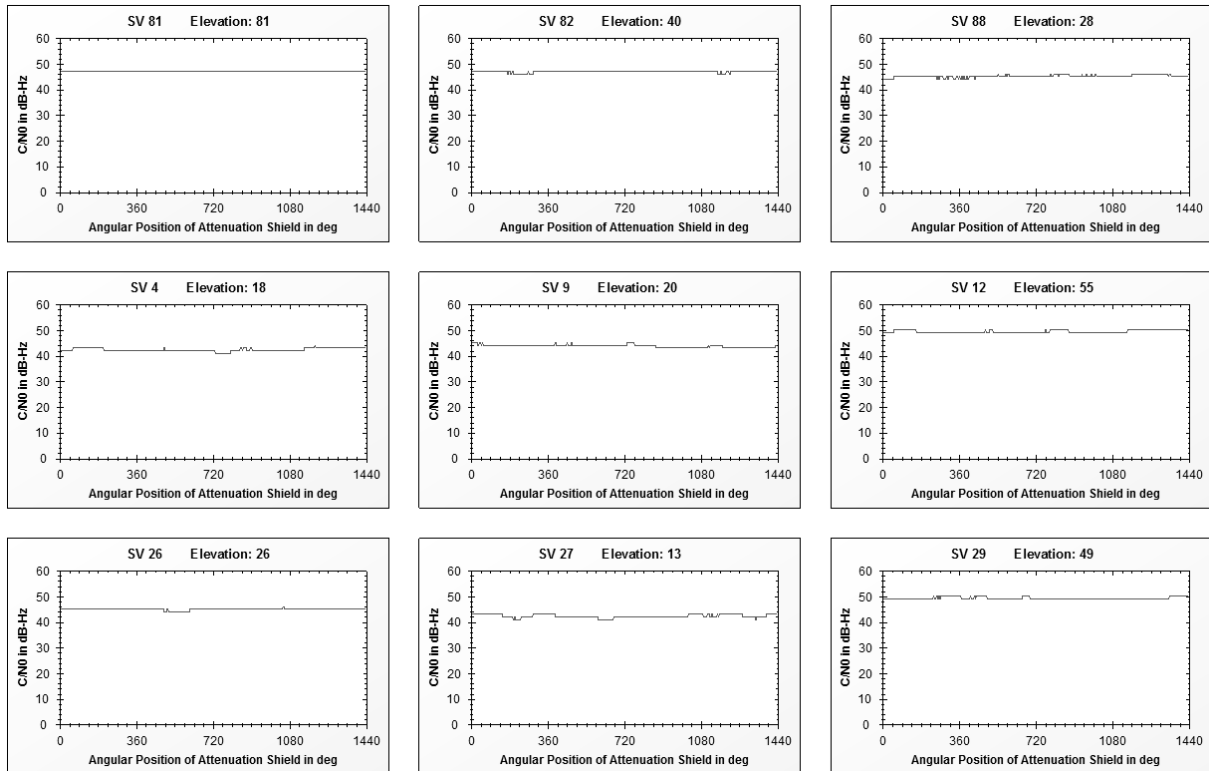
Figure 5.9 C/N_0 densities from nine different satellites during four revolutions of the acrylic bracket without attenuation material, measured with the Leica antenna ATX1230 GG.

The objective of the attenuation is to determine the angle of entrance of each satellite's signal. As shown above, a specific attenuation can distinctly influence the C/N_0 (Figure 5.7 and Figure 5.8). When the material covers the antenna only partially, the influence on the incoming signals varies depending on the angle of entrance, which is given by the azimuth of the satellite. The shape of the attenuation shield that covers one quarter of the antenna (Figure 5.6) was effective. A smaller size could not sufficiently influence the signal while a larger size would unnecessarily attenuate the signal.

This quarter-sized shield can be rotated around the antenna to affect every part of the antenna successively. Thus, a geometric relation can be determined between the position of the attenuation and the corresponding changes in the received satellite signals. By analysing the C/N_0 in respect to the rotating attenuation, the DOA of the satellite signals can be determined.

5.3.5 Motor Speed

The value for the motor speed is a trade-off between angular resolution and time needed for one revolution. A time of 36 s for one revolution leads to 720 measurements per revolution by collecting the data at 20 Hz. Consequently, an angular resolution of 0.5 deg is achieved. The value that has to be sent to the motor controller for a revolution time of 36.07 s is 424. Because of the discrete steps of the motor controller, it is the closest possible value to 36 s.

5.3.6 Encoder for Inner Orientation

The motor implemented in NORDIS has a built-in encoder with 512 pulses per revolution and a built-in gear reduction with a ratio of 189733/2500. The gear reduction from the motor to the gear ring has a ratio of 100/25. Accordingly, the encoder counts 155429.2736 pulses for each revolution of the attenuation. Theoretically, this setup would lead to an angular resolution of 0.002 deg, which could be read out via the RS 232 interface. However, the interface is subject to a time delay because a query must be sent from the computer to the controller to obtain the position reading. Within this time delay, the attenuation moves further. To reach the requested standard measurement uncertainty of < 1 deg, the position of the attenuation together with the corresponding timestamp must be known within a time uncertainty of 5 ms. This value cannot be achieved with the motor encoder when the motor is continuously in motion. Consequently, the inner orientation is realised by an additional pulse sensor that triggers a pulse when a magnetic mark below the attenuation passes the sensor.

To link the shield position with the GNSS measurements, the timestamp must be given in GPS-time. The pulse indicates the time when the attenuation passes the encoder. At this point, the angular value for the rotating attenuation is zero. In the following, the timestamps are termed *zero cross*. The electrical pulse from the encoder is sent to the event input interface of the GNSS receiver, where it is tagged with the actual GPS-time. On the connected laptop, the timestamps are stored in a text file. Because a timestamp is created in the GNSS receiver, any delay caused between the GNSS receiver and the laptop is irrelevant. The evaluation of the uncertainty of the inner orientation can be found in Section 7.2.3.

5.3.7 Autocollimation for Outer Orientation

The reference of NORDIS within the superior coordinate system is necessary for the absolute comparison. Autocollimation is chosen for this purpose because an autocollimation mirror can be easily mounted on the body of the measuring system and autocollimation ensures an orientation standard measurement uncertainty below 0.001 deg. The orientation of the NORDIS hardware is expressed in relation to the surface normal of the mirror. For autocollimation, a theodolite with an illumination is used. The illumination projects the theodolite's reticle through the telescope. On an autocollimation mirror, the image of the reticle is reflected. As the main principle of autocollimation, the reflected image is brought in collimation with the real reticle by aligning the mirror of NORDIS perpendicular to the theodolite. More details are explained in Appendix 9.7. For adjusting, the horizontal fine drive of NORDIS is used. As an alternative to autocollimation, a sighting telescope could be mounted on the hardware body.
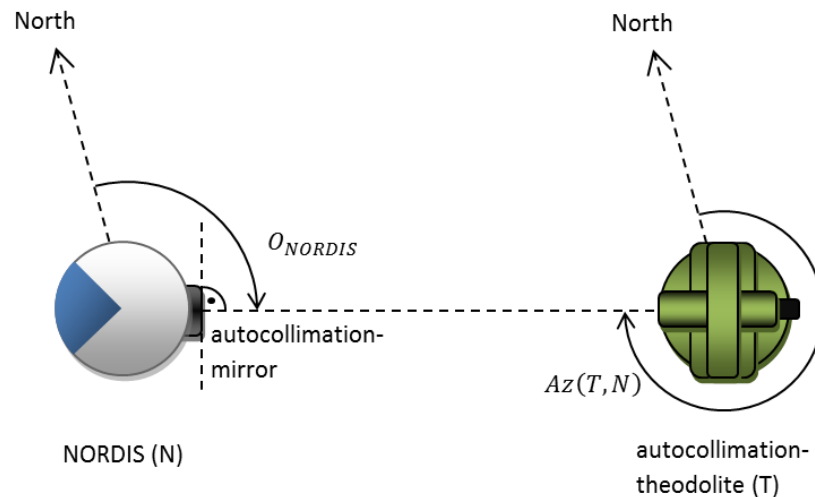
Figure 5.10 Configuration of autocollimation procedure with theodolite and NORDIS (top view).

Once the autocollimation mirror is perpendicular to the theodolite's line of sight, as shown in Figure 5.10, the theodolite is used to measure the direction to the mirror. To determine the azimuth of the normal to the mirror, the theodolite must be oriented. The orientation of NORDIS, given in direction of the surface normal of the mirror in deg, is calculated using Equation (5.5).

$$O_{NORDIS} = Az(T,N) - 180 \qquad (5.5)$$

where $Az(T,N)$ is the measured azimuth between theodolite and NORDIS.

5.3.8 Constant Offset between Inner and Outer Orientation

The location of the pulse encoder used for the inner orientation does not coincide with the surface normal of the autocollimation mirror. This constant offset, which was inevitable for constructive reasons, was determined by calibration measurements. For the calibration measurements, a second autocollimation mirror was mounted on the rotating support (see Figure 5.12). Through autocollimation measurements with a theodolite, the planes of the two mirrors were brought to coincidence. The determined offset value is 128.72 deg, with a standard measurement uncertainty of 0.03 deg.
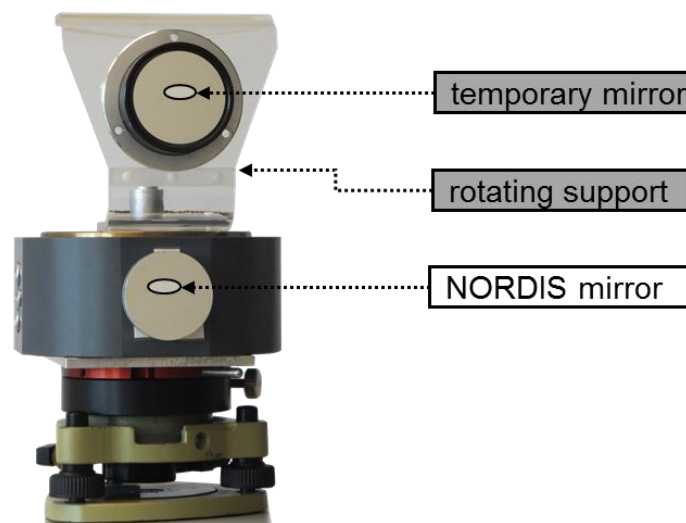
Figure 5.11 NORDIS with a second temporary autocollimation mirror to calibrate the constant offset between pulse encoder and NORDIS mirror.

5.4 Experimental Setup

Most measurements were taken on the roof of the HIL building at the Hoenggerberg campus of ETH Zurich. NORDIS was mounted on a geodetic pillar with known coordinates (Figure 5.12 and Figure 5.13). The coordinates of the pillar serve to calculate the reference orientation and are used to estimate the influence of the attenuation shield on the position solution of the GNSS antenna (see Section 7.2.1).

Figure 5.12 NORDIS on measurement pillar 1013 on the HIL building. View from south. (Picture: D. Grimm)

Figure 5.13 NORDIS on measurement pillar 1013 on the HIL building. View from north. (Picture: D. Grimm)
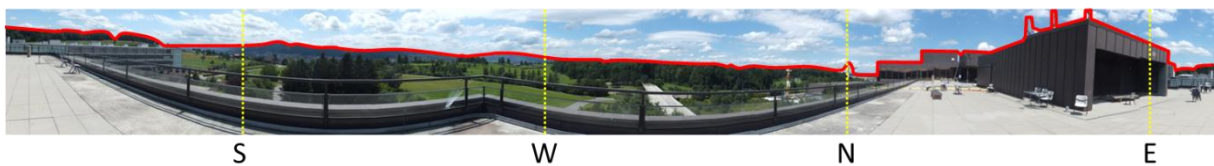
Figure 5.14 360 deg panoramic view from the pillar 1013. (Picture: L. Steiner)

Figure 5.14 shows the field of view as a 360 deg panoramic view. The skyplot is shown in Figure 5.15 and Figure 5.16. On a second pillar, the autocollimation theodolite was mounted to determine the outer orientation. In this present work, three data sets with observation times of 24 h were acquired. In addition, several shorter test measurements were performed. To verify the independency of the location (and thus the specific multipath environment of such a location), measurements were also conducted outside the ETH. Two different methods for data recording were used, as explained in the following sections.
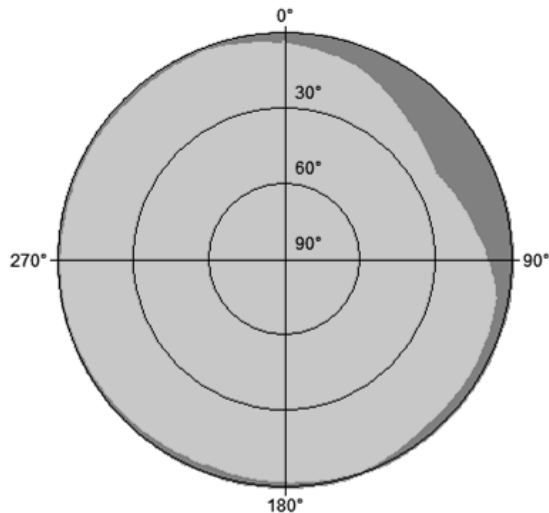
Figure 5.15 Skyplot of pillar 1013
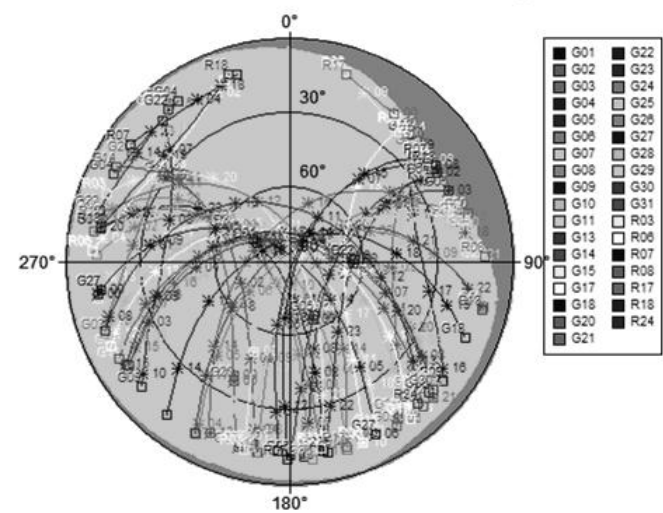
Figure 5.16 Skyplot of pillar 1013 with satellites in view (almanac from 14.04.2012)

5.4.1 Real-Time NMEA Stream

GNSS observational data can be given out from the receiver in real time as NMEA stream. The GNSS receiver sends the data in the NMEA format via serial interface to a connected laptop. The NMEA-0183 format is defined by the National Marine Electronics Association (NMEA). Table 5.3 shows the seven most commonly used sentences, defined in the NMEA standard.

Table 5.3 NMEA Standard Sentences

GGA	GPS Fix Data, fixed data for the Global Positioning System
GGL	Geographic Position – Latitude/Longitude
GSA	GPS DOP and Active Satellites, degradation of accuracy and the number of active satellites in the Global Satellite Navigation System
GSV	GNSS Satellites in View, satellites in view in the Global Satellite Navigation System
RMC	Recommended Minimum Specific GNSS Data
VTG	Course over Ground and Ground Speed, horizontal course and horizontal velocity
ZDA	Time & Date

Source: Zogg (2009)

For NORDIS, the GSA and GSV sentences from the NMEA stream are used as input. However, the values for azimuth, elevation, and C/N_0 are only given as integers, complicating attaining the required standard measurement uncertainty of < 1 deg. The maximal measurement frequency is 20 Hz using a cable connection and 5 Hz using the Bluetooth® link.

5.4.2 Data Recording on the Receiver

As a second possibility, the measurements can be stored directly on the memory card of the GNSS receiver. Because the data are stored in a proprietary format, additional software is needed to export the desired values for azimuth, elevation, and C/N_0 (see Appendix 9.9.2). The values are stored in a higher resolution than the data sent via NMEA. However, because the data are stored on the memory card, they cannot be processed in real time. Nevertheless, a combination of real time NMEA and recording for post processing would be possible though not implemented here.

5.5 Chapter Conclusion

This chapter introduced the measuring concept and the hardware of the **NOR**th **D**irection **I**ndication **S**ystem, NORDIS. The goal for the standard measurement uncertainty for NORDIS was fixed at 1 deg to meet the accuracy requirements of three use cases. NORDIS has several components that contribute to the final results. Therefore, the uncertainties of the single components are listed. A pre-analysis of the uncertainties of the used components has shown that the uncertainty of the carrier-to-noise density is limiting the system. Because it is difficult to estimate the uncertainty of the relationship between the attenuated carrier-to-noise density values and the angular position of the attenuation shield, a certain degree of fuzziness must be expected therefore. In the last part, the experimental setup and method of data collection were described.

6 Orientation Calculation

The C/N_0 time series of different satellite signals measured with NORDIS are not only influenced by the rotating attenuation shield but also vary depending on the satellite's elevation and azimuth. Figure 6.1 shows the measured C/N_0 density of two exemplary satellites (SV 16 and SV 21) as a function of the turning attenuation shield. Both satellites were received at the same time. During the time of data acquisition, the attenuation shield performed four revolutions. The influence of the attenuation caused the changes in the received signal strength. Because the attenuation shield rotated with a constant speed $(T = 36.07\,\text{s})$, the changes in C/N_0 were periodical. In consequence of the different azimuths of the satellites, the first minimum occurs sooner for SV 16 than for SV 21.
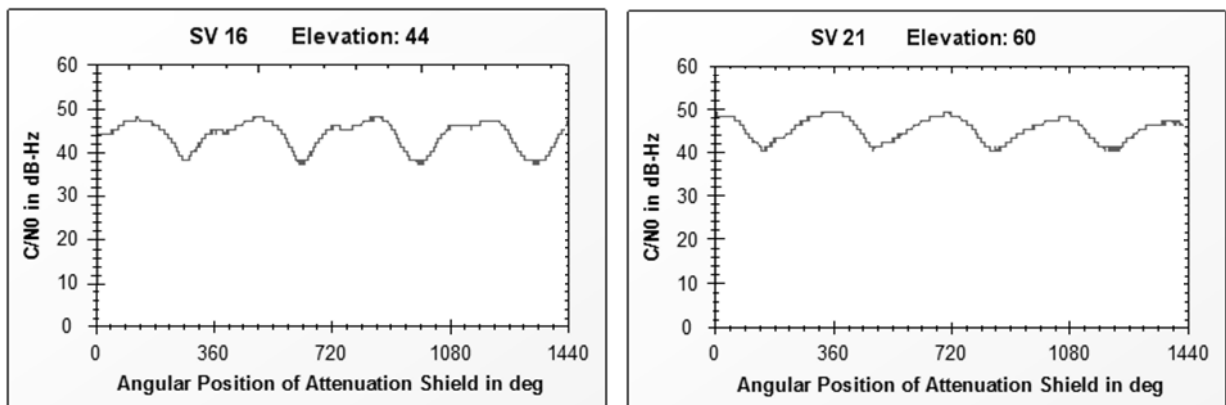
Figure 6.1 Signal strength of SV 16 and SV 21, influenced by 4 revolutions of the attenuation shield.

The antenna receives the most power when the antenna surface is perpendicular to the oncoming signals (see Section 3.6.5). Hence, the mean signal power depends on the elevation of the satellite and the emitted power of the specific satellite. In addition, the elevation influences the attenuation factor of the rotating attenuation shield. That is, the attenuation has a characteristic influence on the signal strength, depending on the cosine of the elevation of the incoming signal.

Influences from the attenuation shield on the C/N_0 function include the following:

- attenuation factor: depending on the used material
- frequency of the function: depending on the angular velocity of the attenuation shield
- number of periods: depending on velocity of the shield and measuring time

Influences deriving from the satellite constellation on the C/N_0 function include the following:

- mean received signal power
- attenuation factor, depending on the elevation of the satellite
- phase shift, depending on the azimuth of the satellite
- local influences, depending on multipath and reflected signals

The theoretical functions for the C/N_0 time series for each satellite (as shown in Figure 6.1) are unknown. However, a simple functional model can be set up with parameters determined empirically. The time series have a periodicity that corresponds to one revolution of the attenuation shield. This periodicity is not of the harmonic type, but because each revolution of the attenuation shield is triggered and recorded, the number of periods is known. In combination with the number of measurements and the time, the frequency (number of cycles per time interval) is known as well. The attenuation factor of the material and, therefore, the theoretical amplitude are known from test measurements. Finally, the positions of the satellites are known from the ephemerides.

The task now is to link the angular position of the attenuation shield with the observed time series. To estimate the corresponding position, two approaches will be discussed: the periodic model and the correlation approach.

6.1   Periodic Model

As input, the periodic model uses the data from the NMEA stream. The model is based on the periodic behaviour of the signal. It is assumed that the unknown function of the measured data can be approximated by a sine curve, as shown in Figure 6.2.
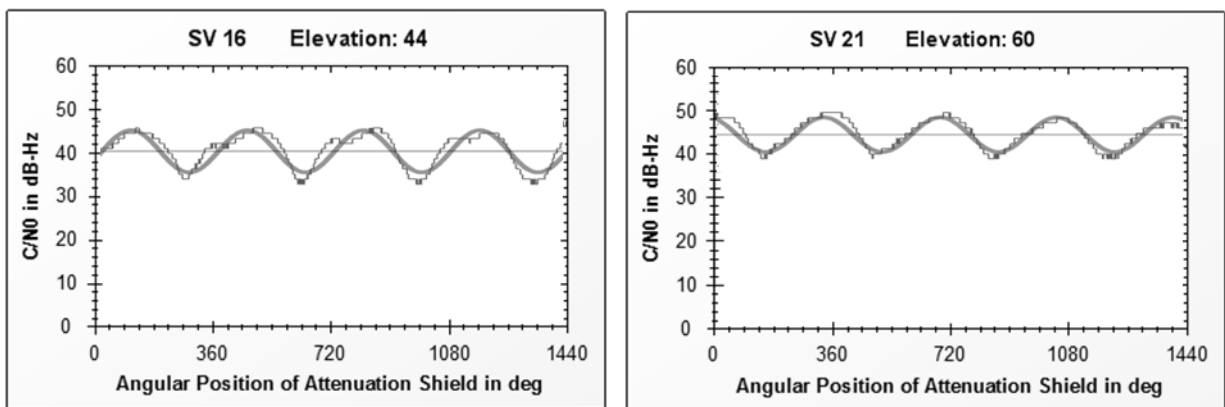
Figure 6.2 Approximation of the series of measurements by sine curves.

Because the angular velocity and the number of revolutions are measured, the frequency parameter of the sine function is known, and the two parameters phase ϕ and amplitude a remain unknown. The phase quantifies the shift of the sine on the time-axis and is dependent on the position of the attenuation shield and on the satellite's azimuth. The phase refers to the starting position of the attenuation shield.

6.1.1 Calculation of Phase and Amplitude

The signal $y(x)$ is modelled as the harmonic function

$$y(x) = a \cdot \sin(fx + \phi). \tag{6.1}$$

Using the addition theorem for trigonometric functions, Equation (6.1) is rewritten to

$$y(x) = a \cdot \sin(fx)\cos(\phi) + a \cdot \cos(fx)\sin(\phi). \tag{6.2}$$

Using the substitution,

$$A = a \cdot \cos(\phi) \text{ and } B = a \cdot \sin(\phi) \tag{6.3}$$

the signal y(x) is brought into the form

$$y(x) = A \cdot \sin(fx) + B \cdot \cos(fx). \tag{6.4}$$

The amplitude a and phase ϕ can be calculated with

$$a = \sqrt{A^2 + B^2} \text{ and } \phi = \arctan\left(\frac{A}{B}\right)\,{}^{[19]}. \tag{6.5}$$

To calculate the elements A and B, a normal equation system is set up. The model for the present data set requires only one frequency[20]. Therefore, the normal equation system can be simplified according to Mautz (2001):

$$\begin{bmatrix} A \\ B \end{bmatrix} = \begin{bmatrix} S & G \\ G & C \end{bmatrix}^{-1} \begin{bmatrix} a \\ b \end{bmatrix}. \tag{6.6}$$

The elements of the normal equation system are

$$S = \sum_{i=1}^{n} \sin^2(fx_i) \quad C = \sum_{i=1}^{n} \cos^2(fx_i) \quad G = \sum_{i=1}^{n} \sin(fx_i)\cos(fx_i)$$

$$a = \sum_{i=1}^{n} \sin(fx_i)\, y_i \quad b = \sum_{i=1}^{n} \cos(fx_i)\, y_i \tag{6.7}$$

where n is the number of measurements and y_i the measured data at time x_i.

Because the measurements are equidistant, the elements of the normal equation matrix (S, G, C) and of the observation vector (a, b) can be calculated as follows (Mautz, 2001):

$$x_i = 2\pi \frac{i}{n} \tag{6.8}$$

with $i = 1, \dots, n$.

The calculation of ϕ and amplitude a is implemented in the NORDIS evaluation software. The code of implementation is shown in Appendix 9.8.

---

[19] Quadrant rule: For $A < 0$, add 180 deg; for $A > 0$, add 360 deg if result <0.
[20] In this context, the frequency of the modulated signal is referred to, not the frequency of the satellite carrier wave (L1, L2, etc).

6.1.2 Calculation of Orientation

The phase shift corresponds to the angle of entrance of the respective satellite signals and is calculated independently using the algorithm shown previously. Table 6.1 shows the computed values for each satellite in view. The parameters PRN[21] number, azimuth, and elevation are derived from the NMEA stream. The orientation is the calculated angle of entrance for each satellite minus its azimuth. The model uncertainty indicates the standard deviation between the sine function as model function and the measured data for each satellite.

Table 6.1 Results of the Calculation

PRN-number	Azimuth in deg	Elevation in deg	Orientation in deg $\tilde{\alpha}_i$	Model Uncertainty	Number of Measurements
15	174	29	98.5253	1.0939	800
17	50	29	102.3563	2.0433	800
18	249	11	119.3076	2.4422	545
22	283	15	103.3056	1.8509	800
26	169	31	95.6214	1.1763	800
27	90	75	105.0596	0.6203	800
30	246	19	108.8710	2.0240	727
66	245	18	90.7509	1.4392	734
67	300	27	94.9899	1.3142	800
75	91	33	96.8674	0.9699	800
77	301	27	80.0531	1.7674	594
85	52	43	83.7664	1.2025	800
86	138	48	98.2125	0.6413	800
87	178	9	88.3763	2.3765	709
9	51	82	124.2930	0.6075	799
12	246	55	87.0747	0.6752	799
median (all values)			97.540		
mean (only green values)			96.843		
standard measurement uncertainty (only green values)			1.552		
standard measurement uncertainty of mean			0.694		

The differences of up to 44 deg between the orientation values in Table 6.1 indicate that the used model of approximation with sine curve is insufficient for the description of the data. The results from the sine approximation are not normally distributed, and averaging all measurements is not possible, thus systematic deviations in the data are assumed. Therefore, the values that are affected by systematic errors are eliminated empirically on the basis of specific criteria. Each single criterion has three conditions (colour coded in Table 6.1), aggregated in the quality variable κ:

    0   value is used (white and green)
    1   value is critical: warning criterion (yellow and blue)
    2   value is not used: exclusion criterion (red)

The following schema illustrates the selection process in three steps. The used criteria were determined by empirical trials and test measurements.

The steps are performed for all i satellites (rows in Table 6.1).

---

[21] The pseudo random noise number serves to identify the GPS satellites.

Step 1	Parameter	Warning Criterion	κ	Criterion for Exclusion	κ
	elevation	< 20 deg	+1	< 10 deg	+2
	amplitude	< 1 dB	+1	< 0.7 dB	+2
	model uncertainty	> 1	+1	> 1.7	+2
	number of data	< n	+1	< n/2	+2
			$\sum \kappa$		$\sum \kappa$

Step 2   If $\sum \kappa < 2$ → use satellite

If $\sum \kappa \geq 2$ → exclude satellite (red)

Calculate:
- mean value[22]
- standard measurement uncertainty of mean value ($stdv$)
- standard measurement uncertainty of single value ($stdv_i$)

In step 3, values with too large standard measurement uncertainties are excluded.

Step 3   if $stdv_i > 3 \cdot stdv$ → blunder: exclude satellite (blue)

calculate mean value and standard measurement uncertainty of mean value ($stdv$)

After the selection process, the 4 remaining measurements are averaged. An orientation value with a standard measurement uncertainty of the single measurements of 1.5 deg and a standard measurement uncertainty of the mean of 0.7 deg is achieved.

6.1.3   Conclusion of the Periodic Model Approach

Although this result looks promising, the periodic model does not seem to satisfy the requirements. The span of 44 deg in the orientation values in Table 6.1 indicates the periodic model is insufficient. The selection by criteria helps to improve the reliability of the results, but only one quarter of the satellites in view could be used in the example shown. Using more satellites would improve the accuracy and reliability. Therefore, another algorithm must be considered. The influence the attenuation shield has on the C/N_0 density values does not appear to be independent of the elevation of the satellites. Another issue is that the available data from the NMEA stream are rounded to integer values. Consequently, a better approach has been considered and is presented in Section 6.2. However, the periodic model could still be used for rough orientation determination.

6.2   Correlation Approach

To improve the results, C/N_0 densities with higher resolutions and a better model are necessary. C/N_0 densities with a resolution of a 0.25 dB are attainable by using raw data from the receiver instead of the NMEA stream. To get the C/N_0, azimuth, and elevation values from the raw data, several steps are necessary, as explained in Appendix 9.9.

6.2.1   Influence of the Satellites' Elevation

To gain better understanding of the influence of the satellites' elevation on the attenuated signal, measurements over one astronomic day were collected under optimal conditions. For a

---

[22] The "circular-safe" averaging function is used (see Appendix 9.10).

measuring location, a meadow hill with a view of the open sky and a low multipath environment was chosen. A detailed view of the measurement setup is shown in Figure 6.3 and Figure 6.4 while Figure 6.5 shows the 360 deg panorama of the view from the top of the hill.
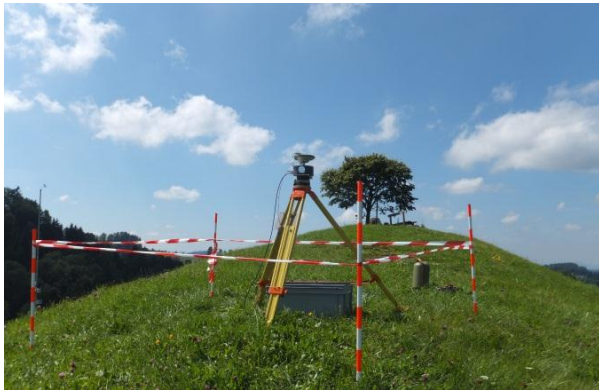
Figure 6.3 Measurement setup on a meadow hill (17.08.2012). View from East. (Picture: L. Steiner)

Figure 6.4 View from the south. (Picture: D. Grimm)
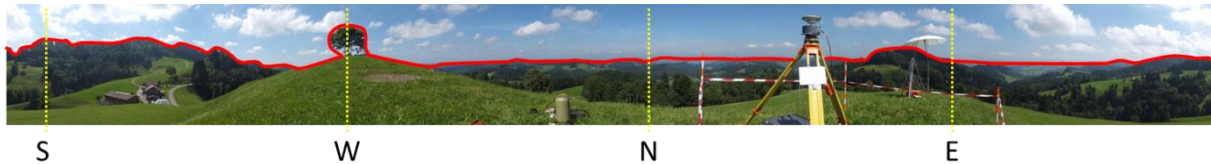
Figure 6.5 360 deg panoramic view of the measurement area from a meadow hill. (Picture: L. Steiner)

The map in Figure 6.6 shows the measuring location (near to point x 950) and its surrounding area. Figure 6.7 shows the areal image of the selected area in Figure 6.6 in larger scale.
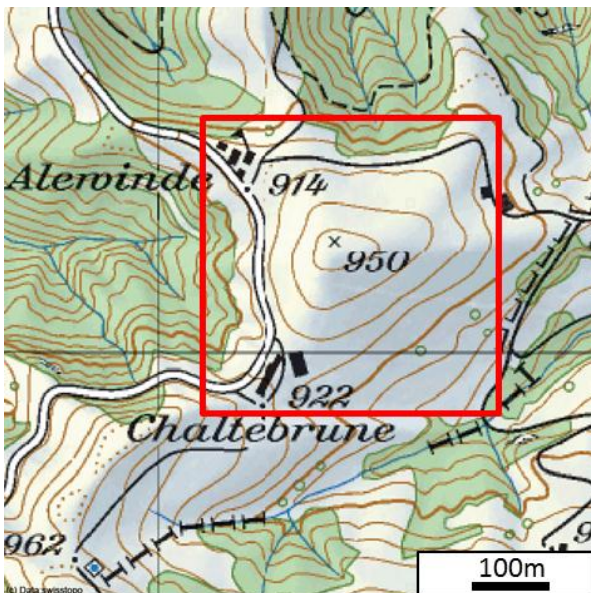
Figure 6.6 Situation map of the measurement area. (Picture: swisstopo, 2012)

Figure 6.7 Aerial image of the measurement area. (Picture: swisstopo, 2012a)

The measurements from this location are analysed to obtain the characteristic influence of the attenuation shield in relation to the satellites' elevation. For each degree of elevation, beginning with 0 deg to 90 deg, a separate C/N_0 curve is generated, as shown in Figure 6.8. Each single curve represents an average of the C/N_0 density for satellites of the same elevation during one revolution of the attenuation shield from 0 deg to 360 deg.
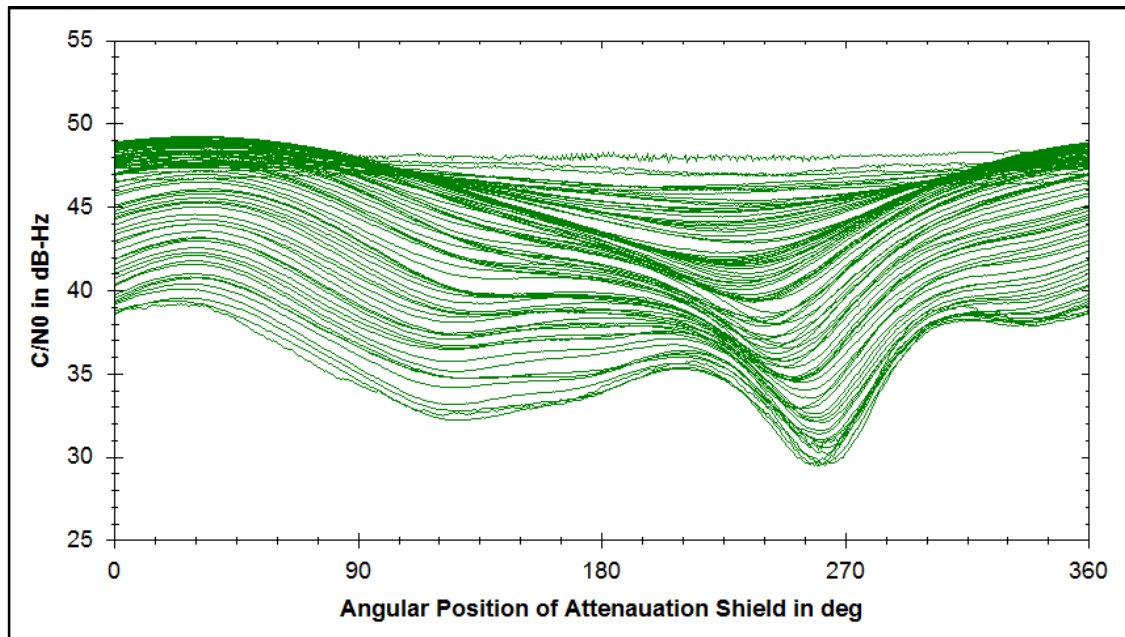
Figure 6.8 Functionality of the influence of attenuation and elevation on the C/N$_0$ from the L1 signal (S1) with 1 deg elevation isolines.

Before averaging the data, the azimuth of each satellite's position (Azi$_i$) was subtracted from the angular position of the attenuation shield (α_i) as shown in Equation (6.9).

$$\tilde{\alpha}_i = \alpha_i - \text{Azi}_i \qquad (6.9)$$

This can be understood as a virtual constellation in which all satellites would broadcast their signals from the same position in respect to the azimuth but from different elevation angles. Figure 6.9 illustrates the real constellation while Figure 6.10 illustrates the virtual constellation with all satellites at the same azimuth. The reduction is permitted when the C/N$_0$ can be assumed as constant for all azimuths. A prerequisite for doing so is an omnidirectional antenna (see Section 3.3.3). However, a location-specific multipath or reflections may lead to deviations and must be considered.
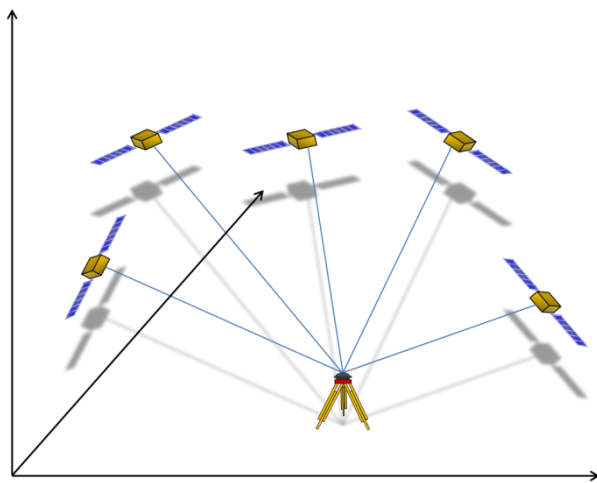
Figure 6.9 Real satellite constellation.
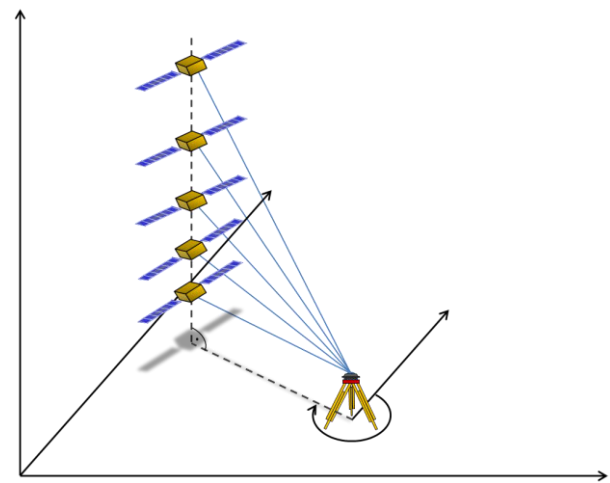
Figure 6.10 Virtual constellation: All satellites have the same azimuth.

The result is a reference curve per 1 deg elevation, independent of the satellite's azimuth. Signals from satellites with low elevations generate lower C/N$_0$ compared to satellites with higher

elevations. This difference is caused by the gain of the used antenna being maximal when the signals are parallel to the antenna boresight vector (see Section 3.6.5), as is the case for satellites with an elevation of 90 deg, thus the wide range of curves in Figure 6.8. Signals of satellites at higher elevations (upper lines) are modulated almost like a sine while signals of satellites at lower elevations (lower lines) indicate a different function. The difference in shape from a sine function and, particularly, the shift of the minimum of the curves are the reason the periodic approach in Section 6.1 is not an appropriate model function. From low to high elevations, a gradual change in the curves occurs. Consequently, not only the amplitude of the curve but also the shape generated by the attenuation shield on the C/N_0 depends on the satellite's elevation.

6.2.2 Cross-Correlation Instead of Sine Approximation

Instead of approximating the modulated signal of each satellite by a sine function as presented in Section 6.1, the signals can be compared with a specific reference curve for each elevation. The reference curves are generated from data, measured at an undisturbed location, as e.g. the place shown in Section 6.2.1. Such reference curves (e.g. Figure 6.8) are used as the basis for the correlation approach. The process flow of the correlation approach is described in Appendix 9.9.

6.2.3 Calculation of the Antenna's Orientation with NORDIS

Figure 6.11 shows the reference data for the L1 signal (S1), measured on the pillar 1013 on the HIL building (see Figure 5.12 to Figure 5.16). Curves exist for all 1 deg steps of elevation between 0 deg and 90 deg. The smoothness of the curves is due to averaging over 24 h. Figure 6.12 shows the curves for the L1 signal (S1), collected to determine the orientation of the antenna. The antenna was mounted on pillar 1013 again, however with a 270 deg different orientation. The data were collected over 52 min. Because of the shorter measuring time, curves do not exist for all elevations, as can be seen by the gaps between the curves, and the curves are not as smooth. However, the data are sufficient for applying the correlation method.
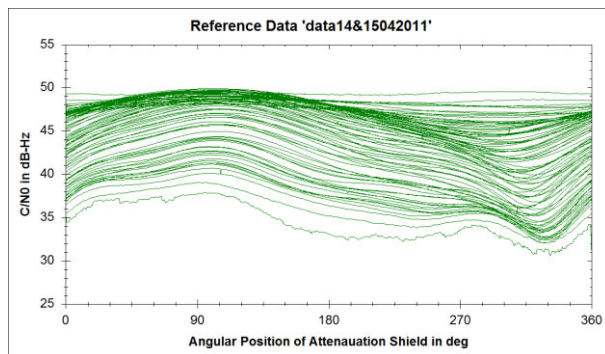
Figure 6.11 Reference data S1 (observation time: 24 h).
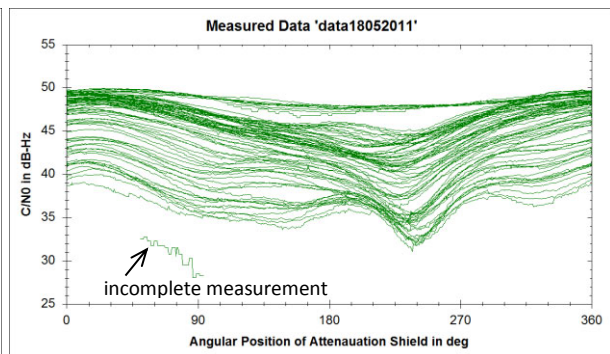
Figure 6.12 Measured data S1 (observation time: 52 min).

The phase shift of the corresponding curves (with the same elevation) indicates the different orientation of the antenna for the reference data and the measured data. The orientation of NORDIS is known in the case of the reference data. Consequently, it is possible to obtain the absolute orientation for the measurements shown in Figure 6.12.

6.2.4 Cross-Correlation Function

To find the phase shift of the two corresponding curve pairs, the measurement curves are shifted against the reference curves incrementally until the curves approach the best possible match. The mathematic method for this procedure is the cross-correlation. In the context of cross-correlation, the steps are referred to as *delay* or *lag*.

The cross-correlation value at delay δ is defined as:

$$corr(\delta) = \frac{\sum_{i=1}^{n}\left[(\xi_i - m_\xi) \cdot (v_{i-\delta} - m_v)\right]}{\sqrt{\sum_{i=1}^{n}(\xi_i - m_\xi)^2} \cdot \sqrt{\sum_{i=1}^{n}(v_{i-\delta} - m_v)^2}} \tag{6.10}$$

using the two data series ξ_i (reference data) and v_i (measured data), where $i = 1, 2, \ldots, n$ and m denotes the mean value of the series ξ and series v, respectively. The source code of implementation of the cross-correlation algorithm is presented in Appendix 0.

For this application, the series are circular because the attenuation is rotating from $n = 0$ deg to 360 deg while 360 deg corresponds with 0 deg: $\xi_{-1} = \xi_{n-1}$, $\xi_{n+2} = \xi_2$.

The denominator in Equation (6.10) serves to normalize the correlation coefficients within the range of -1 to 1. A correlation coefficient of 1 is an indicator of a perfect correlation, and 0 indicates no correlation. A negative correlation indicates a correlation with the inverse of one of the series. A correlation coefficient > 0.7 indicates a significant correlation. The phase shift of the measurement curve is indicated by the delay of the maximal correlation value as shown in Equation (6.11)

$$\delta_{max} = \max[corr(\delta_i)] \tag{6.11}$$

with $i = 0, \ldots, 719$ for the case of measurements each 0.5 deg.

Figure 6.13 shows the correlation coefficients over the delay from 0 deg to 360 deg for all available corresponding curve pairs for the data shown in Figure 6.11 and Figure 6.12. The outliers in Figure 6.13 are caused by incomplete measurement series. One incomplete measurement is marked in Figure 6.12, the second is at an elevation of 76 and hidden within the other curves. For these two series, the maximal value for the correlation coefficient is below the threshold value of 0.7; therefore, they are identified as outliers and ignored.
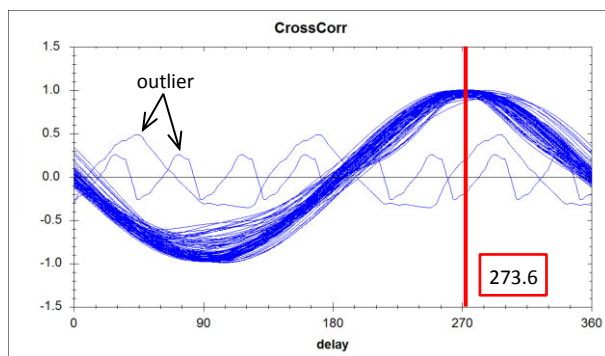
Figure 6.13 Result of the cross-correlation.   **Figure 6.14 Deviations from the mean.**
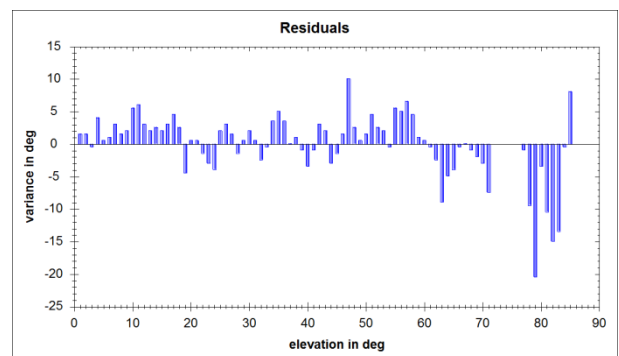
The average[23] delay of the maximal correlation coefficient of all series is 273.6 deg. Figure 6.14 shows the corresponding variance from the mean, sorted by elevation. Results with residuals > 10 deg indicate that the measured data and the reference curve for the correspondent elevation do not fit properly. The majority of the residuals > 10 deg are at elevations > 75 deg. Satellites at high elevations are not suitable for orientation determination because of the steep incidence angle, which leads to inaccurate association between satellite position and position of

---

[23] The circular-safe averaging function is used (see Appendix 9.10).

the attenuation shield. Thus, exclusion of satellites with elevation > 75 deg is necessary. Individual large residuals at lower elevations can be explained by location-based influences such as multipath and reflected signals. The recalculated residuals after excluding all measurement with elevations > 75 deg are shown in Figure 6.15.
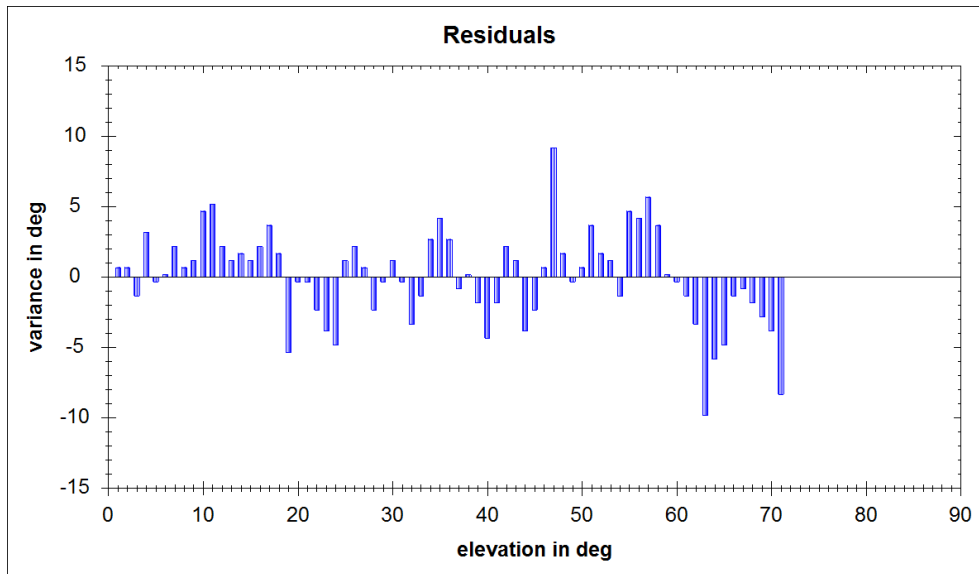
Figure 6.15 Deviations from the mean for values < 75 deg elevation.

An overview of the results is shown in Table 6.2.

Table 6.2 Results

average	273.6	deg
number of used curves for averaging	71	
measuring time	1:52	h
standard measurement uncertainty of maximal correlation value based on data of a single elevation curve	3.25	deg
standard measurement uncertainty of the mean of all elevation curves $(s/\sqrt{71})$	0.38	deg
reference value, determined by autocollimation measurement	270.000	deg

The verification of the results follows in Section 7.

6.2.5   Conclusion of the Correlation Approach

The advantage of the correlation approach is that the elevation-dependent influences on the attenuation shield are considered. Therefore, a different reference curve for every 1 deg of elevation is used. The input data are more useful because the stored data have higher resolutions than the data from the NMEA stream. However, post-processing is necessary. It could be done in real time if an alternative data stream to NMEA with float values were accessible. The disadvantage of a huge amount of data that must be processed to obtain proper reference data is solved by using MySQL database (see Appendix 9.9.4).

6.3 Chapter Conclusion

In the first section of this chapter, the attenuating effect on the C/N_0 density was shown. The C/N_0 density values of all satellites are continuously influenced by the rotating attenuation shield; thus, an association between the influenced signal and the angular position of the shield can be established. To calculate the DOA of the satellites' signals, two different approaches were presented. The periodic model approach uses a sine curve to approximate the C/N_0 data series, thereby determining the phase shift. The phase refers to the starting position of the attenuation shield. Elevation dependent effects reduce the accuracy of this approach. To minimise these effects, a second approach was presented. A specific curve for each 1 deg of elevation is used as reference. The DOA can be calculated by cross-correlating the actual measurements with the corresponding reference curves.

7 Verification of the Results

An investigation of how the measurement duration influences the accuracy of the orientation is discussed in the first section of this chapter. A verification and uncertainty analysis of all contributing subsystems of NORDIS is presented in Section 7.2.

7.1 Dependency of the Measuring Duration on the Orientation Uncertainty

To evaluate the influence of the measurement duration on the orientation accuracy, an additional 24 h measurement was taken on the same pillar where the reference data were measured. The antenna was oriented identically as for the reference data. Hence, the data were measured under the same conditions but on different days. The data are divided into nine subparts, with different measurement durations from 2 min up to 18 h, as shown in Table 7.1. The second row indicates the number of existing corresponding-curve pairs with the same elevation. These curve pairs are used for cross-correlation. After a measuring time of 1 h, all possible curves from 1 deg to 75 deg elevation were available. Satellites with elevation > 75 deg were not taken into account (see Section 6.2.4). The last row indicates the difference between the reference orientation from the reference measurement ($ref = 0$) and the average (avg) from the actual measurement.

Table 7.1 Orientation Parameters for Different Measuring Times

measurement time	2min	5min	15min	30min	1h	2h	6h	12h	18h
reference orientation	0	0	0	0	0	0	0	0	0
averaged orientation $\bar{O}$ in deg	358.474	358.603	359.04	359.762	0.787	0.187	0.120	0.120	0.113
number of corresponding curves	19	29	50	65	75	75	75	75	75
standard measurement uncertainty in deg (u_A)	13.387	6.659	5.321	5.243	2.885	1.879	1.493	1.096	0.698
standard measurement uncertainty of the average in deg (u_A avg)	3.071	1.237	0.753	0.65	0.333	0.217	0.172	0.127	0.081
reference orientation - average in deg (ref-avg)	1.526	1.397	0.960	0.238	0.787	0.187	0.120	0.120	0.047

Figure 7.1 and Figure 7.2 show the achieved standard measurement uncertainty of the orientation depending on the measuring time. In Figure 7.1, the data are plotted linearly while Figure 7.2 shows the same data in a logarithmic scale. The blue line (u_A avg) shows the standard measurement uncertainty of the average value (row 4 in Table 7.1). The green line (ref-avg) indicates the absolute value (without regard to its sign) of the deviation between the calculated

orientation and the known reference value (last row in Table 7.1). Because the reference value can be assumed as known, the green value indicates the measurement error[24] of the determined orientation.

Figure 7.1 Dependency of the orientation uncertainty and the measuring time (linear plot).
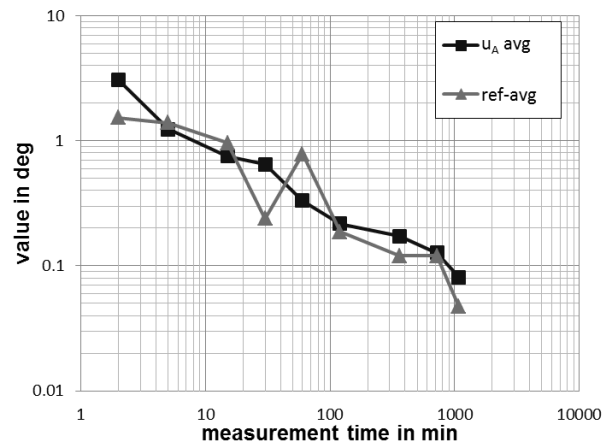
Figure 7.2 Dependency of the orientation uncertainty and the measuring time (logarithmic plot).

For measuring times longer than 15 min, the difference between the determined orientation and the reference value is less than 1 deg. In general, it can be seen that the orientation gets better with increasing measuring time. For this data set, the standard measurement uncertainty of the average has a high accordance with the deviation from the known true value. However, the fourth and fifth values show a greater discrepancy, a possible indication that the standard measurement uncertainty of the average is not representative. As a consequence unmodeled systematic effects should be considered. Thus, it would be wise to enlarge the interval of the reasonable values and use, for instance, a 2 sigma standard measurement uncertainty.

7.1.1 Comparison Measurement at Different Location

The measurement data introduced in Section 6.2 were collected on a different pillar from the reference data. The orientation of the antenna was rotated by 270 deg. The measuring time was 52 min. A division into five subparts is shown in Table 7.2.

Table 7.2 Orientation Parameters for Different Measuring Times

measurement time	2min	5min	15min	30min	52min
reference orientation	270	270	270	270	270
averaged orientation $\bar{O}$ in deg	273.900	273.960	272.459	272.799	272.700
number of corresponding curves	2	5	15	30	52
standard measurement uncertainty in deg (u_A)	3.860	4.191	4.759	3.689	3.250
standard measurement uncertainty of the average in deg (u_A avg)	0.997	0.838	0.680	0.451	0.380
reference orientation -average in deg (ref-avg)	3.900	3.960	2.459	2.799	2.700

---

[24] Measurement error is the measured quantity value minus a reference quantity (Joint Committee for Guides in Metrology, 2008).

The fact that the determined value for the orientation is too large (> 270 deg) for all epochs consolidates the hypothesis of possible presence of one or more systematic deviations, which can also be seen in Figure 7.3 and Figure 7.4. Because the data were collected on a different pillar from the reference data, the lower accuracy could be caused by location-specific influences, which leads to the angular bias of about 3 deg.
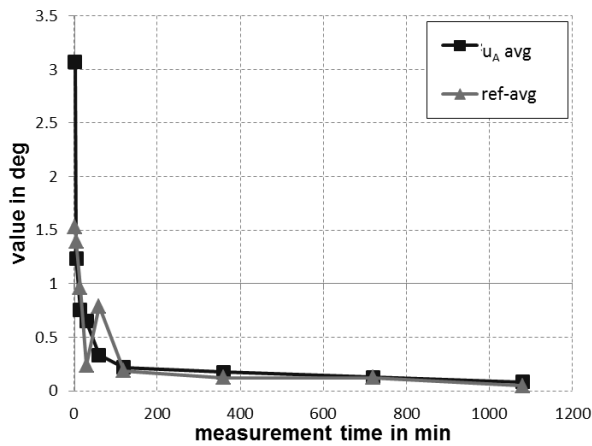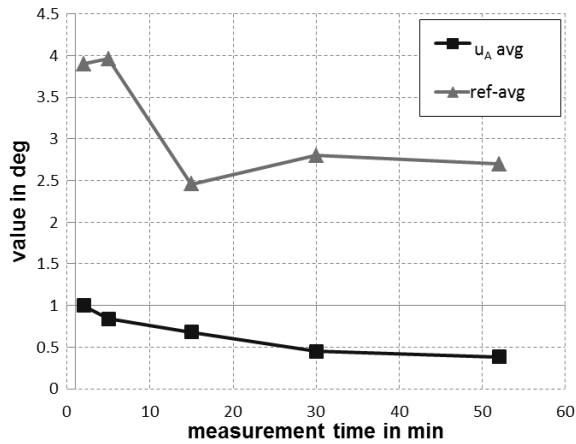

Figure 7.3 Dependency of the orientation uncertainty and the measuring time (linear plot).
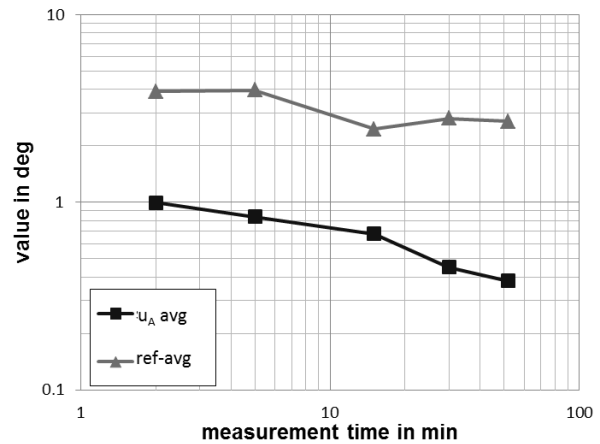
Figure 7.4 Dependency of the orientation uncertainty and the measuring time (logarithmic plot).

7.1.2 Section Conclusion

Observations of longer duration lead to better precision and accuracy. The precision is improved by using a larger data set that can be averaged. The accuracy improves because more satellites from different azimuth and elevations are taken into account, causing a better geometric distribution. Location-specific influences could lead to inaccuracies. However, some systematic effects are suspected and must be analysed in a further step.

7.2 Verification of the Components

The uncertainty of the components introduced in Section 5.2.2 are analysed by using real data from the measurements.

7.2.1 Influence of the Attenuation on GNSS Position

The influence the attenuation shield has on the position solution of the GNSS receiver is analysed in Friedli (2011). The variation of the position solution is within centimetres and, therefore, only visible with differential GNSS. For the test, NORDIS was mounted on a pillar with known coordinates. A reference station for differential GNSS was set up on a nearby pillar (distance between the pillars = 22.5 m). On both pillars, measurements with 20 Hz were recorded. A baseline for each data pair was calculated in post-processing. Therefore, the baseline calculation was performed in kinematic mode, which means that no measurements were averaged. A control measurement performed with the same antenna, without attenuation shield, is presented in Figure 7.7.
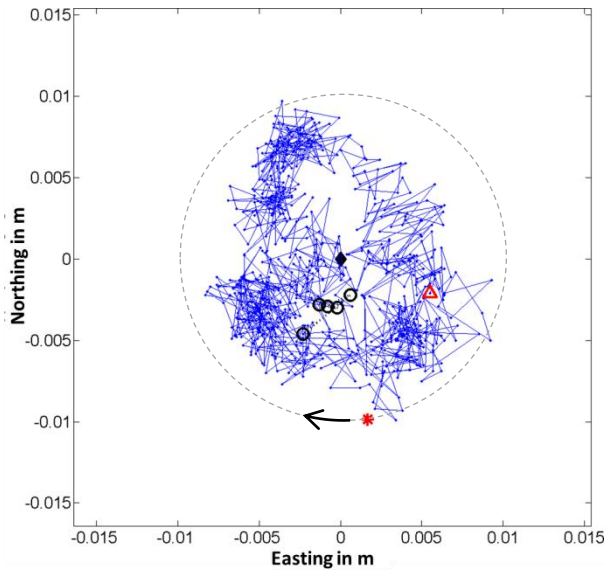
Figure 7.5 Influence of one revolution of the attenuation shield on the GNSS position according to Friedli (2011).
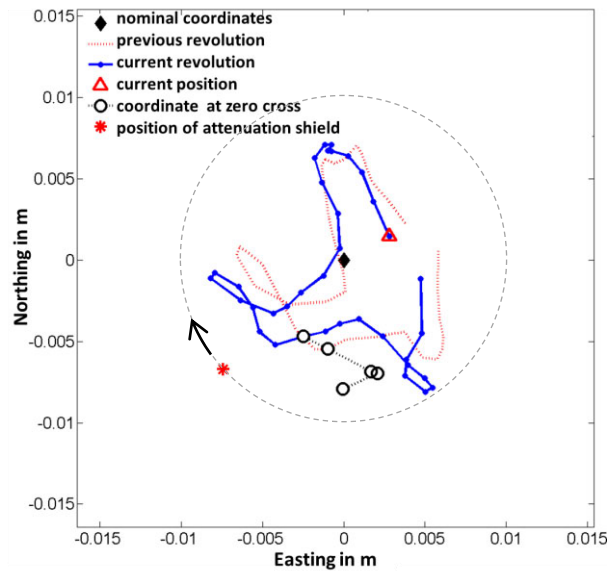
Figure 7.6 Averaged influence of the attenuation shield on the GNSS position according to Friedli (2011).

Figure 7.5 shows a visualisation of the position variation caused by one revolution of the attenuation shield. To provide a clearer view, Figure 7.6 shows a filtered curve; where each point is equal to the moving average of 40 coordinate pairs. The average is calculated for each second, leading to 36 points per revolution of the attenuation shield. The nominal coordinates of the antenna reference point (ARP) are at position (0/0). The actual position solution is marked with a triangle while the asterisk marks the actual position of the attenuation shield moving along the dotted circle. The influence of the attenuation shield can clearly be seen; however, the position coordinates of the GNSS solution are not collocated in a circular distribution around the nominal coordinates as could be expected. Nevertheless, the influence is systematic for successive revolutions as can be seen by evaluating the current revolution (blue line) with the previous revolution (red dotted line). As comparison, Figure 7.7 shows the position variation during the control measurement without attenuation shield.
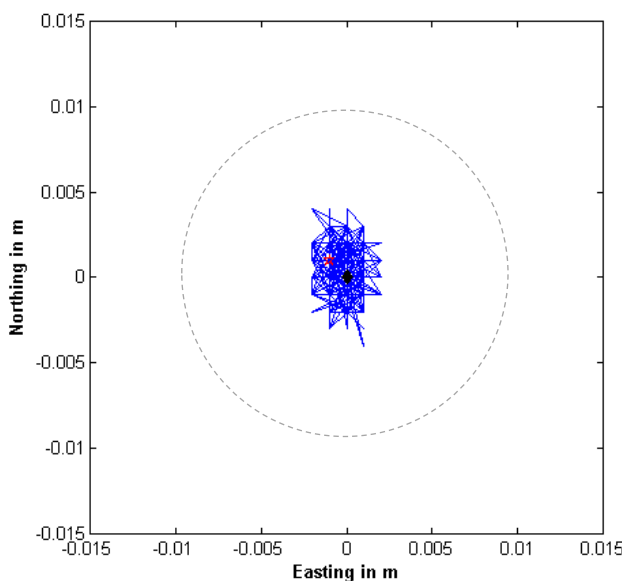
Figure 7.7 Control measurement without attenuation shield. (Plot: L. Steiner)

The variations of the easting and northing values during five successive revolutions are presented in Figure 7.8. The two curves are shifted by a quarter revolution, corresponding to the 90 deg difference between northing and easting. The influence on the northing value is stronger, and the average is above zero while the average for the easting direction is nearly zero. This result can be explained by the geometric distribution of the satellites that is unsymmetrical (i.e. less satellites in the north direction at 47 deg north latitude) because of the inclination of the orbits.
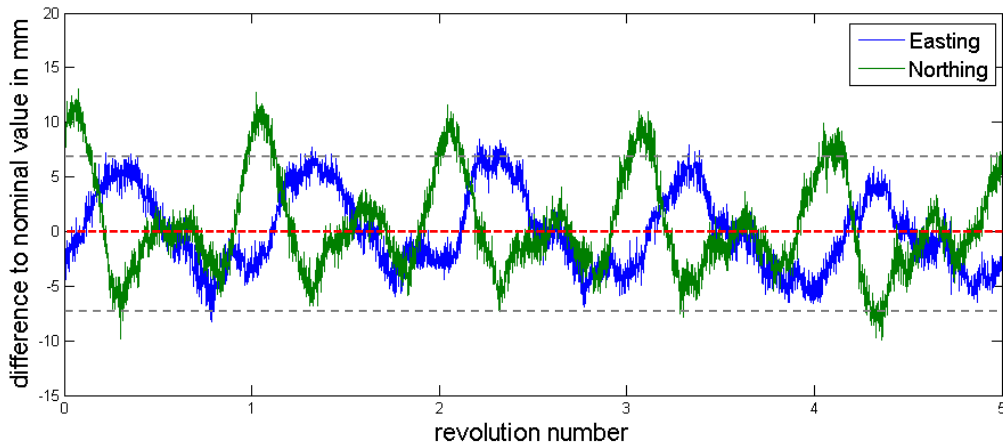
Figure 7.8 Variation of easting and northing plotted for five revolutions (Friedli, 2011).
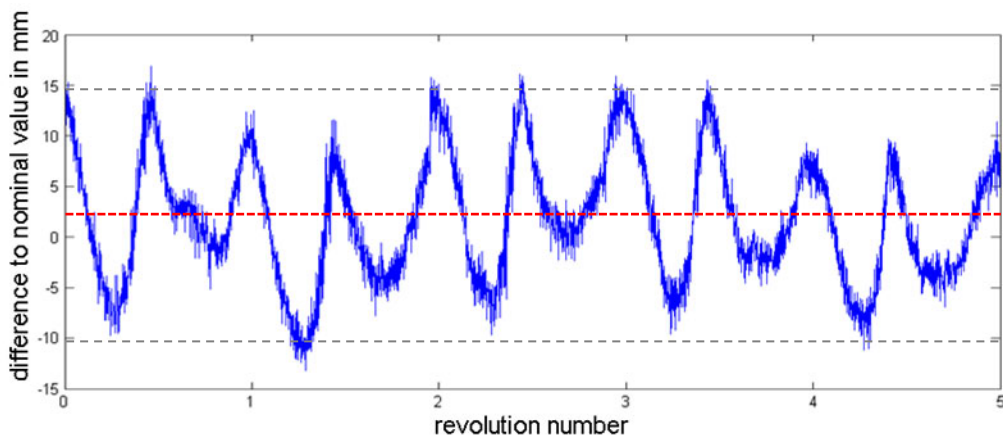
Figure 7.9 Variation of the height component plotted for five revolutions (Friedli, 2011).

Figure 7.9 shows the variation in the height component. The variation is larger, and the average (red dashed line) is above zero. Assuming that the attenuation shield delays the signals, this result can be explained again by the geometric distribution of the satellites in which satellites are only above the antenna, not below. In consequence the offset is not cancelled through the geometrical constellation.
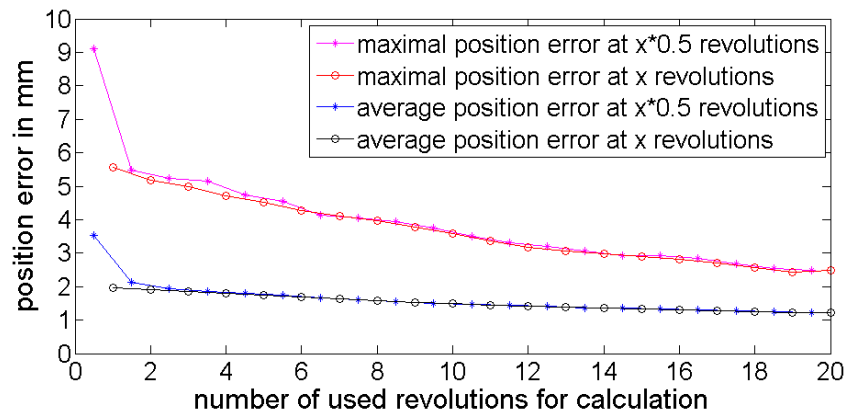
Figure 7.10 Position error (absolute value) in relation to the number of measured revolutions (Friedli, 2011).

Figure 7.10 shows that the position error is maximal for less than one revolution. The position error of the average for more than one revolution is below 2 mm.

7.2.2 Influence of the Attenuation Shield on the Antenna Phase Centre and Gain Pattern

The effect the attenuation shield has on the gain pattern is essential as basis for the measurement principle used in NORDIS. However, the attenuation shield does not only influence the C/N_0, but in addition influences the GNSS position as shown in Section 7.2.1. It is therefore important to not impair the position determination to a greater extent than is inevitable.

The reason for the variance of the position coordinates probably lies in the modification of the electrical phase centre of the antenna caused by the attenuation shield. To verify this statement, measurements of the antenna phase centre (antenna calibration[25]) with applied attenuation shield were carried out. On the roof of the TU Dresden, NORDIS was mounted on the DRB2[26] (Figure 7.11) to perform a relative field calibration of the entire system, including antenna, attenuation shield, bracket and body). The results of this calibration are shown in Figure 7.16.

Figure 7.11 NORDIS mounted on DRB2 at TU Dresden. (Picture: D. Grimm)

---

[25] Further information concerning GNSS antenna calibration can be found in IGS (2012).

[26] http://tu-dresden.de/die_tu_dresden/fakultaeten/fakultaet_forst_geo_und_hydrowissenschaften/ fachrichtung_geowissenschaften/gi/gg/dienstleistungen/akalib

In addition, antenna tests were performed in the measuring chamber of University of Bonn[27] (Figure 7.12). The experimental setup in the measuring chamber consists of a transmitter, which simulates a satellite signal on one end and a movable base for the test antenna on the other end of the test range. Pyramid-shaped absorbers, mounted on the inner walls of the chamber (see Figure 7.12), minimise multipath effects. By pivoting the antenna, different satellite directions are simulated. For the calibration in the anechoic chamber, attenuating material with the same properties and shape was stuck on an identical antenna to the one used in NORDIS (Figure 7.13).
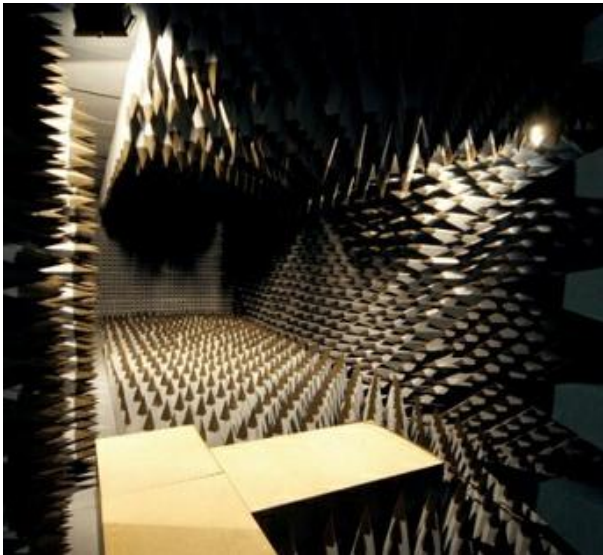
Figure 7.12 Antenna measuring chamber of University of Bonn (Institute for Geodesy and Geoinformation, 2011).

Figure 7.13 Leica ATX 1202 GG antenna with stuck on attenuating material (Zeimetz, 2009)

Figure 7.14 shows the gain pattern for L1 and Figure 7.15 for L2, as measured in the antenna measuring chamber in Bonn. The displayed segment represents the attenuation shield. The values on the colour scale indicate the gain in dB. The different elevation angles are plotted from the edge (horizon) to the centre (zenith) in steps of 10 deg. The gain increases from the edge towards the zenith, in accordance with the theory in Section 3.6.5. In addition, a slight shift of the gain maximum towards the attenuation can be noted. This is the reason for the measurable change in the C/N_0 depending on the position of the attenuation shield.
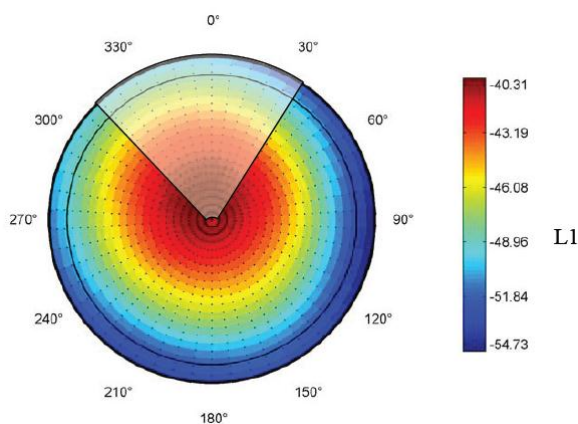
Figure 7.14 Influence of the NORDIS attenuation shield on the gain pattern. L1 phase C/N_0 in dB-Hz (Zeimetz, 2009).
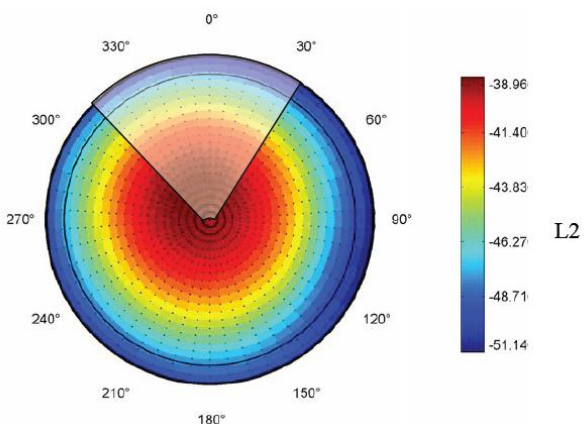
Figure 7.15 Influence of the NORDIS attenuation shield on the gain pattern. L2 phase C/N_0 in dB-Hz (Zeimetz, 2009).

---

[27] http://www.gib.uni-bonn.de/forschung/gnss/antennenmesskammer

The deviation of the phase centre variation resulted in a value of up to 20 mm for the used attenuation material in the case of the measurements in Bonn (Zeimetz, 2009). The measurements performed at TU Dresden show a similar result and are presented in Figure 7.16.

The plots in Figure 7.16 show the phase centre offset (PCO) and the phase centre variation (PCV) from the antenna calibration at TU Dresden for an unshielded antenna on the left and with attenuation shield on the right. The plots show the GPS L1, GLONASS L1, GPS L2, and GLONASS L2 from top down. The values for the PCO are written in the box. The colour scale reflects the PCV in mm. The attenuation shield, mounted in a fixed position in regard to the antenna during the calibration measurement, is represented by the displayed segments in the plots on the right side. The calibrations show deviations of the regular phase centre up to 20 mm, equivalent to the results from the calibration in Bonn. The maximal deviation is not located below the attenuation shield but in an angular offset. The reason for this effect may derive from the design of the spiral antenna used. Although the effect is repeatable, and the measurements presented in Figure 7.6 confirm this value. However, the measurement process in Section 7.2.1 is different from the antenna calibration. In the case of the antenna calibration at TU Dresden and in Bonn, the attenuation shield was fixed on the antenna. In the case of the analysis of the position deviation shown in Figure 7.6, the attenuation shield was rotating, and the antenna was held stable. The deviations of the resulting coordinates shown in Figure 7.8 are with 15 mm within the same magnitude as the calibration measurements for the phase centre variation.
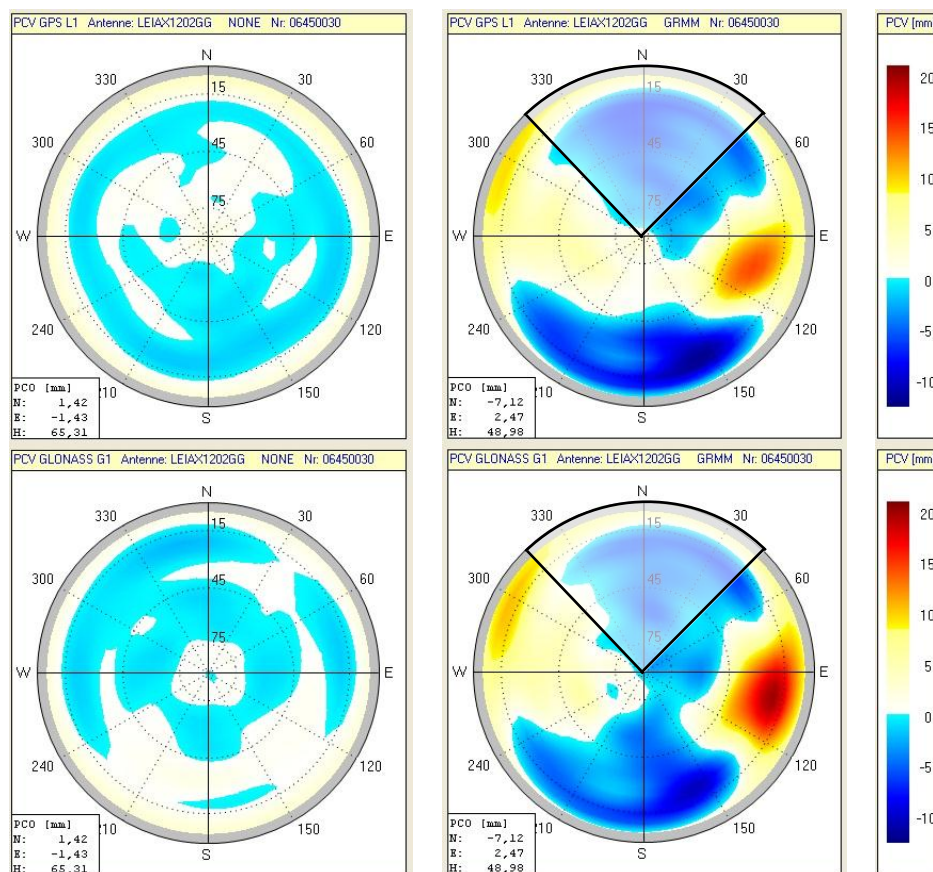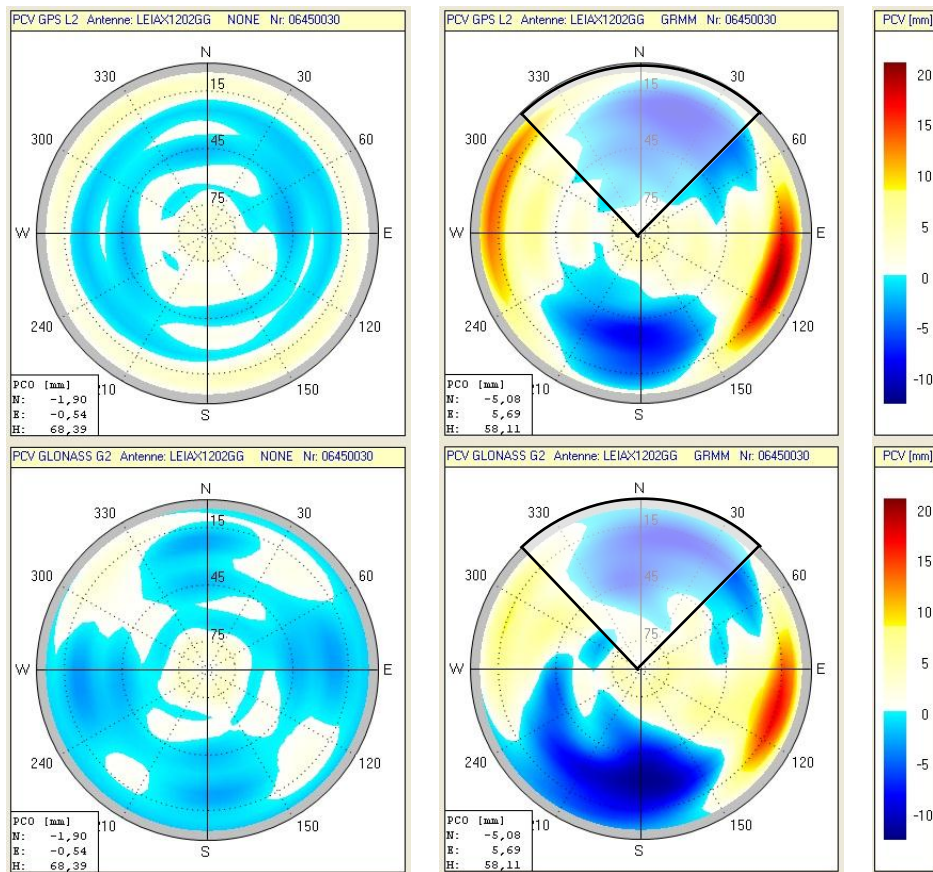
Figure 7.16 Influence of the NORDIS attenuation shield on the L1 and L2 phase centre variation (Frevert, 2010).

7.2.3 Uncertainty of Inner Orientation

The speed of the motor is kept constant by the motor controller. The GPS time for the beginning of one revolution is given by the zero cross event. The following evaluation of the stability of the time that is needed for one revolution has been conducted in Friedli (2011). To analyse the variation of the time needed for one revolution, durations of 450 revolutions were measured, as shown in Figure 7.17.
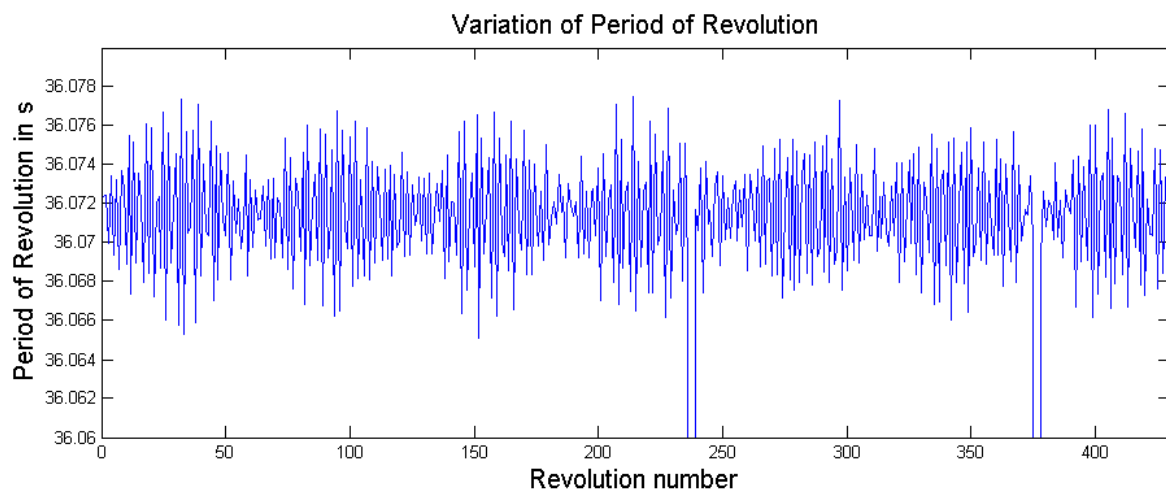
Figure 7.17 Variation of period of revolution according to Friedli (2011).

Four gross errors can be seen at revolution numbers 236, 239, 375, and 378. The gross errors appear in pairs and are caused by multiple pulses per event (see Section 7.2.4). After excluding

this gross errors, the average value for one revolution is 36 seconds and 71 milliseconds, at a standard measurement uncertainty of 3 ms.

To estimate the standard measurement uncertainty of the angular position u_{A_α}, the influence of the temporal uncertainty s_T must be converted by multiplying with the average angular velocity of the attenuation shield ω_{AS}, as shown in Equation (7.1).

Empirical standard
measurement uncertainty: $\quad s_T = 3$ ms

Average period of revolution: $\quad T_{AS} = 36.07$ s

$$\omega_{AS} = \frac{2\pi}{T_{AS}} = 0.174 \text{ rad/s} \tag{7.1}$$

$$u_{A_\alpha} = s_T \cdot \omega_{AS} = 5.2 \cdot 10^{-4} \text{ rad} = 0.03 \text{ deg} \tag{7.2}$$

The result of Equation (7.2) indicates that the standard measurement uncertainty of the angular accuracy for one revolution of the shield is 0.03 deg.

In addition, a systematic effect can be seen in Figure 7.17. Too short and too long time periods (max 6 ms) alternate, causing a superposition (beat) of the two slightly different frequencies. The effect has a period of about 60 revolutions that correspond to about 36 min and could be modelled by an additional sine component. The reason for this result probably lies in a small uncertainty of the motor speed controller. Because its angular effect (max 0.06 deg) is significantly smaller than the targeted standard measurement uncertainty of 1 deg, the influence is not relevant to the final result; therefore, no further investigation was done in this work.

7.2.4 Multiple Pulses per Event

While recording the events, multiple pulses per event could be detected, indicating that two electrical pulses instead of one were induced. In most cases, only one correct pulse was induced. Nonetheless, multiple pulses can be handled in two ways:

1. on the hardware
2. with the processing software

Figure 7.18 shows the effect of multiple pulses.

a) Event = real event at the expected time
b) Event pulse = additional (wrong) pulse
c) Time guard = time span between two expected pulses
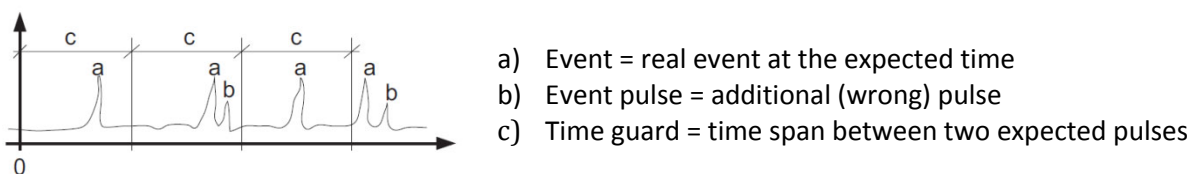
Figure 7.18 Multiple pulses (Leica, 2007a).

The time guard is optional and can be activated in the hardware settings by indicating a value for parameter c. Consequently, only one pulse per time span is recorded. However, doing so could be problematic when the wrong pulse is recorded. Therefore, in NORDIS, all pulses are recorded, and multiple pulses are identified within the software.

7.2.5 Uncertainty of Outer Orientation

The outer orientation is needed twice: to determine the absolute antenna orientation for the reference data set and for validation of the calculated orientation. The reference value for the orientation is calculated from coordinates of the geodetic pillars at ETH. The pillar coordinates derive from an adjustment from annually static GNSS and TPS measurements since 2007. The standard measurement uncertainty of the pillar coordinates can be assumed within 3 mm what results in a standard measurement uncertainty of 0.007 deg for the azimuth. The standard measurement uncertainty of the autocollimation measurements is estimated with 0.001 deg.

7.2.6 Difference Between L1 and L2

On NORDIS, the antenna bandwidth design leads to different influences of the attenuation shield on L1 and L2, as can be seen in Figure 7.19 and Figure 7.20. Figure 7.19 shows the influence of the attenuation shield on the L1 signal (S1) (see Section 6.2). Figure 7.20 shows the influence on the L2 signal (S2) for the same observation.
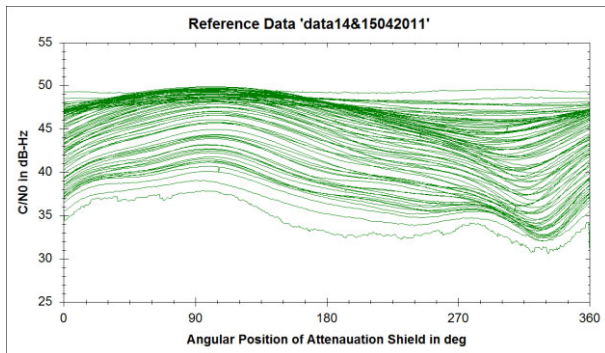
Figure 7.19 Influence of the attenuation on the signal strength S1 on the L1 signal.
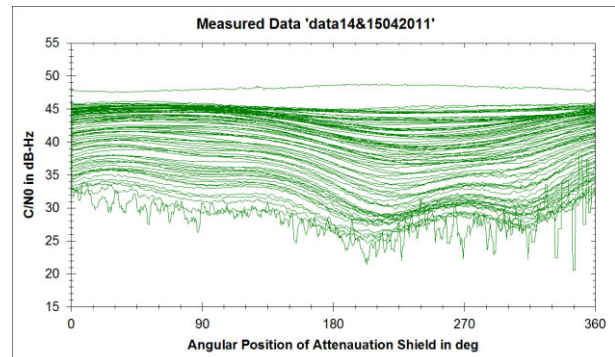
Figure 7.20 Influence of the attenuation on the signal strength S2 on the L2 signal.

The different effects the attenuation shield has on L1 and L2 require a separate calculation of reference data for L1 and L2. Consequently, data measured on L1 must be correlated with reference data for L1 and data from L2 with reference data for L2. For further analyses only L1 is used.

7.2.7 Relevance of the Antenna Field Regions

In the far field (see Section 3.2.1), the oncoming wave front can be assumed as planar and the rays as approximately parallel, simplifying the wave propagation path. Many effects that occur from the electromagnetic wave, like diffraction, refraction and multipath, can be treated by geometric assumptions as long as the effects happen in the far field.

In the near field (see Section 3.2.2), the wave forms are more complicated, and determination of the propagation path is not successful if based on geometric treatment. In NORDIS, the attenuation is placed in the near field of the receiving antenna. Consequently, calculating the effects that the attenuation shield causes on the electromagnetic wave is difficult. A geometric model cannot be applied. However, the effects caused by the attenuation shield are repeatable for the same antenna type and the same frequency. Therefore, the approach of this work is based on exploitation of empirical data.

7.2.8 Manufacturer Differences in C/N$_0$

The signal strength is not available as analogue channel for a single satellite because all GPS (for GLONASS see Section 3.6.1) satellites broadcast at the same frequencies of L1 1575.42 MHz and L2 1227.60 MHz. The signals from different satellites must be identified first, requiring the use

of a separation technique. Because each manufacturer of receivers has a proprietary technique, the indicated signal strength values differ significantly (see Section 3.6.8).

In this present work, signal strength is an important observable. The variation of the signal strength, dependent on the position of the attenuation, is used to detect the DOA of the entering satellite signals. However, because the calculation of the angle is performed with help of a cross-correlation function, the absolute values of the signal strength do not matter. The cross-correlation function calculates the angular phase shift of two functions but does not take into account the amplitude of the function. Accordingly, it would even be possible to calculate the cross-correlation between one data set in SNR and another in C/N_0 because the shape of the function would be the same.

7.3 Chapter Conclusion

Under the best conditions, the resulting orientation value has a measurement uncertainty below 1 deg. However, results with a measurement uncertainty ranging up to 3 deg are reasonable to expect. When an orientation with a measurement uncertainty of below 4 deg is required, a measuring time of 2 minutes is sufficient. For results that require a measurement uncertainty of below 1 deg, a measuring time of at least 2 hours should be considered.

Verification of the components shows that all components used meet the requirements. The influence the attenuation shield has on position uncertainty is less than 2 mm, averaging across full revolutions, and can be neglected in most cases. Thus, the antenna can still be used for position determination. Because the attenuation shield influences the L1 and L2 in different ways, reference curves for both curves are required. A location-specific multipath may reduce the accuracy of the orientation determination as shown in Section 7.1.1.

8 Conclusion and Outlook

The results of Chapter 6 and 7 showed that the objectives stated in Section 5.1 have been met. Under optimal conditions, orientation information with uncertainty ranging between 1.5 deg and 4 deg is achievable after a few minutes of measurement. Orientation with an uncertainty below 1 deg is achievable by measuring over several hours. A comparison of the obtained orientation value with a reference value verifies the correctness of the system. However, systematic influences deriving from the antenna's surroundings (e.g., multipath or diffracted signals) can lead to a bias of the DOA determination and worsen the measurement uncertainty. The orientation determination is impossible, when the reception of the signal is no longer ensured (e.g., due to effects from the ionosphere or from interfering signals).

8.1 Conclusion

Although the idea of using an attenuation shield to determine the DOAs of satellites' signals was already formulated in patent applications (Kahlmann and Ingensand, 2007 and Wiklund, 1992, certain outstanding issues remained to be addressed before a functional model could be realised. In terms of hardware, suitable material, the shape of the attenuation shield, and the support had to be found. Using acrylic glass for the support turned out to be the best solution because it does not attenuate the signals itself. In terms of software, the data analysis was not straightforward. The initial idea to approximate the measured curves for each satellite by a sine curve seemed promising. The mathematic model was simple and, therefore, easy to implement. However, the model was incomplete. During the evaluation of the model, the influence of the attenuation shield proved to be strongly dependent on the elevation of the satellites. This problem could be solved by using a specific reference curve for each integer degree of elevation instead of using a sine function as an approximation. To find the best match of the measured curve and the reference curve, cross-correlation was used. Therefore, it was necessary to collect huge amounts of data to create the reference curves. To include the whole satellite constellation, data for one astronomic day were collected. With a sampling frequency of 20 Hz, the amount of data required efficient data management. The use of MySQL database solved the data handling.

8.2 Possible Use Cases

The presented preliminary model has not been designed for use in the everyday environment. The size is too large, and the measurement procedure is too complicated for direct application. However, the intention was to create a proof of concept of an idea that was, as yet, available only in theory. Even if NORDIS is not ready for the mass market, some tasks could be accomplished with the present system.

8.2.1 Initial Orientation for Tachymeter

One immediate use could be determining the initial orientation for a tachymeter. In the case of a tachymeter with a GNSS antenna on top, an attenuation shield could be mounted as shown in Figure 1.7. By rotating the tachymeter, the attenuating effect can be achieved. The accuracy achieved with NORDIS meets the requirements specified in Section 5.1.1. However, the synchronisation between C/N_0 value and angular position of the tachymeter needs to be solved as an integral part of the on-board software.

8.2.2 Orientation Determination for Permanent Antennas

For long-term monitoring tasks, GNSS antennas are often installed permanently. For tasks in which a high accuracy is desired, correction models for the phase centre variation (PCV) are required. To correctly apply the PCV model, the orientation of the antenna must be known. However, it is not easy to determine the orientation of the antenna by ordinary means. In this case, the principle of NORDIS could be used to initially orient the antenna. After the orientation, the attenuation has to be removed to avoid disturbing regular measurements.

8.2.3 Use of NORDIS with Ultra-Wide Band Antenna for non-GNSS Applications

A test conducted with an ultra-wide band (UWB) antenna showed that the NORDIS hardware could also be used for non-GNSS applications. The tested UWB antenna is part of an indoor positioning system used for a building information system, as presented in Blankenbach and Norrdine (2011. The system is composed of several mounted devices positioned at known coordinates and consisting of an antenna and a connected transceiver (transmitter and receiver) and one mobile device consisting of two antennas, one transceiver, and a camera (see Figure 8.1). The system is intended to deliver images with known camera position and orientation as input data for augmented reality applications. Because the camera is levelled, knowing the orientation within the horizontal plane x, y [Figure 8.1 (a)] is sufficient. The actual setup uses two UWB antennas mounted on a baseline [Figure 8.1 (b)] to calculate the orientation from coordinate differences (see Section 2.2.7).
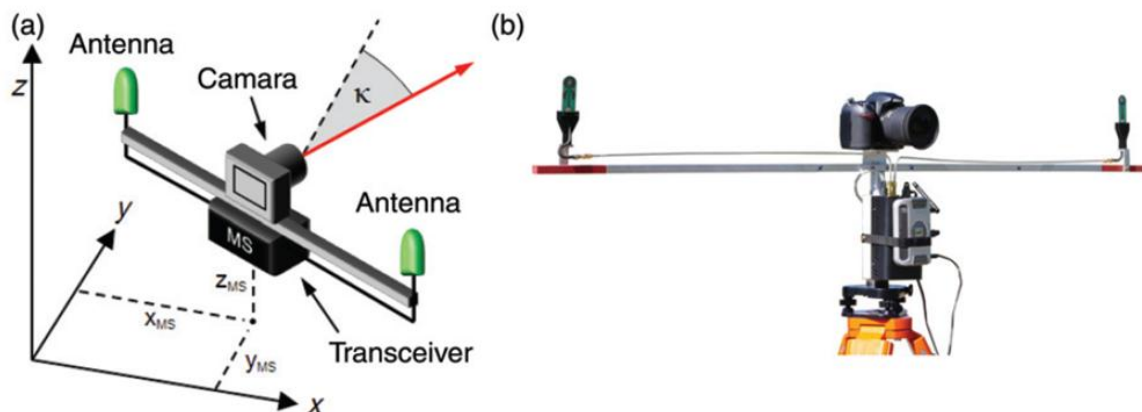
Figure 8.1 Setup for camera orientation using two UWB antennas mounted on a baseline (Blankenbach and Norrdine, 2011).

Alternative to the two antennas, the NORDIS approach could be used to determine the orientation. To test the feasibility of this idea, a UWB antenna was mounted on the NORDIS hardware, as shown in Figure 8.2. An additional UWB antenna was placed, first, at position 1 and, second, at position 2 (see Figure 8.3).
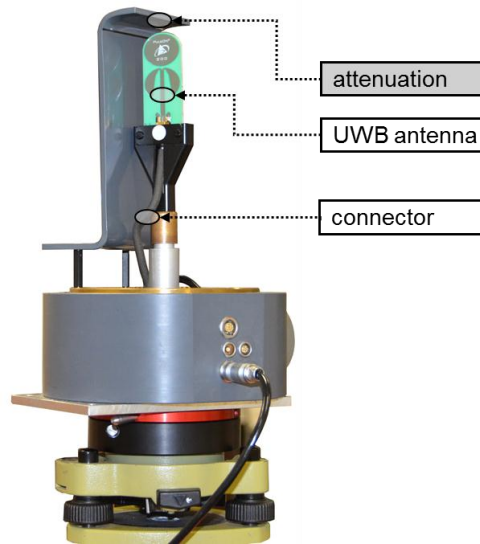
Figure 8.2 UWB antenna mounted on the NORDIS hardware (Picture D. Grimm).
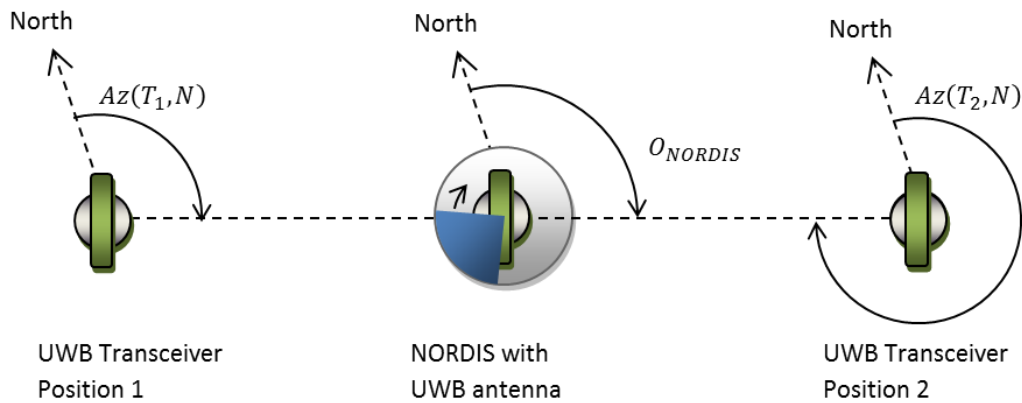
Figure 8.3 Measurement setup. First, the UWB transceiver was placed at position 1, then moved to position 2.
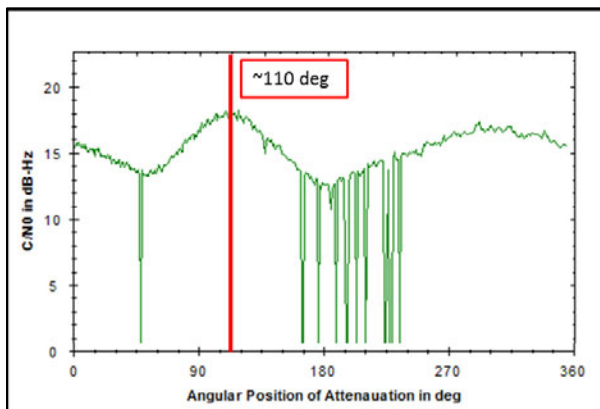
Figure 8.4 Signal strength with transceiver at position 1 during one revolution of the attenuation shield.
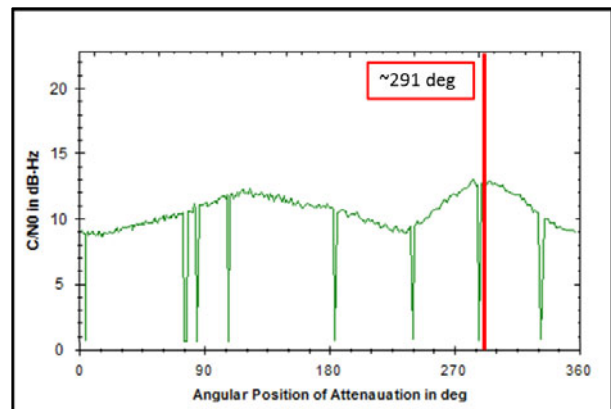
Figure 8.5 Signal strength with transceiver at position 2 during one revolution of the attenuation shield.

The signal strength was measured at the antenna on the NORDIS hardware during one revolution of the attenuation shield. Figure 8.4 shows the signal strength received from the transceiver at position 1 and Figure 8.5, the signal strength from position 2. The signals are significantly modified by the attenuation shield and have a dependency on the angle of entrance of the signal.

Because the distance to position 1 is shorter than the distance to position 2, the signal strength is stronger for position 1. The phase shift of the two curves is 291-110=181 deg, which corresponds to the measurement setup shown in Figure 8.4.

The first results look promising; however, a sophisticated analysis must still be undertaken.

8.2.4 Detection of Multipath and Reflected Signals (Multipath Scanner)

Given that the DOA of each satellite's signal can be measured, NORDIS can be used to detect erroneous signals reaching the antenna. Assuming the antenna orientation is known, the DOA of each signal can be calculated from the ephemerides in relation to the antenna. The observed DOA, determined with NORDIS for each satellite, can then be compared with the values expected from the ephemerides. Signals received from multiple directions indicate a multipath. One signal coming from the wrong direction indicates a reflected or diffracted signal. Such a result is particularly interesting when only the reflected signal reaches the antenna and the original signal is not detectable. To test the influence of erroneous signals with NORDIS, two data series were measured on the roof of the HIL building. The second data series was measured 23 h 56 min after the first, to ensure the same constellation, at least for the GPS satellites.

Figure 8.6 Measurement setup on the roof of the HIL building on 10.07.2012. View from north. (Picture: L. Steiner)

Figure 8.7 Follow-up measurement at the same place on 11.07.2012. View from south. (Picture: D. Grimm)

Figure 8.8 360 deg panoramic view from the HIL roof. (Picture: L. Steiner)

8.2.4.1 Multipath Detection

Figure 8.9 shows the curve of the C/N_0 densities for SV 18 during one revolution of the attenuation shield (green) with minor deviations from the reference curve (red). Figure 8.10 shows again the C/N_0 density for SV 18 during one revolution (green) and the reference curve (red) after 14 revolutions of the attenuation shield. The time difference between the two measurements is ca. 8 min. During these 8 min, the satellite shows an azimuthal change of ca. 4 deg, which is corrected for the plots by subtracting the azimuth from the angular position [see Equation (5.3)]. Nevertheless, the C/N_0 in Figure 8.10 does not fit the reference curve, indicating a disturbed reception of the signal.
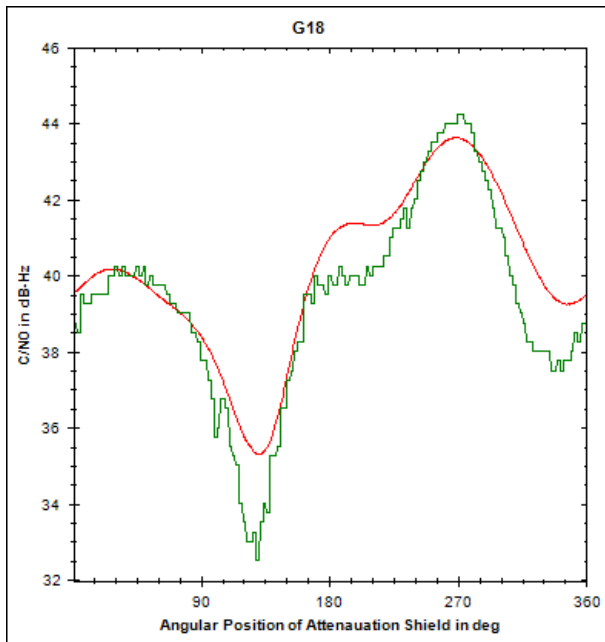
Figure 8.9 C/N$_0$ during one revolution of the attenuation shield (green) and the reference curve (red)
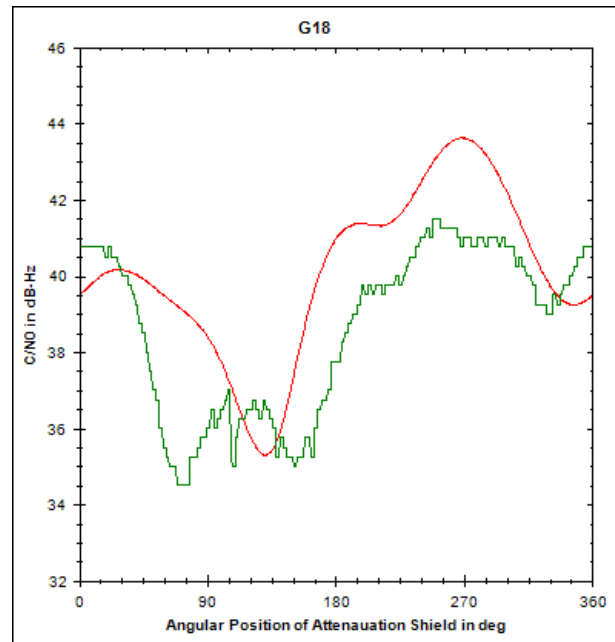
Figure 8.10 C/N$_0$ during one revolution of the attenuation shield (green), showing significant deviation from the reference curve (red)

Figure 8.11 and Figure 8.12 show the skyplot for the measurements from 10.07.2012 and 11.07.2012, during the same satellite constellation. The colour of each dot of the satellite tracks in Figure 8.11 and Figure 8.12 represents the value of the correlation coefficient, calculated from one revolution of the attenuation shield (e.g., Figure 8.9 or Figure 8.10). The colour indicates how well the measured curve and the reference curve fit together. To calculate the correspondence, the curve of the actual revolution is cross-correlated with a reference curve at the corresponding elevation (see Section 6.2).
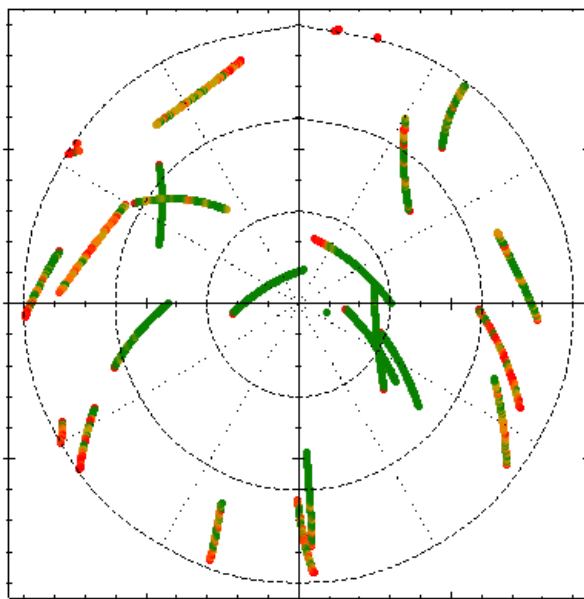
Figure 8.11 Coloured skyplot from 10.07.2012 during 91 revolutions of the attenuation shield. The red parts of the tracks indicate a disturbed signal reception.
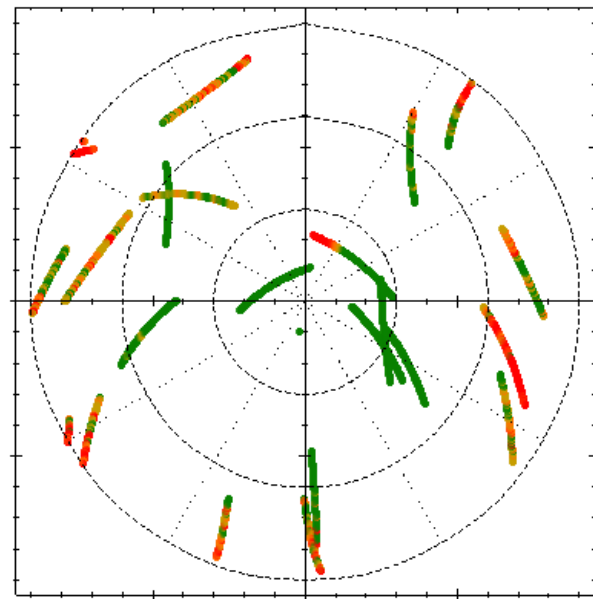
Figure 8.12 Follow-up measurement from 11.07.2012 with 95 revolutions of the attenuation shield.

For a correlation coefficient > 0.9, the signal reception can be assumed to be undisturbed, and the dot is plotted in green. For correlation coefficients < 0.4, the dot is plotted in red. The values between 0.4 and 0.9 change gradually from red to orange. Thus, the green part of the satellite track indicates an undisturbed measurement with no multipath, reflected, or diffracted signals while the orange indicates some deviations from the reference curve and the red part is a strong indication of a disturbed signal.

Comparing the two figures indicates a remarkable recurrence of the patterns. The signals of single satellites are disturbed at the same positions for both measurement days, indicating an influence in the local antenna environment. In a next step, the critical curves are further analysed to distinguish multipath from reflected or diffracted signals. Knowing the critical positions of the satellites allows for excluding these satellites during the critical time from the position calculation, resulting in reduced coordinate uncertainty.

8.2.4.2 Comparison of Measurements in Multipath Intensive and Low Multipath Areas

To verify the detection of multipath and reflected signals, measurements were conducted in a low multipath area (Figure 8.13), with NORDIS placed in an open meadow, and in an area with expected multipath (Figure 8.14) signals, with the antenna placed in front of a wall. The wall is situated to the north, with ca. 1 m distance to the antenna. A second wall is to the east at a distance of ca. 10 m. Both measurements were conducted with corresponding satellite constellations for GPS.
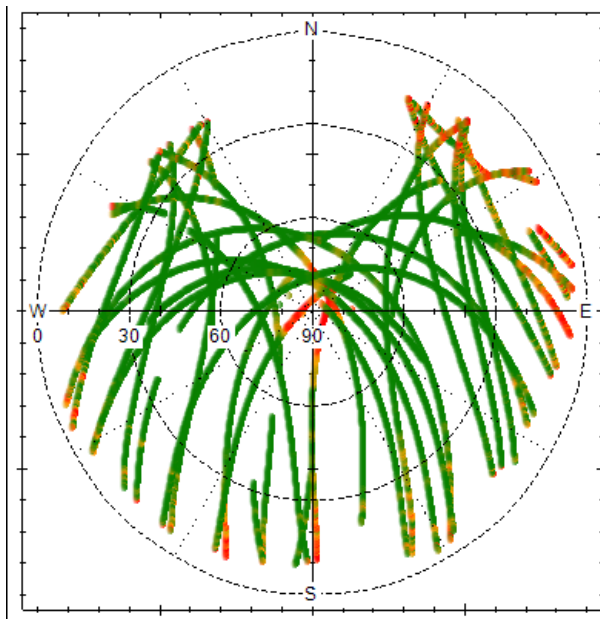
Figure 8.13 Coloured skyplot from measurements of a meadow area with low multipath. (Grimm et al., 2012)
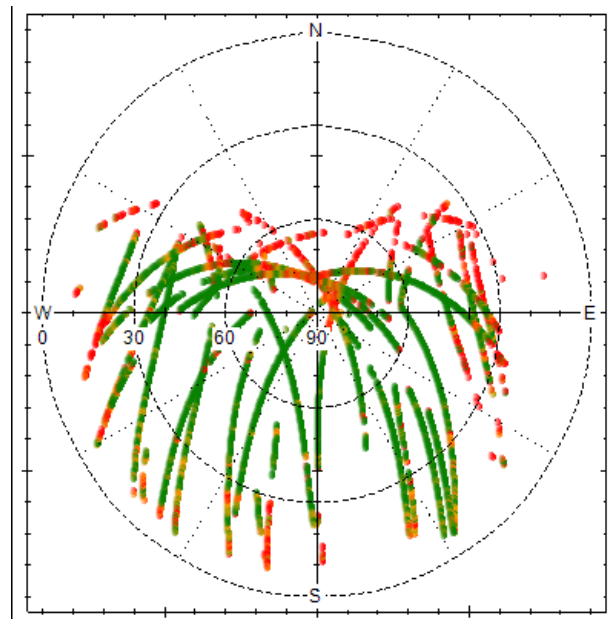
Figure 8.14 Coloured skyplot from measurements with the antenna placed in front of a wall. The multipath is clearly visible by the red dots. (Grimm et al., 2012)

Figure 8.13 shows largely undisturbed measurements. The red dots in the zenith are caused by the weak influence of the attenuation shield for satellites at high elevations and are, thus, random. Some effects can be seen for low elevations, in particular in the north-eastern part. In Figure 8.14, the multipath effects caused by the walls in the north and east are clearly visible.

8.2.4.3   Analysis of a Single Satellite Track

The following section is based on Grimm et al. (2012.

Figure 8.15 shows one exemplary satellite in the measurements shown in Figure 8.13 and Figure 8.14. The two upper graphs show the skyplot of SV27, using data from the almanac for azimuth and elevation. For the bottom graphs, the azimuth value originates from observed DOAs derived from NORDIS. In the case of undisturbed measurements (left in Figure 8.15), the observed DOA (bottom left in Figure 8.15) corresponds to the expected DOAs (top left in Figure 8.15) for each satellite position, although some systematic deviations exist for low elevations. In contrast, most observed DOAs from the measurements in the high multipath location (right in Figure 8.15) do not correspond to the expected DOAs.
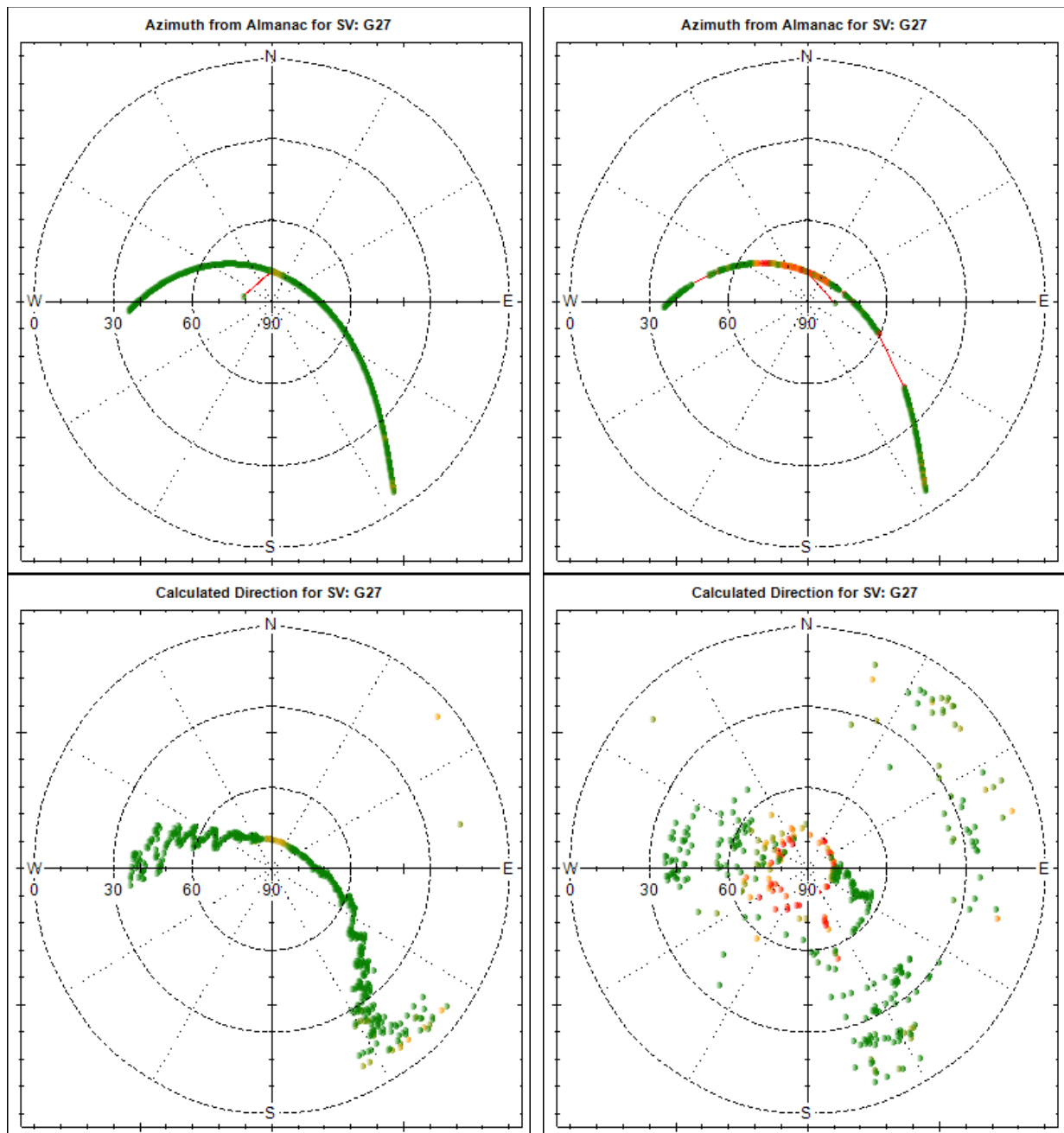
Figure 8.15 Skyplot of SV27 from the meadow area (left) and next to a building (right). Expected DOA (top) and observed DOA (bottom). Multipath free is shown on the left and near a wall on the right. (Grimm et al., 2012)

Green dots reflect good correlation with the reference data (correlation-coefficient greater than 0.9) indicating a signal from one direction only. Although this particular data point represented by a green dot has a high correlation with the shape of the reference data, this signal still could potentially have a phase shift and thus arrive from a different direction than expected. To evaluate if the signal has arrived from a different direction, the difference between the expected DOA and observed DOA is calculated. All points which lie within a range of 15 degrees from the expected position are considered to have arrived directly at the antenna and are plotted in green (Figure 8.16). (Grimm et al., 2012)

This threshold value is based on the assumption that the observed DOAs in the case of the undisturbed area shown in Figure 8.18 are directly received. The deviation within 15 deg is caused by thus far unknown system effects. Signals arriving from a different direction (> 15 deg) compared to the nominal direction are categorised as reflected and, therefore, plotted in blue in Figure 8.16 and Figure 8.17.
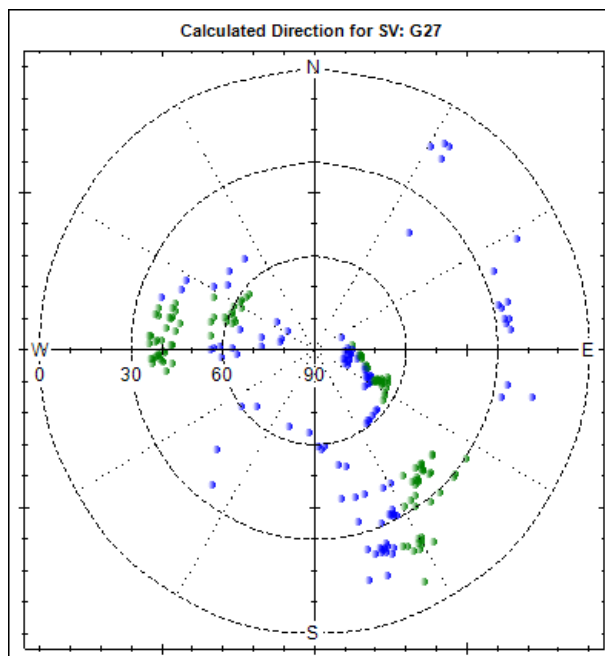
Figure 8.16 Satellite signals corresponding to the expected DOAs are plotted in green while signals with unexpected DOAs are plotted in blue.
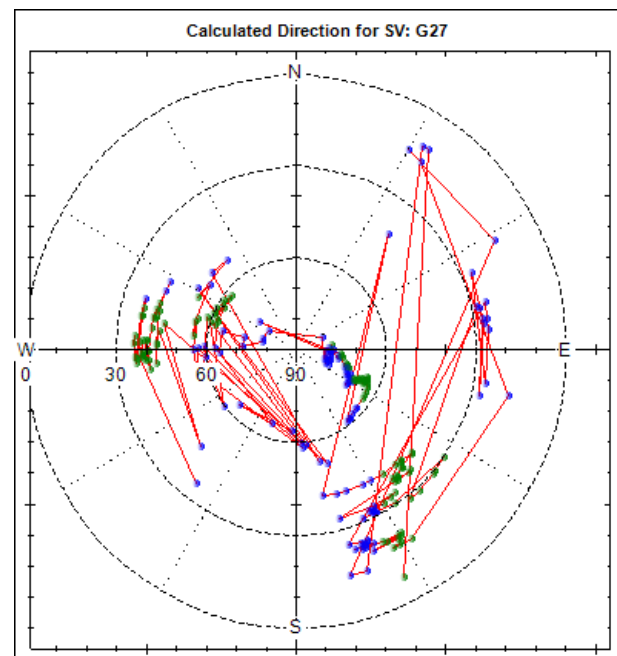
Figure 8.17 Detected DOAs connected by a red line to show the chronological order.

8.2.4.4 Workflow for Signal Quality Control

From the analysis of the multipath and reflected or diffracted signals, a workflow for GNSS signal quality control can be composed, as presented in Figure 8.18.

In a first step, the correlation-coefficient (cc) between the observed data and the reference data is analysed. This allows a distinction of signals arriving the antenna from one direction (cc = 1 and cc > 0.9) or arriving the antenna from multiple directions (cc < 0.9). For signals arriving only from one direction, the DOA is compared with the expected DOA in a second step. This allows a distinction between directly received signals and reflected signals. (Grimm et al., 2012)

© L. Steiner
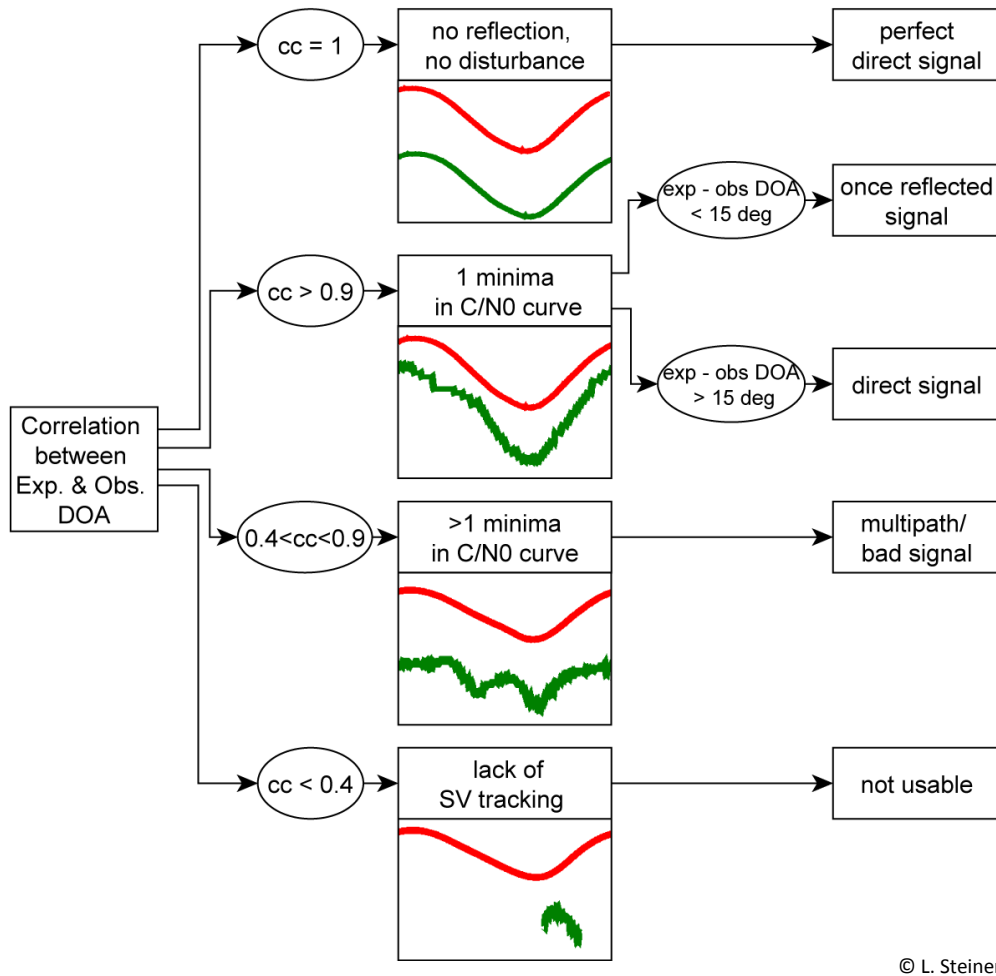
Figure 8.18 Workflow to identify multipath and reflected signals (Grimm et al., 2012).

The output of this analysis must be evaluated by comparing it with other multipath and diffraction mitigation approaches as presented in Rost (2011) and Wieser (2001).

8.2.5   Human Body as Attenuation Shield

Pedestrians using a mobile device (Figure 8.20) are attenuating satellite signals with their body when the signals arrive from behind the person. This effect could be taken advantage of to use the human body instead of an attenuation shield. Similar to the presented NORDIS approach, the C/N_0 can be used to detect the DOAs of the satellites' signals.
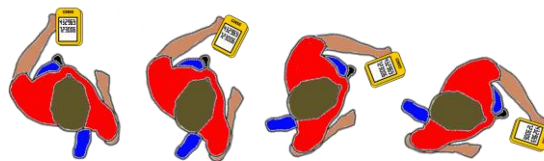
Figure 8.19 Human body as attenuation shield for satellites signals reaching the GNSS device from behind the person.

The upper graphs in Figure 8.20 show the C/N_0 of three exemplary satellites during one rotation of the person holding the GNSS handheld device as shown in Figure 8.19. The lower graphs in Figure 8.20 show the C/N_0 of the same satellites while the person stands still.
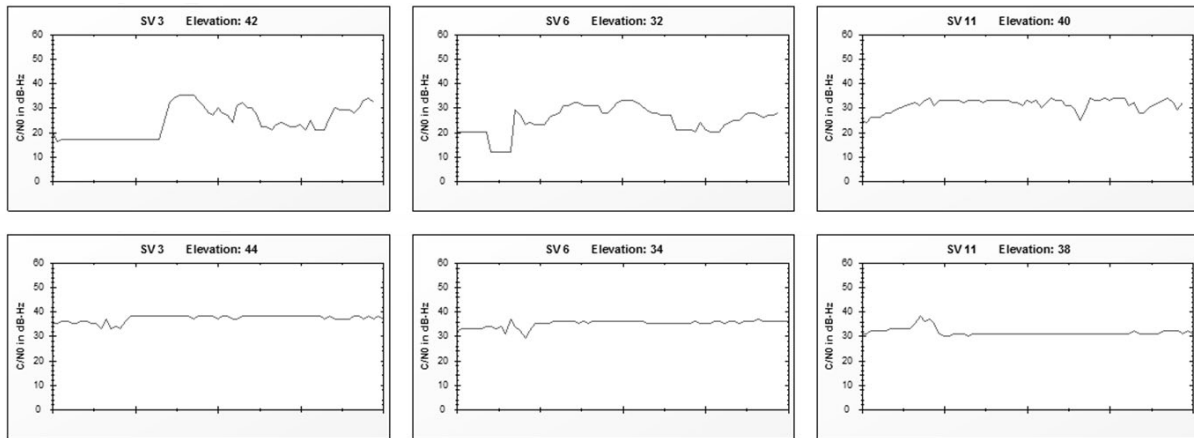
Figure 8.20 C/N_0 values during one revolution of the person (upper graphs) and while standing still (lower graphs).

Comparing the different graphs, the influence of the human body is visible. However, the influence is irregular, and determination of the DOA is not clearly possible. Nevertheless, improving this approach could allow GNSS to provide pedestrians, at least, with course orientation information.

8.3 Possible Improvements of NORDIS

The functional model presented in this thesis is a proof of concept. However, the presented system could and should be improved in several ways:

- The rotating attenuation should be miniaturised and included in the antenna or, even better, be realised electronically. The present system with a mechanical rotating attenuation shield is unsuitable for daily use. However, it is far from clear whether an electronic attenuation shield is feasible at all.
- Instead of using a reference curve for each degree of elevation, a mathematic function could be found to describe the behaviour.
- To make the system real-time capable, a real-time stream of the C/N_0 densities in float instead of integer accuracy should be established. Further, the analysis algorithm must be improved. Instead of averaging the values after the completion of all measurements, linear regression could be implemented to update and average the values continuously.
- Finding the reason for the systematic effects (Figure 8.15) would increase the reliability and improve the accuracy of both, orientation and determination of multipath and reflected signals.

8.4   Limitations of NORDIS

Because the C/N_0 estimation for each satellites signal is correlated between the GNSS satellites, the influence of the attenuation shield cannot be treated as completely uncorrelated. Thus, the attenuation shield has an influence not only on the incoming signals of the specific satellites in the line of sight of the attenuation shield but also on all received signals. The level of correlation depends on the implemented C/N_0 calculation approach, which classically is the narrowband-wideband power ratio method (NWPR) (see Section 3.6.10). Possibly, the output from NORDIS differs when using alternative estimators for C/N_0 as presented in Falletti et al. (2011. This could be the reason for the present systematic effects. In addition, it is important to recognise that diffraction and influences from the ionosphere or interfering signals can impede the satellite signal reception completely. In such a case, orientation determination is no longer possible.

9 Appendix

9.1 Acronyms and Abbreviations

AGC .... Automatic Gain Control

AR .... Axial Ratio

ARP .... Antenna Reference Point

ATR .... Automatic Target Recognition

BIH .... Bureau International de l'Heure

C .... Carrier Power

C/A .... Coarse Acquisition

CHTRF .... Swiss Terrestrial Reference Frame

CIO .... Conventional International Origin

C/N$_0$ .... Carrier-to-Noise Density

CTP .... Conventional Terrestrial Pole

CTRS .... Conventional Terrestrial Reference System

dB .... Decibel

dBm .... power ratio in decibels (dB) of the measured power referenced to one milliwatt

dBW .... power ratio in decibels (dB) of the measured power referenced to one watt

deg .... Degree

DLL .... Delay Lock Loop

DOA .... Direction of Arrival

DR .... Dead Reckoning

E .... East

ECEF .... Earth-Centered Earth-Fixed

EGNOS .... European Geostationary Navigation Overlay Service

EIRP .... Effective Integrated Radiate Power

EM .... Electro Magnetic

EOP .... Earth Orientation Parameters

ETH .... Swiss Federal Institute of Technology

ESA .... Electrically Small Antenna

FM ....Frequency Modulation

GAGAN ....GPS Aided Geo Augmented Navigation

GB...Giga Byte

GLONASS. Globalnaja Nawigazionnaja Sputnikowaja Sistema (Global Navigation Satellite System)

G-MoDe..GNSS-Movement Detection

GNSS .... Global Navigation Satellite System

GPS ....Global Positioning System

HIL...Building at ETH

IDOT..stands for a small letter i with a dot representing the first derivative

IEEE..Institute of Electrical and Electronics Engineers

IERS..International Earth Rotation Service

INS ....Inertial Navigation System

IMU...Inertial Measuring Unit

IRM...IERS Reference Meridian

IRP ....IERS Reference Pole

ITRF ....International Terrestrial Reference Frame

ITU...International Telecommunication Union

L1 .... Carrier Frequency (GPS + GLONASS)

L2 .... Carrier Frequency (GPS + GLONASS)

L3 .... Carrier Frequency (GLONASS)

L5 .... Carrier Frequency (GPS + GLONASS)

LHCP .... Left-Handed Circular Polarisation

LNA... Low Noise Amplifier

MEO.. Medium Earth Orbit

MUSIC...MUltiple SIgnal Classification

N .... North

NBW.. Noise Bandwidth

NMEA .... National Marine Electronics Association

NORDIS..NORth Direction Indication System

NWPR.. Narrowband-Wideband Power Ratio

OP.. Observation Point

PCO.. Phase Centre Offset

PCV .... Phase Centre Variation

PLL...Phase Lock Loop

PRN .... Pseudo Random Noise

RINEX.. Receiver Independent Exchange Format

RHCP.. Right-Handed Circular Polarisation

S ....South

Sapos .... Satellite Positioning Service

SNR.. Signal-To-Noise-Ratio

SV .... Space Vehicle (expression for Satellite)

Swipos... Swiss Positioning Service

UWB... Ultra Wide Band

W ....West

WAAS..Wide Area Augmentation System

WRC .... World Radio Conference

WGS 84 ....World Geodetic System 1984

9.2   Conventions

GPS and GNSS

The abbreviation **GPS** is used when only the U.S. Global Positioning System is concerned. For general statements that include the Russian GLONASS, the European Galileo, the Chinese COMPASS and other systems, the abbreviation **GNSS** (Global Navigation Satellite System) is used.

Expression of Uncertainty in Measurement

In this thesis, uncertainties in measurements are indicated according to the **International Vocabulary of Basic and General Terms in Metrology** (Joint Committee for Guides in Metrology, 2008). See Appendix 9.4 for an extract of the most frequently used definitions.

Italic Face

Terms used for a concept to be defined are printed in italic face the first time they appear.

Referenced Figures

Adopted figures are referenced. Unreferenced figures origin from the author.

9.3 Symbols

Further symbols are introduced when used.

a	semi major axis
A	substitution variable, used in Equation (6.3)
A_m	azimuth between the running axis of a gyroscope and the local meridian
α	angular position of the attenuation shield
α_t	angular position of the attenuation shield at time t
$\tilde{\alpha}$	reduced α
$Az(A, B)$	azimuth between A and B
Azi	azimuth
b	semi minor axis
B	substitution variable, used in Equation (6.3)
$\boldsymbol{B}$	magnetic field vector
c	propagation velocity of electromagnetic waves in air ($2.9979 \cdot 10^8$ m/s)
C	carrier power
C_{ic}	amplitude of the cosine harmonic correction term to the angle of inclination
C_{is}	amplitude of the sine harmonic correction term to the angle of inclination
C_{rc}	amplitude of the cosine harmonic correction term to the orbit radius
C_{rs}	amplitude of the sine harmonic correction term to the orbit radius
C_{uc}	amplitude of the cosine harmonic correction term to the argument of latitude
C_{us}	amplitude of the sine harmonic correction term to the argument of latitude
d	distance
D	precession
D_A	normalised directivity
δ	delay (cross-correlation function)
Δn	mean motion difference from computed value
e	eccentricity
$\boldsymbol{E}$	electric field vector
ε	attenuation factor of absorbing material
ε_r	relative permittivity (dielectric constant)
Ele	elevation
G_G	GPS system gain

Symbols

H	magnetic H-Field
i	inclination
IDOT	rate of inclination angle
j	control variable
k	Boltzmann constant ($1.38 \cdot 10^{-23} \, J/K$)
κ	quality variable
l	radian lenght (antenna)
L	size (antenna)
λ	geodetic latitude
λ_w	wavelength
Λ	longitude
m	control variable
M_0	mean anomaly at epoch
n	number
N	noise
N_0	standard thermal noise floor
N_T	ambient thermal noise (at 290 K)
v_a	true anomaly
v_c	corrected true anomaly
O_{NORDIS}	unknown orientation of NORDIS
$\bar{O}$	averaged orientation of the antenna
ω	argument of perigee
ω_{AS}	average angular velocity of the attenuation shield
ω_E	Earth angular momentum
Ω	longitude of ascending node
Ω_0	right ascension angle measured from the zero meridian (GPS)
$\dot{\Omega}$	rate of right ascension
P	ellipse parameter
φ	geodetic latitude
φ_A	longitude (antenna coordinate system)
ϕ	phase angle
Φ	latitude
$\vec{r}_o$	position vector in the orbital system
$\vec{r}_e$	position vector in the equatorial system

$r(\lambda)$	function for position vector of a satellite, dependent on the true anomaly
$\boldsymbol{R}$	transformation matrix
R_1	radius for the antenna near field
R_2	radius for the antenna far field
R_G	running axis of the gyroscope
s	empirical standard deviation
σ	standard deviation
T	revolution period
T_a	absolute temperature
τ	transformation
θ	zenith angle (antenna coordinate system)
u_A	standard measurement uncertainty of the type A
u_B	standard measurement uncertainty of the type B
u_C	combined standard measurement uncertainty (type A and type B)
ξ_i	data series (cross-correlation function)
x_s , y_s	Cartesian coordinates of the satellite in the orbital system
x_t, y_t, z_t	Cartesian coordinates of the satellite in the topocentric horizontal system
X_s, Y_s, Z_s	Cartesian coordinates of the satellite in the geocentric system
v	Fresnel diffraction parameter
v_i	data series (cross-correlation function)

9.4 Expressions of Uncertainty in Measurement

The following definitions are taken from the **International Vocabulary of Basic and General Terms in Metrology** (Joint Committee for Guides in Metrology, 2008)

9.4.1 Measurement Accuracy

Closeness of agreement between a measured quantity value and a true quantity value of a measurand

NOTE The concept 'measurement accuracy' is not a quantity and is not given a numerical quantity value. A measurement is said to be more accurate when it offers a smaller measurement error.

9.4.2 Measurement Error

Measured quantity value minus a reference quantity value

9.4.3 Measurement Precision

Closeness of agreement between indications or measured quantity values obtained by replicate measurements on the same or similar objects under specified conditions

NOTE Measurement precision is usually expressed numerically by measures of imprecision, such as standard measurement uncertainty, variance, or coefficient of variation under the specified conditions of measurement.

9.4.4 Measurement Uncertainty

Non-negative parameter characterizing the dispersion of the quantity values being attributed to a measurand, based on the information used

NOTE 1 Measurement uncertainty includes components arising from systematic effects, such as components associated with corrections and the assigned quantity values of measurement standards, as well as the definitional uncertainty. Sometimes estimated systematic effects are not corrected for; instead, associated measurement uncertainty components are incorporated.

NOTE 2 The parameter may be, for example, a standard measurement uncertainty called standard measurement uncertainty (or a specified multiple of it) or the half-width of an interval having a stated coverage probability.

9.4.5 Measurement Trueness

Closeness of agreement between the average of an infinite number of replicate measured quantity values and a reference quantity value

NOTE Measurement trueness is not a quantity and, thus, cannot be expressed numerically, but measures for closeness of agreement are given in ISO 5725.

9.5 GNSS Receiver

For all antennas with a coaxial cable connection, the Leica GX 1230 GG receiver was used in these tests.
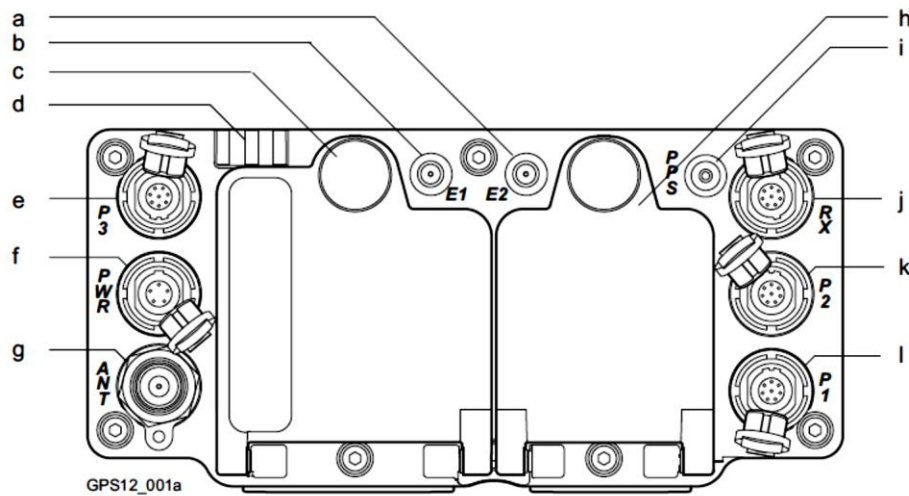
a) Port E2: Event input 2, on GX 1200 with PPS / Event option
b) Port E1: Event input 2, on GX 1200 with PPS / Event option
c) Battery compartment A
d) LED indicators
e) Port P3: Power out, data in/out, or remote interface in/out. 8-pin LEMO
f) Port PWR: Power in. 5-pin LEMO
g) Port ANT: GNSS antenna in

h) Battery compartment B
i) Port PPS: PPS output, on GX 1200 with PPS / Event option
j) Port RX: RX 1200 in/out or remote interface in/out. 8-pin LEMO
k) Port P2: Power out, data in/out, or remote interface in/out. 8-pin LEMO
l) Port P1: Power out, data in/out, or remote interface in/out. 8-pin LEMO

Figure 9.1 Interface ports of the receiver Leica GX 1230 GG (Leica, 2007a).

Because the Leica GX 1230 GG receiver supports neither Bluetooth® nor the digital input from the smart antenna (ATX1230 GG), the receiver RX 1250 has to be used for this antenna type. However, such receiver types are not equipped with an event input interface. Therefore, an additional Leica GX 1230 GG receiver with its own Leica AX1202 GG antenna can be used, in particular to record the events from the encoder of the inner orientation.

9.6 Absorbing Materials Specification

For the attenuation shield in NORDIS, the material WX-020 is used.

WAVE-X® WX Series

High Permeability Absorbers & Suppressors

Wave-X WX series combines the highly effective energy absorption properties of proprietary high performance magnetic materials with the desirable physical characteristics of flexible elastomer. Precisely refined fillers are blended in exacting ratios with various substrate materials to create thin, flexible EMI absorption sheets which attenuate over a wide range of frequencies.

Wave-X products provide superior EMI absorption through inductive coupling and are designed for close proximity placement to the transmission source. These thin, flexible absorber sheets attenuate the radiated noise by suppressing magnetic fields at the source.

• Hi Temperature   • SAR - Mobile Phone

WX Series Typical Performance

Wave-X WX-010
Wave-X WX-020
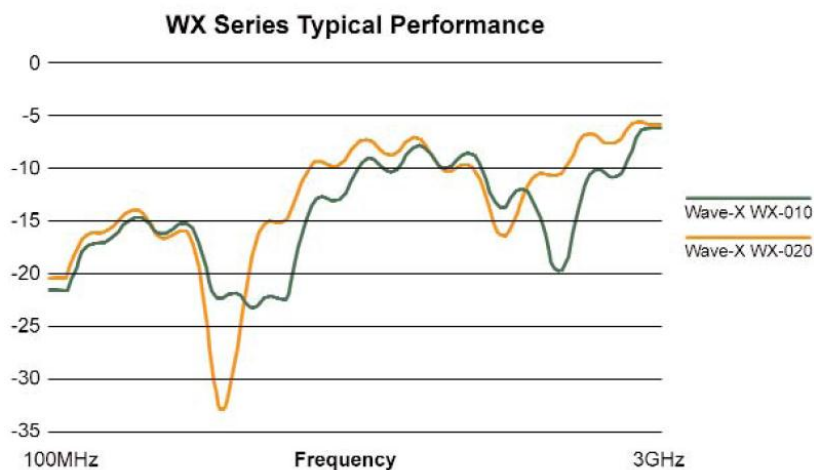
Technical Specifications

FREQUENCY RANGE	100 MHz - 3GHz
OPERATING TEMPERATURE	-65° to +350°F / -54° to +177°C
AVAILABLE THICKNESS (excluding adhesive)	.005", .010", .020", .040" 0.13, 0.25, 0.5, 1.0mm (custom sizes available)
SURFACE RESISTANCE	>1MΩ
ELONGATION	75%
PRODUCT FORMAT	Sheets or Rolls Cut to Size & Shape Pressure Sensitive Adhesive (optional) Ground Plane (optional)

WAVE-X® WD Series
Tailored Permeability, UL94-V0 Rated Absorbers & Suppressors

Wave-X WD Series absorbers are made from soft magnetic metal powders encapsulated in flexible thermoplastic rubber sheets. Within the WD series range ARC has included several product categories designed to optimize absorber thickness and permeability against the frequencies to be controlled. All products in the WD Series are UL94-V0 certified.

Like all Wave-X products, the WD Series provides superior EMI absorption through inductive coupling and are designed for close proximity placement to the transmission source. These thin, flexible absorber sheets attenuate the radiated noise by suppressing magnetic fields at the source. The Wave-X WD-HS absorbers are designed to enhance the transmission range of RFID systems operating at 13.56MHz.
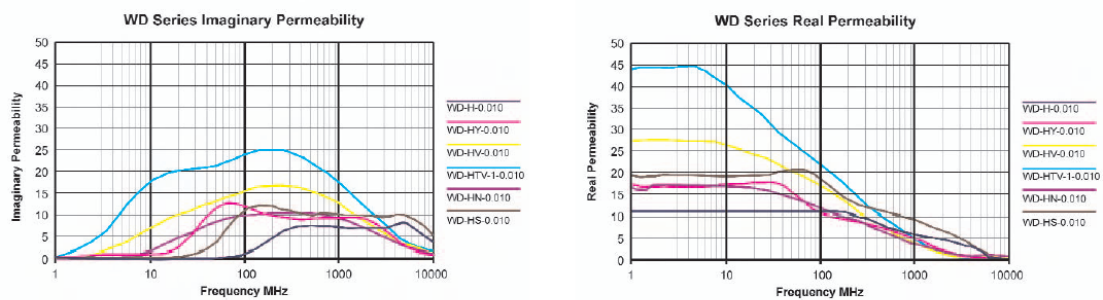

Technical Specifications

WD CATEGORY	H / HY Broadband	HV High Permeability	HTV-1 Ultra-High Permeability	HN Halogen Free	HS For RFID
FREQUENCY RANGE	200MHz - 10GHz / 30MHz-4GHz	10MHz - 3GHz	5MHz - 3GHz	20MHz - 3GHz	13.56MHz and below
OPERATING TEMPERATURE	-25° to 194°F / -31° to 90°C	-25° to 194°F / -31° to 90°C	-25° to 194°F / -31° to 90°C	-25° to 194°F / -31° to 90°C	-25° to 194°F / -31° to 90°C
THICKNESS IN/MM	0.002", 0.004", 0.010", 0.020, 0.040" 0.05, 0.1, 0.25, 0.5, 1mm	0.002", 0.004", 0.010", 0.020" 0.05, 0.1, 0.25, 0.5mm	0.004", 0.010", 0.020" 0.1, 0.25, 0.5mm	0.004", 0.010", 0.020" 0.1, 0.25, 0.5mm	0.010", 0.020 0.25, 0.5mm
SURFACE RESISTANCE (ref.)	1MΩ - WD-H 200MΩ - WD-HY	10MΩ	1600MΩ	10MΩ	$1 \times 10^{4}\Omega$
FLAMMABILITY RATING	UL94-V0	UL94-V0	UL94-V0	UL94-V0	
ELONGATION	50% / 60%	60%	20%	60%	30%
PRODUCT FORMAT	Sheets or Rolls Max. width 9" (230mm) Pressure Sensitive Adhesive (optional) Ground plane (optional)	Sheets or Rolls Max. width 9" (230mm) Cut to Size & Shape Pressure Sensitive Adhesive (optional) Ground plane (optional)	Sheets 17.7x16.9 (450x430mm) Cut to Size & Shape Pressure Sensitive Adhesive (optional) Ground plane (optional)	Sheets or Rolls Max. width 9" (230mm) Cut to Size & Shape Pressure Sensitive Adhesive (optional) Ground plane (optional)	Sheets 11.7x8.3" (297x210mm) Cut to Size & Shape Pressure Sensitive Adhesive (optional) Ground plane (optional)

Source and further data sheets: http://www.arc-tech.com/wavex2.php

9.7   Principle of Autocollimation

To use a theodolite for autocollimation, a special illumination of the reticle is needed. The illumination is not to be confused with the illumination of the reticle for night measurements, but rather, it is a special illumination that projects the picture of the reticle through the telescope. Special autocollimation-theodolites with built-in illumination are available; however, an add-on allows using a common theodolite. Figure 9.2 illustrates the principle of autocollimation.
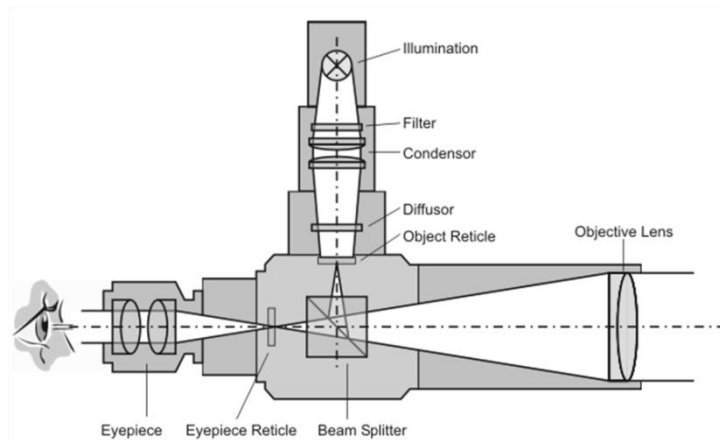
Figure 9.2 Principle of autocollimation (Davidson Optronics, 2011).

> After passing through the beamsplitter, light enters the objective lens where it is collimated prior to exiting the instrument. Collimation simply means that the light rays exit the instrument parallel to one another. After being reflected by a mirror or other high-quality reflective surface, light re-enters the autocollimator and is focused by the objective lens. The return image appears in sharp focus on the measuring reticle in focal plane [. . .] after being redirected 90 deg by the beamsplitter. An eyepiece is used to view the return image. Deviation of the mirror [. . .] will cause the return image to be laterally displaced [. . .] with respect to the measuring reticle. (Davidson Optronics, 2011)

9.8 Implementation of Calculation of Phase and Amplitude in Visual Basic

The equations presented in Section 6.1.1 can be converted into code in which one loop is needed as shown in Figure 9.3. The code was written in Visual Basic 2010.

```
For j = 0 To n - 1

        sin = Math.Sin(f * x(j))
        cos = Math.Cos(f * x(j))

        sumS += sin * sin
        sumC += cos * cos
        sumG += sin * cos
        suma += sin * y(j)
        sumb += cos * y(j)
Next

    _S = sumS
    _C = sumC
    _G = sumG
    _a = suma
    _b = sumb

    _Aa = (_C * _a - _G * _b) / (_S * _C - _G * _G)
    _Bb = (_S * _b - _G * _a) / (_S * _C - _G * _G)

    _phi = Math.Atan2(_Bb, _Aa)
    _am = Math.Sqrt(_Aa ^ 2 + _Bb ^ 2)
```

Figure 9.3 Code of implementation written in Visual Basic.

9.9   Process Flow of the Correlation Approach

The flow chart in Figure 9.4 illustrates the process flow for acquisition of reference data and acquisition of further measurement data. The reference data are saved to hard disk and can be repeatedly reused for the correlation. Consequently, the reference data must be acquired only once as long as the same type of antenna is used.
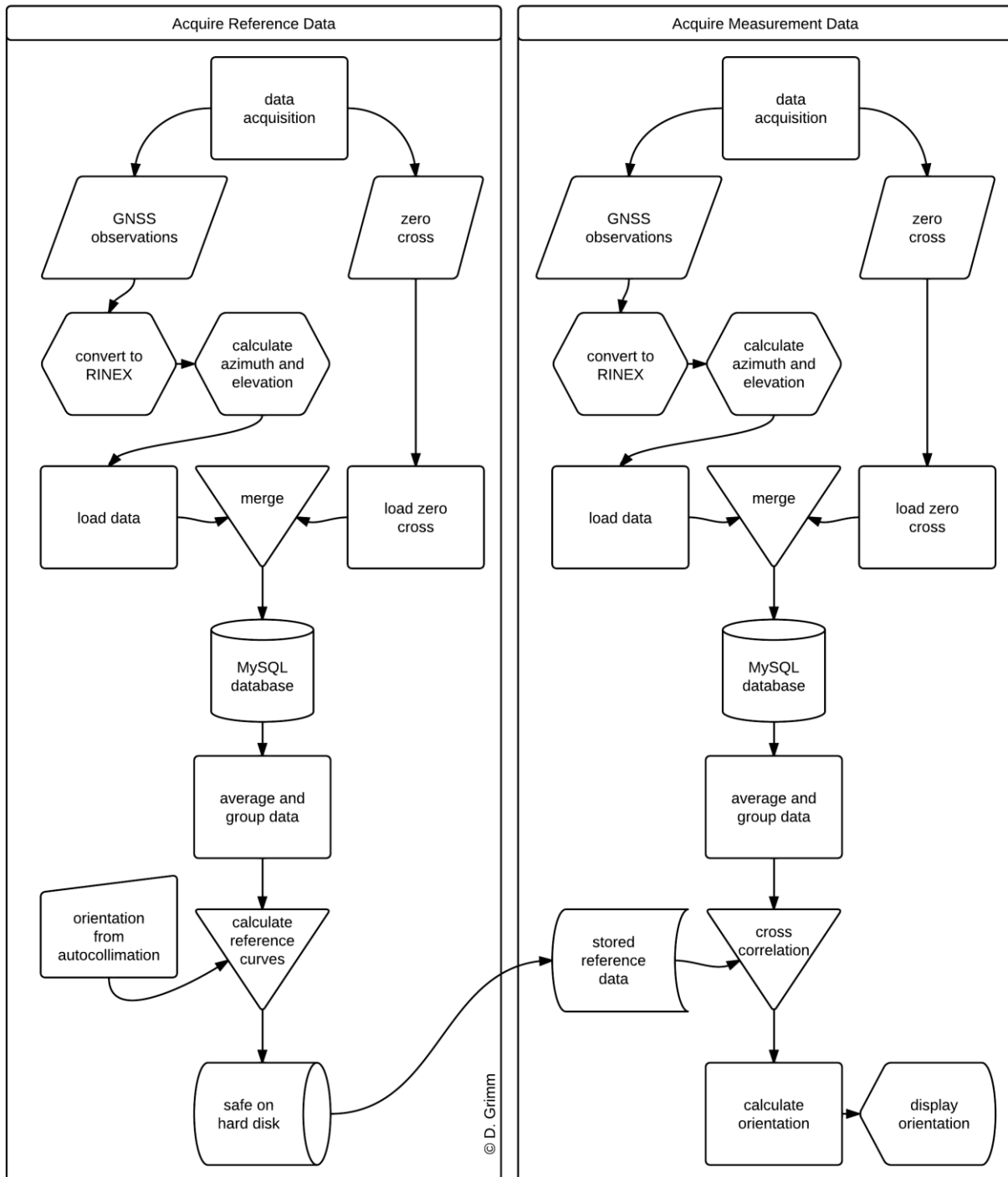

Figure 9.4 Process flow for the generation of reference data (left) and observation process (right).

9.9.1   Data Acquisition

The GNSS measurements are saved in a data format specific to the manufacturer (e.g., Leica). In addition, the timestamps of the zero crossings are saved in a separate text file. To calculate the angle of entrance in terms of the antenna, the satellite positions must be established by elevation and azimuth in the local horizontal coordinate system. Because the positions of the satellites are given in the ephemerides as orbital elements (see Section 4.1.1), the positions from the ephemerides must be converted into the horizontal system from the antenna location as explained in Section 4.1. This calculation process is implemented in the software WaRINEX[28], which needs the GNSS observation file in the RINEX[29]-observation-format and the broadcast ephemerides for GPS and GLONASS as input. Broadcast ephemerides for GPS and GLONASS can be either downloaded from the NASA-webpage[30] or exported from the collected data. The broadcast ephemerides are given in the RINEX navigation message format. Furthermore, the signal strength values S1 and S2 are required.

9.9.2   Data Conversion to RINEX

In the RINEX observation file, the observation types S1 and S2 indicate the signal strengths for L1 and L2. Normally, they correspond to the C/N_0, but they also can differ depending on the manufacturer (for more information about C/N_0, see Section 3.6.8). S1 and S2 are not part of the official RINEX version 1 or 2, but they can be included optionally. RINEX version 3 includes these observation types by default.

To convert the Leica measurement data into a RINEX observation file, the following two methods have been tested.

9.9.2.1   Leica Geo Office RINEX Export

Until the release of Leica Geo Office (LGO) version 8, the observations S1 and S2 were not included in the RINEX export. In LGO version 8, it is still not possible to specify the types of observation that should be included in the RINEX export. However, the observations S1 and S2 are exported by default. In addition to the RINEX observation file, the RINEX navigation files for all used SV systems (GPS and GLONASS) are exported.

9.9.2.2   Translating with "teqc"

An alternative method to convert a proprietary format into RINEX is the use of teqc[31]. Teqc is a toolkit for various pre-processing tasks with GNSS data: **t**ranslation, **e**diting, and **q**uality **c**heck.

"Teqc is being enhanced to handle a number of native binary formats from various receivers. For now, teqc handles common formats for many dual-frequency (L1 and L2) and a few single-frequency (L1) receivers," (Unavco, 2011). The RINEX export using teqc is nearly 3 times faster than that using LGO.

WaRINEX and teqc both process batch jobs, non-interactive programs that execute a series of calculations without manual intervention. To run them, a start command has to be entered. The start command includes the filename of the files to process. The command for "teqc" to convert the Leica raw date into RINEX is as follows:

---

[28] Documentation can be found at http://www.wasoft.de/wrnx/index.html
[29] Documentation can be found at ftp://ftp.unibe.ch/aiub/rinex/rinex300.pdf
[30] ftp://cddis.gsfc.nasa.gov/
[31] Documentation can be found at http://facility.unavco.org/software/teqc/teqc.html

"teqc.exe +nav GPS_navFile.11n,GLO_navFile.11g inputfile.m00 > RINEXfile.11o"

The *inputfile.m00* contains the raw data of the observation in Leica's raw data format. "*RINEXfile.11o*" is the output filename, with the data in RINEX format. The file is automatically created. Existing files with the same name are overwritten. The files "*GPS_navFile.11n*" and "*GLO_navFile.11g*" are automatically created as well and contain the broadcast ephemeris for GPS and GLONASS, which are required in the next step.

If only the RINEX observation file is desired, the command is as follows:

"teqc.exe inputfile.m00 > RINEXfile.11o"

9.9.3 Azimuth and Elevation of the Satellites with WaRINEX

The software WaRINEX is used to convert the orbital information of the satellites' positions into azimuth and elevation in the horizontal coordinate system with the antenna as the centre.

"WaRINEX performs editing and manipulation of GPS, GLONASS, and SBAS observations given in the Receiver Independent Exchange Format (RINEX)" (WaSoft, 2011). Besides different editing possibilities, special manipulation options are implemented:

- Application of antenna phase centre corrections
- Interpolation of GNSS observations
- Moving the antenna to a new position

The following command is used to calculate the azimuth and elevation values and write them together with the GNSS observations:

"WaRINEX.exe RINEXfile.11o +Xoutputfile.txt"

Character "X" is a control parameter to include the satellite position in the output. Broadcast ephemerides for GPS and GLONASS are therefore needed. The RINEX observation and navigation files must be stored in the same folder. The resulting file ("outputfile.txt") is automatically created. Existing files in the same folder with the same names are overwritten. Figure 9.5 shows the data format of the output of the WaRINEX executable.

```
#### dreh_18052011.11o (input file)
####GLONASS_k_01-16   1  -4  -6  -5   1  -4   5   6  -2  -7   0  -1  -2  -7   0  -1
####GLONASS_k_17-32   4  -3   3   2   4  -3   3   2   #   #   #   #   #   #   #   #
####    time    SV     azi      ele        C1              P2              L1                  L2            S1       S2
1636 303974.40 G  5  204.6671  48.2615  21556612.700    21556614.760   113280763.601 0    88270733.614 0   49.250   45.000
1636 303974.40 G 15  297.8083  31.9636  22643541.960    22643544.000   118992616.439 0    92721526.147 0   46.000   40.250
1636 303974.40 G 26  314.9688  70.9811  19991680.800    19991682.520   105056990.997 0    81862596.544 0   48.000   46.000
1636 303974.40 G 27  251.7809  19.0872  23655313.820    23655317.180   124309514.710 0    96864569.601 0   44.000   37.250
1636 303974.40 G 28  117.6500  57.4767  21338792.180    21338792.200   112136109.529 0    87378783.331 0   45.500   33.750
1636 303974.40 R  2  165.6853  23.5473  22345654.100    22345662.200   119240687.994 0    92742806.090 0   39.750   38.250
1636 303974.40 R  3  247.3629  38.6191  21059333.380    21059342.740   112297612.070 0    87342623.630 0   45.500   44.250
1636 303974.40 R 12   45.9744  27.9279  21852165.040    21852173.540   116730346.381 0    90790312.584 0   39.000   30.000
1636 303974.40 R 13  346.9883  75.6477  19369193.060    19369198.440   103430410.207 0    80445897.677 0   46.000   44.500
1636 303974.40 R 14  245.8767  35.7734  21252724.800          #        113288983.025 0          #     #   44.000      #
1636 303974.45 G  5  204.6668  48.2612  21556635.200    21556637.260   113280881.847 0    88270825.756 0   49.250   45.000
```

Figure 9.5 Outputfie.txt, output of WaRINEX.exe.

Lines beginning with "###" contain comments. The fourth line is the header line for the following rows. For each satellite observation, a new line is appended. The time is given by GPS-week, followed by time of week in seconds (for GPS-week and time of week, see Section 4.1.3). The satellite system is indicated by "G" for GPS and "R" for GLONASS, followed by the name of the space vehicle (SV). The azimuth and elevation of the satellite are given for each observation time. The last six columns show the observations from the RINEX file. (Depending on the data

stored in the RINEX file, the number and order of columns can differ.) Columns C1, P2, L1, and L2 are not used in NORDIS. The last two columns show the signal strength (normally C/N_0) for L1 and L2, which are the essential values. The values are given with a resolution of a 0.25 dB. In contrary, the values are given as integer values for the NMEA-stream. Hence, the resolution is better with the RINEX data. Missing values are indicated with "#".

The reformatting steps from raw-data to RINEX to the text file are completed as preparation for using LGO or teqc for conversion to RINEX and WaRINEX for calculation of the azimuth and elevation values. The following steps and calculations are included in the NORDIS evaluation software, which is written in Visual Basic 2010.

9.9.4   MySQL Database

For fast processing, the data are stored in a MySQL database. To register new data, a new table must be created. Table 4.2 shows the setup of the data table. All relevant values from the file *outputfile.txt* are written into this table.

Table 9.1 Data Table in MySQL.

Column Name	ID	SV	ele	azi	s1	s2	alpha	alphaT	Round
Data type	INT	TEXT	FLOAT	FLOAT	FLOAT	FLOAT	FLOAT	FLOAT	INT
Conditions	PK, NN, UQ, AI	NN	NN	NN			NN	NN	NN
Example 1	1	G15	42.5489	201.066	43.5	42.0	61.5	219.9511	4
Example 2	16	R12	70.9362	6.7303	49.5	45.5	28.5	21.7697	6

PK: primary key
NN: not null
UQ: unique value
AI: auto increment

The primary key for the dataset is the ID. The value "alpha" (α henceforth) indicates the angular position of the attenuation. The value alphaT ($\tilde{\alpha}$ henceforth) is the alpha value reduced by the azimuth.

$$\tilde{\alpha} = \alpha - \text{Azi} \tag{9.1}$$

In case of negative numbers for $\tilde{\alpha}$, 360 deg are added. By subtracting each satellite's azimuth from α, a constellation with the same azimuth for all satellites is generated (see Figure 6.10). Subtracting the azimuth from α is also necessary to make the calculation independent from the movement of the satellites (see Section 4.3.2).

The value "Round" indicates the total number of rounds the attenuation completed. It is incremented for each completed revolution.

To create the MySQL table the following query was used:

```
query = "CREATE TABLE `nordis11`.`" & tableName & "` (`ID` INT NOT NULL
AUTO_INCREMENT, `SV` TEXT NOT NULL, `ele` FLOAT NOT NULL, `azi` FLOAT NOT NULL, `s1`
FLOAT,  `s2` FLOAT, `alpha` FLOAT NOT NULL, `alphaT` FLOAT NOT NULL, `Round` INT NOT
NULL, PRIMARY KEY (`ID`),  UNIQUE INDEX `ID_UNIQUE` (`ID` ASC) ) ENGINE = MyISAM
DEFAULT CHARACTER SET = latin1;"
```

Figure 9.6 mySQL query to create a new data table (Visual Basic syntax)

The query is run in the NORDIS evaluation software; thus, Visual Basic syntax is used.

Before writing the data into the table, the single observations must be allocated to a specific angular position (α) of the attenuation. This step is accomplished by using the zero crossing timestamps. For an observation at the time of the zero cross, the value for α is set to 0. The revolution speed of the attenuation is kept constant by the motor controller. Consequently, there is a linear dependency from the time elapsed since the last zero cross event, which can be used to estimate the angular position $\alpha(t)$. To enable the use of the zero crossing values, the file containing the timestamps must be loaded into the software as well.

9.9.5 Load Zero Cross

The zero crossings are stored in a separate text file. The format of the sentence is shown in Figure 9.7.

```
$PLEIR,EI1,304738177,136250,1636,4,4*44
$PLEIR,EI1,304774250,436200,1636,5,5*4A
$PLEIR,EI1,304810322,559600,1636,6,6*4F
$PLEIR,EI1,304846392,804600,1636,7,7*42
$PLEIR,EI1,304882464,304300,1636,8,8*4A
$PLEIR,EI1,304918540,258850,1636,9,9*49
```
Figure 9.7 Example of event message with zero crossing values.

9.9.5.1 Syntax in ASCII

The lines of the zerocross file are structured in the following way:

$PLEIR,EIX,sssssssss,ttttttt,nnnn,cccc,dddd*hh<CR><LF>

Table 9.2 Event Input Notify Message Format (Leica, 2007a).

Field	Description
$PLEIR	Header
EIX	Message identifier X = 1 for port E1 X = 2 for port E2
sssssssss	GPS time of week of event in ms
ttttttt	GPS time of week of event in ns
nnnn	GPS week number
cccc	Event count
dddd	Event pulse count This is the count of all pulses including those violating the specified time guard boundary[32] conditions set in CONFIGURE Event Input. This allows determination of missed events.
*hh	Checksum
<CR>	Carriage return
<LF>	Line feed

Each line indicates the time when a revolution of the attenuation is completed. While loading the zero cross time stamps, the issue of missing and multiple pulses per event (see Section 7.2.4) must be handled. Before storing the timestamp, the time difference ΔT_i between two following timestamps is checked. The admissible range given in milliseconds is as follows:

$$A \coloneqq \{3600, \dots, 3612\}$$

$\Delta T_i \in A$ must be true.

---

[32] The time guard boundary is explained in Chapter 7.2.4.

If ΔT_i is too short, the condition $(\Delta T_i + \Delta T_{i+1}) \, \epsilon \, A$ is tested. If the condition is true, it indicates multiple pulses for one event. Consequently, the two timestamps are added together. If ΔT_i is too long, a pulse is missing. In this case, the time interval is skipped. When loading is completed, a statistic (Figure 9.8) shows the quality of the zero crossing.

first ZeroCross:	18.05.2011 12:38:58
last ZeroCross:	18.05.2011 13:31:16
observation time:	0 h 52:18 min
number of intervals:	87
max value:	36.08 s
min value:	36.06 s
mean value:	36.0715 s
standard measurement uncertainty:	0.042 s
stdv mean:	0.004 s

Figure 9.8 Zero cross statistics.

9.9.6 Load Data

In this step, the data are loaded from the text file output of the WaRINEX software (see Figure 9.5) into the database. As mentioned in Section 9.9.3, the order of the rows in the text file can differ. Therefore, it is necessary to interpret the header of the rows (fourth line in Figure 9.5) first to identify the position of the values of interest. Only the following entries of the file are needed and stored in the database (compare Table 9.1):

- SV number
- elevation
- azimuth
- S1
- S2
- α (in database written as "alpha")
- $\tilde{\alpha}$ (in database written as "alphaT")
- round

Normally, a MySQL table would be accessible to multiple users for writing and reading. However, such accessibility reduces the performance and is not necessary for the present program. To increase the speed of the MySQL database, the table into which the data are written was locked with the following command:

```
query= "LOCK TABLES " & TableName & " WRITE;"
```

To further improve the performance, the rows to write are collected in the NORDIS evaluation software and sent as a group of 120[33] rows. Consider the performance of the database is important; otherwise, processing time would dramatically increase.

---

[33] This is an empirical value and depends on the performance of the computer being used and the settings in the MySQL database.

9.9.7 Average and Group the Data

Until this point, the observations are stored in chronological order, corresponding to the observation times. To draw curves as shown in Figure 6.8 and to calculate the cross-correlation, all available data must be sorted, first, by elevation and, second, by $\tilde{\alpha}$, and then averaged. To obtain data for the calibration curves, all curves for all possible elevations are needed. Therefore, measurements over 24 hours were taken to take advantage of the entire SV-constellation. Doing so resulted in a large amount of data (ca. 2 – 3 GB for 24 h).

To sort and average the data, the following query was used:

```
query = " select round(ele), round(alphaT*2)/2, avg(s1), avg(s2) from  `nordis11`.`"
& inputTableName & "`  group by round(ele), round(alphaT*2)/2 order by round(ele),
round((alphaT*2)/2);"
```

Figure 9.9 MySQL query for ordering and averaging the measurements.

This query computes all data averaged in the desired order. It is crucial to combine the commands "avg(s1)" and "group by round(ele), round(alphaT)". The "group by" statement in combination with the "avg()" statement means that all entries with the same conditions will be averaged. The conditions are written after the "group by" statement. Multiple conditions are separated by commas. Because the values for elevation (ele) and the reduced alpha (alphaT) are originally given as floats, they must be rounded to be averaged together. The "group by" statement does not allow indicating a range, as indicated in the "select where" statement, but groups the same values exclusively. In this case, rounding the values first has the same effect as indicating a range of 1 deg. To improve the resolution to steps of 0.5 deg, the following rounding statement is used: "round (alphaT*2)/2".

The query shown above could also be divided into different queries, and the averaging process could have been computed in Visual Basic code. However, doing so would be much less efficient. The great benefit of sending the whole task in one query to the MySQL database is the implemented "query optimizer":

> The task of the query optimizer is to find an optimal plan for executing an SQL query. Because the difference in performance between "good" and "bad" plans can be orders of magnitude (that is, seconds versus hours or even days), most query optimizers, including that of MySQL, perform a more or less exhaustive search for an optimal plan among all possible query evaluation plans. (Oracle, 2011)

Normally, it would be sufficient to execute the query of the corresponding data table in the database and use the results for calculation. Because the reference table is used for each new calculation, the query above must be executed each time for the reference table. Therefore, storing the results in a new table and save the table to hard disk for further use saves time.

```
query = "CREATE TABLE `nordis11_mean`.`" & MeanTableName & "` (`ID` INT NOT NULL
AUTO_INCREMENT, PRIMARY KEY (`ID`) ) select round(ele) as ele, round(alphaT*2)/2 as
alpha, avg(s1) as s1, avg(s2) as s2 from  `nordis11`.`" & tableName & "` group by
round(ele), round(alphaT*2)/2;"
```

Figure 9.10 MySQL query to create a new table with the results.

9.9.8 Implementation of the Cross-Correlation Algorithm

As arguments, the two series (series1 and series2) and a value for the maximal delay are passed to the crosscorr function, which includes the above-mentioned cross-correlation Equation 4.10.

```
mean1 = series1.Average
mean2 = series2.Average

'part 1
If series1.Count < series2.Count Then
    n = series1.Count
Else
    n = series2.Count
End If

'part 2
For j = 0 To n - 1
    s1 += (series1(j) - mean1) ^ 2
    s2 += (series2(j) - mean2) ^ 2
Next

standardisation = Math.Sqrt(s1 * s2)

'part 3
For d = 0 To maxDelay - 1
    s12 = 0
    For j = 0 To n - 1
        m = j + d

        While m < 0
            m += n
        End While
        m = m Mod n
        s12 += (series1(j) - mean1) * (series2(m) - mean2)
    Next
    r.Add(s12 / standardisation)
Next
```

Figure 9.11 Source code of the core part of the crosscorr function written in Visual Basic.

In part 1, the value n is set to the length of the shorter series. In part 2, the denominator of Equation (6.10) is calculated. Finally, in part 3, the numerator and the correlation series are calculated. To collect all the correlation coefficients, "r" is declared as the list name. To find the maximal correlation factor, the maximal value of the list is given together with the position in the list, which corresponds to the delay "d". Thus, the result is the correlation coefficient "cc" at delay "d". If the list "r" contains more than one maximal value, the first occurrence is reported.

9.10 Averaging Function

Averaging values with circular behaviour (360 deg $\triangleq$ 0 deg) has one crucial point: when the values range around the zero point, the average would be around 180 deg. In the NORDIS evaluation software, it is handled in a circular-safe averaging function. Before averaging, the median of the dataset is calculated. When the median is between 315 deg (or -45 deg) and 45 deg, 180 deg is added to all values. With these new values, the average and standard measurement uncertainty are calculated. Afterwards, 180 deg is subtracted from the result.

9.11 NORDIS Evaluation Software
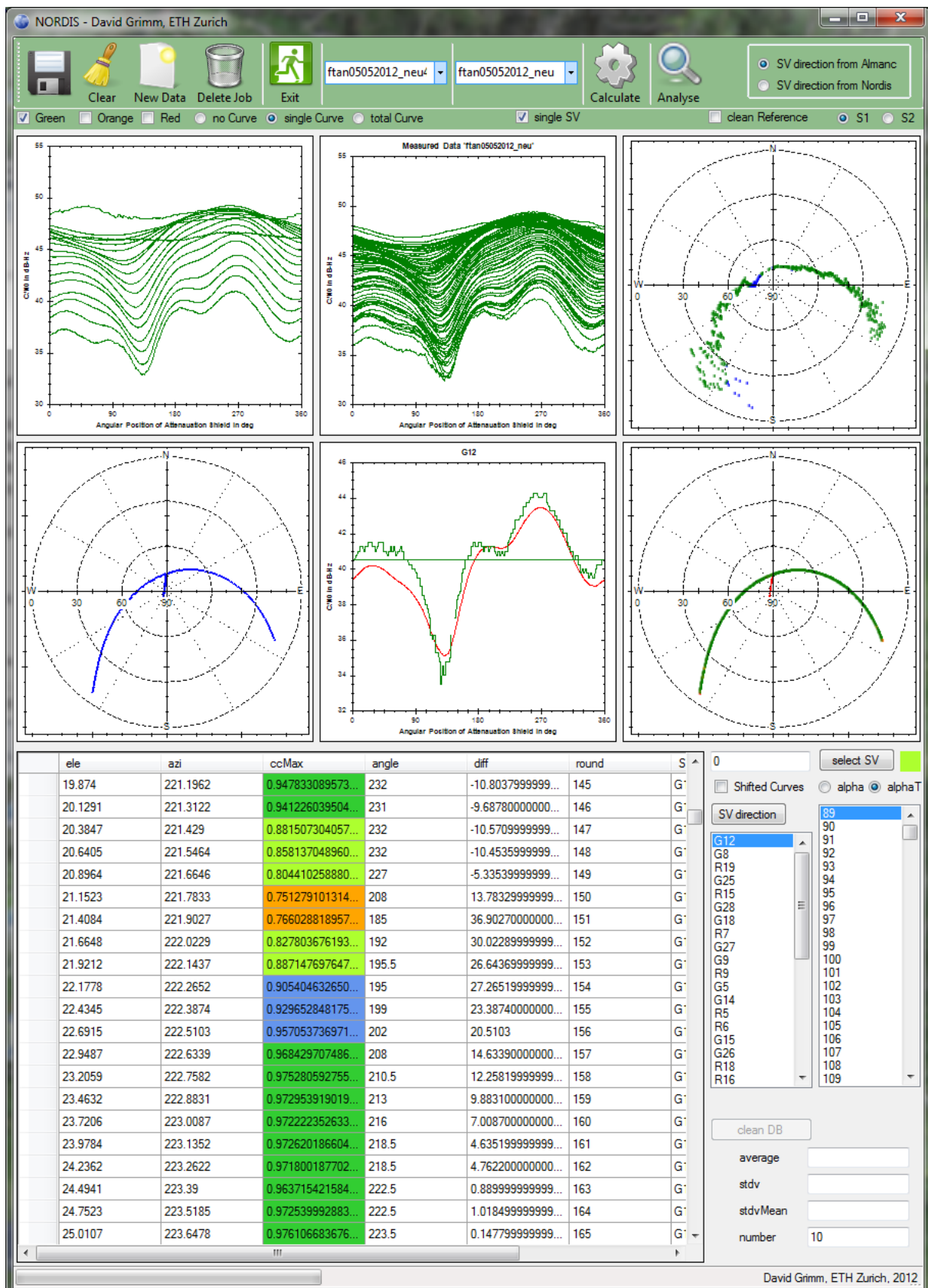
Figure 9.12 Print screen of the NORDIS evaluation software.

10 References

Anschütz, R. 2012. *Proven Gyro Compass Technology for over than 100 years*, (Technical report), Raytheon Anschütz, Kiel. Accessed from www.raytheon-anschütz.com

AppStore 2012. "gpsCompass", *itunes.apple.com*. Accessed from http://itunes.apple.com/us/app/gpscompass/id286550480?mt=8

Axelrad, P. and Behre, C. P. 1999. "Satellite attitude determination based on GPS signal-to-noise ratio", *Proceedings of the IEEE*, vol. 87, no. 1, pp. 133–144. doi:10.1109/5.736346

Badke, B. 2009. "Carrier-to-noise density and AI for INS / GPS integration", *Inside GNSS*, vol. 4, no. 5, pp. 20–23. Accessed from http://www.insidegnss.com/node/1637

Bahder, T. B. 2002. "Attitude determination from single-antenna carrier-phase measurements", *Journal of Applied Physics*, vol. 91, no. 7, pp. 4677–4684. doi:10.1063/1.1448871

Barrows, A. K., Gebre-Egziabher, D., Hayward, R., Xia, R. and Powell, J. D. 1996. "GPS-based attitude and guidance displays for general aviation", in *Proceedings of IEEE Conference Emerging Technologies and Factory Automation EFTA '96*, vol. 2, Kauai, Hawaii, November 18-21, pp. 423–428.

Bauersima, I., Beutler, G., Brunner, F. K., Geiger, A., Gurtner, W., Hogg, D. C., Kaniuth, K., Leitinger, R., Petit, G., Putz, E., Rothacher, M., Schildknecht, T., Shi, P. and Snider, J. B. 1988. *Atmospheric effects on geodetic space measurements*, Brunner, F. K., ed., The Shool of Surveying, University of New South Wales, Kensington, Australia.

Beckmann, A., Larisch, H.-J. and Schuster, O. 1988. Determination of azimuths from GPS measurements and comparison with common methods, in *GPS-Techniques Applied to Geodesy and Surveying*, Groten, E. and Strauß, R., eds., vol. 19 of *Lecture Notes in Earth Sciences*, Springer Berlin; Heidelberg, pp. 459–465. 10.1007/BFb0011339.

Benkner, T. 2007. *Grundlagen des Mobilfunks*, Schlembach, J Fachverlag, Wilburgstetten.

Beutler, G. 1996. GPS satellite orbits, in *GPS for Geodesy*, Kleusberg, A. and Teunissen, P., eds., vol. 60 of *Lecture Notes in Earth Sciences*, Springer, Berlin; Heidelberg, pp. 37–101. 10.1007/BFb0117679.

Bevelacqua, P. J. 2011. "The online source for understanding antennas". Accessed from http://www.antenna-theory.com/basics/radPattern.html

Blankenbach, J. and Norrdine, A. 2011. "Building information systems based on precise indoor positioning", *Journal of Location Based Services*, vol. 5, no. 1, pp. 22–37. doi:10.1080/17489725.2010.538016

Bolljahn, J. 1958. "Effects of satellite spin on ground-received signal", *Antennas and Propagation, IRE Transactions on*, vol. 6, no. 3, pp. 260 –267. doi:10.1109/TAP.1958.1144597

Booker, H. G. 1946. "Slot aerials and their relation to complementary wire aerials (Babinet's principle)", *Journal of the Institution of Electrical Engineers -Part IIIA: Radiolocation*, vol. 93, no. 4, pp. 620–626. doi:10.1049/ji-3a-1.1946.0150

Braasch, M. S. and Van Dierendonck, A. J. 1999. "GPS receiver architectures and measurements", *Proceedings of the IEEE*, vol. 87, no. 1, pp. 48–64. doi:10.1109/5.736341

Broumandan, A., Lin, T., Moghaddam, A., Lu, D., Nielsen, J. and Lachapelle, G. 2007. "Direction of arrival estimation of GNSS signals based on synthetic antenna array", in *Proceedings of the 20th International Technical Meeting of the Satellite Division of The Institute of Navigation (ION GNSS 2007)*, ION GNSS 2007, Fort Worth, TX, September 25-28, 2007, pp. 728–738.

Brown, A. and Gerein, N. 2001. "Test results of a digital beamforming GPS receiver in a jamming environment", in *Proceedings of the 14th International Technical Meeting of the Satellite Division of The Institute of Navigation (ION GPS 2001)*, Salt Lake City, UT, September 11-14, 2001, pp. 894–903.

Brown, A., Gerein, N. and Savage, L. 2001. "Multipath characterization using digital phased arrays", in *Proceedings of ION 57th Annual Meeting of The Institute of Navigation*, NAVSYS Corporation, Albuquerque, NM, June 11-13, 2001, pp. 469 – 476. Accessed from http://www.navsys.com/Index.html

Brown, R. A. 1992. "Instantaneous GPS attitude determination", *IEEE Aerospace and Electronic Systems Magazine*, vol. 7, no. 6, pp. 3–8. doi:10.1109/62.145113

Brown, R. A. and Ward, P. 1990. "A GPS receiver with built-in precision pointing capability", in *Proceedings of IEEE Position Location and Navigation Symposium Record 'The 1990's - A Decade of Excellence in the Navigation Sciences' IEEE PLANS '90*, March 20-23, 1990, pp. 83–93.

Brunner, F. K., Hartinger, H. and Troyer, L. 1999. "GPS signal diffraction modelling: the stochastic SIGMA-D model", *Journal of Geodesy*, vol. 73, pp. 259–267.

Buist, P. J., Hashida, Y., Unwin, M. and Schroeder, M. 2000. "Full attitude from a single GPS antenna: Demonstration of concept with orbital data from PoSAT-1", in *Spacecraft Guidance, Navigation and Control Systems*, Schürmann, B., ed., vol. 425 of *ESA Special Publications*, pp. 493 – 498. Accessed from http://articles.adsabs.harvard.edu/cgi-bin/nph-iarticle_query?2000ESASP.425..493B&defaultprint=YES&filetype=.pdf

Cannon, M. E., Nayak, R., Lachapelle, G., Salychev, O. S. and Voronov, V. V. 2001. "Low-cost INS/GPS integration: Concepts and testing", *Journal of Navigation*, vol. 54, no. 1, pp. 119–134.

Chang, C. C. and Tsai, W. Y. 2006. "Evaluation of a GPS-based approach for rapid and precise determination of geodetic/astronomical azimuth", *Journal of Surveying Engineering © ASCE*, vol. 132, no. 4, pp. 149–154. doi:10.1061/(ASCE)0733-9453(2006)132:4(149)

Chu, Q. and Woerkom, P. V. 1997. "GPS for low-cost attitude determination: A review of concepts, in-flight experiences, and current developments", *Acta Astronautica*, vol. 41, no. 4 - 10, pp. 421 – 433. doi:10.1016/S0094-5765(98)00046-0

Cocard, M. 1995. "High precision GPS processing in kinematic mode", PhD thesis, ETH Zurich, Schweizerische Geodätische Kommission, vol. 52.

Davidson Optronics 2011. "Principles of autocollimation". Accessed from http://www.davidsonoptronics.com/principles-of-autocollimation

Djuknic, G. M. 2003, December 2, "Method of measuring a pattern of electromagnetic radiation", *United States Patent no. 6,657,596 B2*, Washington, DC: U.S. Patent and Trademark Office.

DMT 2012. "Gyromat 3000". Accessed from http://www.dmt.de/fileadmin/PDF/Broschueren/Produkte/DMT_Gyromat.pdf

Dodel, H. and Häupler, D. 2004. *Satelliten-navigation*, 1 edn, Hüthig GmbH, Heidelberg.

Duncan, C. and Dunn, C. 1998. "Estimating attitude from GPS measurements on one antenna", *Technical Support Package, NASA Tech Brief*, vol. 22, no. 6. Accessed from http://www.techbriefs.com/index.php?option=com_staticxt&staticfile=/Briefs/Jun98/NPO20323.html

El-Mowafy, A. and Mohamed, A. 2005. "Attitude determination from GNSS using adaptive Kalman filtering", *Journal of Navigation*, vol. 58, no. 01, pp. 135–148. doi:10.1017/S0373463304003042

Eling, C., Zeimetz, P. and Kuhlmann, H. 2010. "Determination of a GPS-single-epoch orientation based on double differences", in *2nd International Conference on Machine Control & Guidance*, Lammers, P. S. and Kuhlmann, H., eds., University of Bonn, March 9-11, 2010.

Euler, H.-J. and Hill, C. D. 2006, July 26, "Verfahren zur Bestimmung der Orientierung einer Antennenanordnung", *European Patent no. 05001286.3*, Brussels: European Patent Office.

Evans, A. G. 1986. "Roll, pitch, and yaw determination using a global positioning system receiver and an antenna periodically moving in a plane", *Marine Geodesy*, vol. 10, no. 1, pp. 43–52. doi:10.1080/01490418609388010

Falletti, E., Pini, M. and Presti, L. L. 2011. "Low complexity Carrier-to-Noise Ratio estimators for GNSS digital receivers", *IEEE Transactions on Aerospace and Electronic Systems*, vol. 47, no. 1, pp. 420–437.

Flawn, B. J. 1996, November 5, "Compass", *United States Patent no. 5,572,217*, Washington, DC: U.S. Patent and Trademark Office.

Fraunhofer Institut 2011. "Antennendesign", *AoA – Angle of Arrival*. Accessed from http://www.iis.fraunhofer.de/bf/ln/technologie/aoa/anten.jsp

Frei, E., Ryf, A. and Scherrer, R. 1992. "Das GPS (Global Positioning System) und seine Anwendungsmöglichkeiten in der Ingenieurvermessung", in *Ingenieurvermessung 92*, Matthias, H. J. and Grün, A., eds., vol. 1, pp. II 10/1 – II 10/13.

Fresnel, A. 1816. "Sur la diffraction de la lumière", *Annales de chimie et de physique*, vol. 1, pp. 239–281. Accessed from http://books.google.ch/

Frevert, V. 2010. *PCV Antenna LEIAX1202GG*, (Technical report), Technische Universität Dresden.

References

Friedli, R. 2011. "Orientierungsbestimmung mit GNSS", Unpublished bachelor thesis, ETH Zurich.

García-Fernández, M., Markgraf, M. and Montenbruck, O. 2008. "Spin rate estimation of sounding rockets using GPS wind-up", *GPS Solutions*, vol. 12, pp. 155–161. doi:10.1007/s10291-007-0074-8

Garmin 2011. "Handheld GPS". Accessed from https://buy.garmin.com/shop/shop.do?cID=143

Geiger, A. 1988. Modeling of phase center variation and its influence on GPS-positioning, in *GPS-Techniques Applied to Geodesy and Surveying*, Groten, E. and Strauß, R., eds., vol. 19 of *Lecture Notes in Earth Sciences*, Springer Berlin; Heidelberg, pp. 210–222. 10.1007/BFb0011339.

GeoMessTechnik 2012. "Gyromax-Vermessungskreisel". Accessed from http://www.gmt-heger.com/index.php?id=2#technische_daten

Giorgi, G., Buist, P. J., Verhagen, S. and Teunissen, P. J. G. 2011. "GNSS-based attitude determination", *Inside GNSS*, vol. 6, no. 4, pp. 62–71.

GPS Groundtrack 2012. "GPS Groundtrack", *Ground tracks and 3D plots of orbits*. Accessed from http://hakenberg.de/numerics/spacecraft_orbits.htm

gpscompass 2012. "Vector PRO GPS Compass". Accessed from http://www.gpscompass.com.au/Specifications.htm

Grimm, D. E. 2007. "Orientierung einer GPS-Antenne", student thesis, ETH Zurich.

Grimm, D. E. 2007. "Orientierung von GPS-Antennen", diploma thesis, ETH Zurich.

Grimm, D. E. 2008. "GNSS orientation for kinematic applications", in *1st International Conference on Machine Control & Guidance*, Ingensand, H. and Stempfhuber, W., eds., ETH Zurich, June 24-26, pp. 121 – 126.

Grimm, D. E. 2008. "GPS direction finding", *Geodezija ir Kartografija*, vol. 34, no. 3, pp. 100–102. doi:10.3846/1392-1541.2008.34.100-102

Grimm, D. E. 2009. "GNSS Orientierung", in *GNSS 2009: Systeme, Dienste, Anwendungen*, Wanninger, L. and Adelt, U., eds., vol. 57, Deutscher Verein für Vermessungswesen/Arbeitskreis Messmethoden und Systeme, Wißner-Verlag, Augsburg, pp. 203–222.

Grimm, D. E., Steiner, L. and Mautz, R. 2012. "GNSS antenna orientation and detection of multipath signals from direction of arrival", in *Proceedings of the 25th International Technical Meeting of the Satellite Division of the Institute of Navigation (ION GNSS 2012)*, ION GNSS 2012, Nashville TN, September 17-21, 2012.

Guillaume, S., Geiger, A. and Forrer, F. 2012. G-MoDe detection of small and rapid movements by a single GPS carrier phase receiver, in *VII Hotine-Marussi Symposium on Mathematical Geodesy*, Sneeuw, N., Novák, P., Crespi, M. and Sansò, F., eds., vol. 137 of *International Association of Geodesy Symposia*, Springer, Berlin; Heidelberg, pp. 141–145.

Guinot, B. 2003. "Terrestrial polar origin", *Contribution to the Working Group of Nomenclature for Fundamental Astronomy*, pp. 3–5.

Halmos, F. 1966. "Untersuchungen der Kreiseltheodolite sowie deren Anwendungsmöglichkeiten", *Allgemeine Vermessungs-Nachrichten*, vol. 10, no. 73, pp. 424–437.

Hashida, Y. and Unwin, M. J. 1993. "Satellite attitude from a single GPS antenna", in *Proceedings of the 6th International Technical Meeting of the Satellite Division of The Institute of Navigation (ION GPS 1993)*, ION GPS, September 22-24, 1993, pp. 355 – 363. Accessed from http://www.ion.org/search/view_abstract.cfm?jp=p&idno=4431

Hayashi, N. 1996. "Augmentation of GPS with a Barometer and a Heading Rate Gyroscope for Urban Vehicular Navigation", PhD thesis, University of Calgary.

Häberling, S. and Geiger, A. 2010. "Determination of attitude change by a single GPS antenna", in *2nd International Conference on Machine Control & Guidance*, Lammers, P. S. and Kuhlmann, H., eds., University of Bonn, Bonn, March 9-11, pp. 149 – 150.

Hesse, C. 2007. "Hochauflösende kinematische Objekterfassung mit terrestrischen Laserscannern", PhD thesis, Leibniz Universität Hannover, Deutsche Geodätische Kommission bei der Bayerischen Akademie der Wissenschaften: Reihe C, no. 608.

Hill, C. D. and Euler, H.-J. 1996. "An optimal ambiguity resolution technique for attitude determination", in *Proceedings of Position Location and Navigation Symposium IEEE 1996*, April 22-26, pp. 262–269.

Hofmann-Wellenhof, B., Lichtenegger, H. and Collins, J. 1997. *GPS Theory and Practice*, 4th edn, Springer, Wien; New York.

IGS 2012. "IGS product publications and studies". Accessed from http://acc.igs.org/studies.html

Ingensand, H. 2004. *Ingenieurgeodäsie und Geodätische Messtechnik III*, IGP, ETH Zurich.

Institute for Geodesy and Geoinformation 2011. "Absolute GNSS-Antennenkalibrierung am IGG", *Antennenmesskammer Bonn*. Accessed from http://www.gib.uni-bonn.de/forschung/gnss/antennenmesskammer

Institute of Electrical and Electronics Engineers [IEEE] 1983. *Definitions of terms for antennas*, Std 145-1983, Revision of ANSI/IEEE Std 145-1973, IEEE, New York, NY.

International Telecommunication Union 2000. *Nomenclature of the frequency and wavelength bands used in telecommunications*, recommendation ITU-R V.431-7, UN agency for information and communication technologies.

Jablonski, D. G. 1989, November 14, "Apparatus for and a method of determinig compass headings", *United States Patent no. 4881080*, Washington, DC: U.S. Patent and Trademark Office.

Javad 2011. "RTK Umbrella". Accessed from http://www.javad.com/jgnss/products/accessories/

Joint Committee for Guides in Metrology 2008. *International vocabulary of metrology — basic and general concepts and associated terms*, JCGM 200, JCGM/WG 2, Bureau international des poids et mesures (BIPM).

Joseph, A. 2010. "What is the difference between SNR and C/N0", *Inside GNSS*, vol. 5, no. 8, pp. 20–25. Accessed from http://www.insidegnss.com/auto/novdec10-Solutions.pdf

Kahle, H.-G. 2004. *Einführung in die Höhere Geodäsie*, IGP, ETH Zurich.

Kahlmann, T. and Ingensand, H. 2007, January 4, "Method and system for acquiring azimuth information using signals provided by satellites", *International Patent no. WO 2007/000067 A1*, Geneva: World Intellectual Property Organization.

Kahlmann, T., Remondino, F. and Ingensand, H. 2006. "Calibration for increased accuracy of the range imaging camera swissranger", in *Proceedings of the ISPRS Commission V Symposium 'Image Engineering and Vision Metrology'*, vol. 34, ISPRS, Dresden, 25-27 September 2006, pp. 136–141.

Kalman, R. E. 1960. "A new approach to linear filtering and prediction problems", *Journal of Basic Engineering*, vol. 82, Series D, pp. 35–45. doi:10.1.1.129.6247

Kao, W.-W. 1991. "Integration of GPS and dead-reckoning navigation systems", in *Vehicle Navigation and Information Systems Conference, 1991*, vol. 2, pp. 635 – 643.

Kepler, J. 1937. *Astronomia nova*, Caspar, M., ed., vol. 3, C.H. Beck Verlag, München.

Kepler, J. 1940. *Harmonice mundi*, Caspar, M., ed., vol. 6, C.H. Beck Verlag, München.

Kim, D., Serrano, L. and Langley, R. B. 2006. "Innovation: Phase wind-up analysis", *GPS World*, vol. 17, no. 2, pp. 58–64.

Kim, J.-T., Moon, S.-H., Han, D. S. and Cho, M.-J. 2005. "Fast DOA estimation algorithm using pseudocovariance matrix", *IEEE Transactions on Antennas and Propagation*, vol. 53, no. 4, pp. 1346–1351. doi:10.1109/TAP.2005.844459

Krall, A. H. and Bahder, T. B. 2001. "Orientation and velocity effects in the global positioning system", *Journal of Applied Physics*, vol. 90, no. 12, pp. 6513–6525. doi:10.1063/1.1417993

Kunysz, W. 2000. "High performance GPS pinwheel antenna", in *Proceedings of the 13th International Technical Meeting of the Satellite Division of The Institute of Navigation (ION GPS 2000)*, Salt Lake City, UT, September 19-20, 2000, pp. 2506–2511.

Kunysz, W. 2002, September 3, "Aperture coupled slot array antenna", *United States Patent no. 6,445,354 B1*, Washington, DC: U.S. Patent and Trademark Office.

Ladetto, Q. and Merminod, B. 2002. "Digital magnetic compass and gyroscope integration for pedestrian navigation", in *9th Saint Petersburg International Conference on Integrated Navigation Systems*, Saint Petersburg, Russia, May 27-29.

Langley, R. B. 2011. "GLONASS Overview". Accessed from http://gps.pl/arch/GLONASSOverview.pdf

Leica 2007. *Leica GPS 1200 Technical Reference Manual*, 5.5 edn, Heerbrugg, Leica Geosystems AG.

Leica 2007. *Leica TPS 1200 User Manual*, 5.5 edn, Heerbrugg, Leica Geosystems AG.

Leica 2012. "Leica IPAS20". Accessed from http://www.leica-geosystems.com/de/Luftbild-Sensoren-Leica-IPAS20_62633.htm

Leick, A. 2003. *GPS satellite surveying*, 3rd edn, Wiley, New York.

Lockheed Martin 2005. "GPS IIR-M", *Lockheed Martin's photostream*. Accessed from http://www.flickr.com/photos/lockheedmartin/

Marini, J. W. 1971. "The effect of satellite spin on two-way Doppler range-rate measurements", *IEEE Transactions on Aerospace and Electronic Systems*, vol. 7, no. 2, pp. 316–320.

Mautz, R. 2001. "Zur Lösung nichtlinearer Ausgleichsprobleme bei der Bestimmung von Frequenzen in Zeitreihen", PhD thesis, Technische Universität Berlin, Bayrische Akademie der Wissenschaften Reihe C, no. 532.

Mautz, R. 2012. *Indoor Positioning Technologies*, Mautz, R., Müller-Gantenbein, J. and A.Geiger, eds., vol. 86, Schweizerische Geodätische Kommission. Accessed from www.sgc.ethz.ch

McLean, J., Sutton, R. and Hoffman, R. 2002. *Interpreting Antenna Performance Parameters for EMC Applications Part 1: Radiation Efficiency and Input Impedance Match*, (Technical report), TDKRF Solutions, Cedar Park TX. Accessed from http://www.tdkrfsolutions.com/DataPDFs/antenna_paper_part1.pdf

McLean, J., Sutton, R. and Hoffman, R. 2002. *Interpreting Antenna Performance Parameters for EMC Applications Part 2: Radiation Pattern, Gain, and Directivity*, (Technical report), TDKRF Solutions, Cedar Park TX. Accessed from http://www.tdkrfsolutions.com/DataPDFs/antenna_paper_part2.pdf

Menge, F. 2003. "Zur Kalibrierung der Phasenzentrumsvariationen von GPS-Antennen für die hochpräzise Positionsbestimmung", PhD thesis, Universität Hannover, no. 247.

National Imagery and Mapping Agency, U.S. Dapartment of Defense 2000. *Word geodetic system 1984*, 3th Edition, National Imagery and Mapping Agency, U.S. Department of Defense, Washington, DC.

National Instruments 2010. *GPS Receiver Testing*. Accessed from www.ni.com

Northwood Labs 2003. "GPS carrier-to-noise density". Accessed from http://202.114.120.10/gnss/docs/AN101.pdf

NovAtel 2006. *GPS-704X Antenna Design and Performance*, (Technical report), NovAtel Inc., Calgary AB.

Oracle 2011. *7.4. Controlling the query optimizer*. Accessed from http://dev.mysql.com/doc/refman/5.0/en/controlling-optimizer.html

Oxford Technical Solutions 2012. "RT3000", *RT3000 Family Products.* Accessed from http://www.oxts.com/default.asp?pageref=7&gclid=CJ6S7KLV9qsCFUMKfAod3mJURg

Paffenholz, J.-A., Alkhatib, H. and Kutterer, H. 2010. "Direct geo-referencing of a static terrestrial laser scanner", *Journal of Applied Geodesy*, vol. 4, no. 4, pp. 115–126. doi:10.1515/JAG.2010.011

Park, C., Kim, I., Jee, G.-I. and Lee, J. G. 1997. "An error analysis of GPS compass", in *Proceedings of the 36th SICE Annual Conference. International Session Papers SICE '97*, July 29-31, 1007, pp. 1037–1042.

Petovello, M. and Driver, T. 2008. "Satellite almanac life expectancy", *Inside GNSS*, vol. nov/dec, no. 8, pp. 14–19.

precise positioning management 2012. "4011 GPS Compass Antenne und PDA". Accessed from http://www.ppmgmbh.com/pages_de/produkte/gps_empfaenger/mobilfunk/4011_GPS_Compass.html

Right Handed Circular Polarization 2011. "Right Handed Circular Polarization", *wikipedia.org*. Accessed from http://en.wikipedia.org/wiki/File:Circular.Polarization.Circularly.Polarized.Light_With.Components_Right.Handed.svg

Rost, C. 2011. "Phasenmehrwegereduzierung basierend auf Signalqualitätsmessungen geodätischer GNSS-Empfänger", PhD thesis, Technische Universität Dresden, Deutsche

Geodätische Kommission bei der Bayerischen Akademie der Wissenschaften, Reihe C, no. 665.

Rudge, A. 1982. *The Handbook of Antenna Design*, Rudge, A., Milne, K., Olver, A. D. and Knight, P., eds., vol. 1 of *IEE electromagnetic waves series*, P. Peregrinus on behalf of the Institution of Electrical Engineers, London, UK.

Sayre, M. M. 2003. "Development of a block processing carrier to noise ratio estimator for the global positioning system", master thesis, College of Engineering and Technology of Ohio University.

Scappuzzo, F. S. 2009. "Analysis and corrections of non-hydrostatic effects and GNSS antenna errors for accurate GPS and GALILEO IWV estimates", PhD thesis, ETH Zurich.

Schmidt, R. 1986. "Multiple emitter location and signal parameter estimation", *IEEE Transactions on Antennas and Propagation*, vol. 34, no. 3, pp. 276–280. doi:10.1109/TAP.1986.1143830

Schwieger, V. and Hemmert, J. 2008. "Integration of a multiple-antenna GNSS system and supplementary sensors", in *1st International Conference on Machine Control & Guidance*, Ingensand, H. and Stempfhuber, W., eds., ETH Zurich, June 24-26, 2008, pp. 103–112.

Seeber, G. 2003. *Satellite Geodesy*, 2nd edn, W. de Gruyter, Berlin; New York.

Serrano, J., Bernedo, P., Potti, J. and Silvestrin, P. 1995. "A new spacecraft attitude determination scheme based on the use of GPS line-of-sight vectors", in *Proceedings of the 8th International Technical Meeting of the Satellite Division of the Institute of Navigation*, September 12-15, 1995, pp. 1797–1806.

Spinney, V. W. 1976. "Application of the global positioning system as an attitude reference for near-earth users", in *Proceedings of Bicentennial National Aerospace Symposium*, The Institute of Navigation, Warminster, PA, April 27-28, 1976, pp. 132 – 136.

Stempfhuber, W. 2007. "Herausforderungen der 3D-Baumaschinensteuerung", in *Ingenieurvermessung 07*, Brunner, F. K., ed., Herbert Wichmann Verlag, Heidelberg, pp. 343–354.

Stier, K. H. 1962. "Der Vermessungskreiselkompass und seine Einsatzbedingungen", *Zeitschrift für Vermessungswesen*, vol. 1, no. 87, pp. 57–65.

swisstopo 2012. "Arial image", *http://map.admin.ch/*. Accessed from http://www.swisstopo.admin.ch/internet/swisstopo/en/home/swisstopo/legal_bases/use_without_licence.html

swisstopo 2012. "Color map", *http://map.admin.ch/*. Accessed from http://www.swisstopo.admin.ch/internet/swisstopo/en/home/swisstopo/legal_bases/use_without_licence.html

Teunissen, P. J. G., Giorgi, G. and Buist, P. 2011. "Testing of a new single-frequency GNSS carrier phase attitude determination method: land, ship and aircraft experiments", *GPS Solutions*, vol. 15, pp. 15–28. doi:10.1007/s10291-010-0164-x

Thales Navigation 2011. *The precise GPS compass*, Santa Clara, CA, Thales Navigation, Inc. Accessed from http://www.ppmgmbh.com

TomTom 2012. "Car Navigation", *TomTom*. Accessed from https://www.tomtom.com

Torge, W. 2003. *Geodäsie*, 2d edn, W. de Gruyter, Berlin.

Trimble 2009. "Trimble SPS750 and SPS850 Receiver Construction Applications", *SPS750 and SPS850 Modular GPS Receivers*. Accessed from http://www.trimble.com/con_sps750_850.shtml

Trimble 2012. "GCS900 3D with dual GPS for Excavators", *3D Grade and Compaction Control Systems*. Accessed from http://www.trimble.com/construction/heavy-and-highway

TU, C.-H., TU, K.-Y., CHANG, E.-R. and WANG, L.-S. 1997. "GPS compass: A novel navigation equipment", *IEEE Transactions on aerospace and elctronic systems*, vol. 33, no. 3, p. 6.

u-blox 2012. "u-blox ADR", *u-blox Automotive Dead Reckoning technology*. Accessed from http://www.u-blox.com/en/dead-reckoning.html

Unavco 2011. "TEQC - the toolkit for GPS/GLONASS/Galileo/SBAS data". Accessed from http://facility.unavco.org/software/teqc/teqc.html

U.S. Coast Guard Navigation Center 2008. *Global positioning system standard positioning service performance standard*, 4th edn., Assistant Secretary of Defense for Command, Control, Communications, and Intelligence, U.S. Department of Defense, Washinton, DC.

Van Dierendonck, A. J. 1996. GPS receivers, in *Global Positioning System: Theory and Applications*, Parkinson, B. W., Spilker, J. J., Axelrad, P. and Enge, P., eds., vol. 1, American Institute of Aeronautics and Astronautics, Washington, DC, chapter 8, p. 329–407.

Wang, C., Walker, R. A. and Moody, M. P. 2005. "A GPS signal transmission model for improved single antenna attitude determination", in *11th Australian International Aerospace Congress*, Melbourne, March 13-17, 2005.

Wanninger, L. 2000. *Präzise Positionierung in regionalen GPS-Referenzstationsnetzen*, no. 508, Deutsche Geodätische Kommission, C.

Ward, P. W., Betz, J. W. and Hegarty, C. J. 2006. Satellite signal acquisition, tracking, and data demodulation, in *Understanding GPS : principles and applications*, Kaplan, E. D. and Hegarty, C. J., eds., 2nd edn, Artech House, Boston, MA, chapter 5, pp. 153–241.

WaSoft 2011. "Editing and manipulation of GNSS observations". Accessed from http://www.wasoft.de/e/wrnx/index.html

Wen, Z., Li, L. and Wei, P. 2006. "Fast direction finding using modified pseudocovariance matrix", *IEEE Transactions on Antennas and Propagation*, vol. 54, no. 12, pp. 3914–3918. doi:10.1109/TAP.2006.886572

Wheeler, H. A. 1947. "Fundamental limitations of small antennas", *Proceedings of the Institute of Radio Engineers*, vol. 35, no. 12, pp. 1479–1484. doi:10.1109/JRPROC.1947.226199

Wieser, A. 2001. "Robust and fuzzy techniques for parameter estimation and quality assesment in GPS", PhD thesis, Technische Universität Graz, Shaker Aachen.

Wiget, A. and Schneider, D. 1992. "Erfahrungen mit GPS in Staumauer-Überwachungsnetzen", in *Ingenieurvermessung 92*, Matthias, H. J. and Grün, A., eds., vol. 1, pp. II 12/1 – II 12/13.

Wiklund, R. 1992, May 14, "Method and device for position measurement", *International Patent no. WO 92/08105*, Geneva: World Intellectual Property Organization.

xsens 2012. "MTi-G". Accessed from http://www.xsens.com/en/general/products-all

Zanini, M. 1992. *Hochpräzise Azimutbestimmung mit Vermessungskreiseln*, no. 209, Institut für Geodäsie und Photogrammetrie.

Zeimetz, P. 2009. *Antennenexperimente*, (Technical report), Rheinische Friedrich-Wilhelms-Universität zu Bonn.

Zeimetz, P. 2010. "Zur Entwicklung und Bewertung der absoluten GNSS-Antennenkalibrierung im HF-Labor1", PhD thesis, Rheinische Friedrich-Wilhelms-Universität zu Bonn. Accessed from http://hss.ulb.uni-bonn.de/2010/2212/2212.htm URN: urn:nbn:de:hbz:5N-22122

Zogg, J.-M. 2009. *GPS essentials of satellite navigation*, no. GPS-X-02007-D, u-blox AG, Thalwil. Accessed from www.u-blox.com

Curriculum Vitae

Personal Details

Name	David Eugen Grimm
Date of Birth	September 22, 1982
Nationality	Swiss

Education

2008-2012	PhD-Study at ETH Zurich, Switzerland, Institute of Geodesy and Photogrammetry
2002-2007	Study of Geomatic Engineering and Planning at ETH Zurich, Switzerland
2002	Matura Typus B, Hochalpines Institut Ftan, Switzerland

Work Experience

2007-2012	Research and Teaching Assistant Institute of Geodesy and Photogrammetry at ETH Zurich, Geodetic Metrology and Engineering Geodesy (Prof. H. Ingensand)
2005-2007	Teaching Assistantship Institute of Geodesy and Photogrammetry at ETH Zurich, Geodetic Metrology and Engineering Geodesy (Prof. H. Ingensand)
2005-2006	Internship CERN (European Organisation for Nuclear Research) in Geneva, Large Scale Metrology Group

Languages

German	native language
Romansh	native language
English	fluent
French	fluent

Acknowledgements

Acknowledgements